Spring 2016

VACUUM BRAZING OF DIAMOND TO TUNGSTEN CARBIDE

Zhiyong Yin
Montana Tech of the University of Montana

Follow this and additional works at: http://digitalcommons.mtech.edu/grad_rsch

Part of the Metallurgy Commons, and the Other Materials Science and Engineering Commons

VACUUM BRAZING OF DIAMOND TO TUNGSTEN CARBIDE

by

Zhiyong Yin

A thesis submitted in partial fulfillment of the

requirements for the degree of

Master of Science in Metallurgical Engineering

Montana Tech

2016

Abstract

Diamond tools are increasingly gaining importance as cutting and drilling materials for a wide variety of industrial applications. Polycrystalline diamond (PCD) is the main ultrahard material commercially used in the oil and gas drilling industry. In this study, a reactive brazing process was developed to join polycrystalline diamond (PCD) to WC-13 wt% Co, to form the cutter for fixed-cutter drill bit applications.

Most nonmetals including polycrystalline diamond are not wet by and cannot easily be joined with conventional brazing alloys due to their chemical stability. The experimental approach was first to analyze the effect of adding an active metal (Ti, Zr, or V) to copper, silver, or a silver-copper eutectic alloy on the wettability of diamond and WC-Co substrates. Sessile drop tests were utilized to compare wettability between the liquid braze alloy and the substrate. The addition of Ti, Zr, and V decreased the apparent contact angle, which improved both the wetting and bonding behavior between braze alloy and diamond substrate. For all three alloy systems evaluated, all three base alloys (Cu, Ag, and Ag-Cu) with active metal additions (Ti, Zr, or V) exhibited good wettability on diamond and WC-Co substrates.

Microstructural analysis of the diamond and WC-Co sessile drop samples was performed via scanning electron microscopy (SEM) to characterize the interfacial layers formed. Two different types of reactions were observed between the braze alloys and the WC-Co substrates: reduction and dissolution reactions. For the diamond sessile drop samples, only intermetallic solidification products were observed at the interface for the Ag-Cu eutectic based alloys with additions of 2 and 5 wt% Ti. SEM/EDS analysis revealed that the chemical changes at the interface between the braze alloy and diamond substrate were in agreement with the intermetallic solidification products predicted from the phase diagrams. Based on the Gibbs energies of formation for carbides, it is predicted that the formation of TiC is thermodynamically favored at the interface. However, no TiC reaction product was identified within the resolution of SEM/EDS analysis possibly because the TiC reaction layer is too thin.

Based on the results of the wetting studies, an effort was made to optimize the shear strength of diamond brazed to WC-Co. This phase study was focused on the relationship between the braze alloy composition, the braze layer thickness, the brazing thermal cycle, the braze microstructures and the resulting joint mechanical properties. The average shear strength for Ag-2 wt% Ti alloy was approximately constant in the braze thickness range of 0.1 to 0.2 mm. It was observed that the brazed samples failed in the silver braze layer. More visible cracking and larger cracks were observed on the surface region of diamond substrates of the joint thickness of 0.2 mm for the Ag-Cu-2 wt% Ti alloys. It is possible that thermal stresses generated from coefficient of thermal expansion (CTE) mismatch resulted in the formation of interfacial cracks. The Ag-Cu eutectic alloy with addition of a 2 wt% Ti has the highest average shear strength of 95 MPa when the hold time is 30 minutes and the cooling rate is 5 °C/min.

Keywords: polycrystalline diamond (PCD), tungsten carbide (WC), vacuum brazing, active metals, wettability, shear strength

Dedication

This thesis is dedicated to my dear parents, my brother, and all my friends who supported me in all my pursuits. Thanks to my wonderful family for all their love and encouragement.

Acknowledgements

First of all, I would like to thank my advisor, Dr. Alan Meier for his guidance and encouragement throughout this project. I could not have done it without his help and support.

I would also like to thank the other members of my committee, Dr. K. V. Sudhakar, Dr. Bruce Madigan, and Dr. Gagan Saini for their contributions to this research and thesis.

In addition, I would like to thank Hayden Peck and Kleanny Gama for their help with tungsten carbide wetting study and brazing thickness study, respectively. This work would not have been completed without their support.

I want to thank Ronda Coguill of CAMP, Montana Tech for her help with the shear test fixture design and the mechanical testing. I would also like to thank Gary Wyss of CAMP, Montana Tech for his SEM training and his assistance with SEM. I would like to thank Dr. Bill Gleason for his help with vacuum furnace.

Finally, I would like to Dr. Alan Meier, Dr. K. V. Sudhakar, and Dr. Courtney Young for their time and assistance throughout my Ph.D program application process.

Table of Contents

List of Tables

List of Figures

List of Equations

1. INTRODUCTION

Diamond is the hardest known natural material and has found industrial applications in numerous fields including: drilling tools for oil and gas wells, metal machining tools and ultrahard abrasives (American Welding Society, 2007). Diamond has the highest hardness and highest thermal conductivity of any known material at room temperature. Diamond is five times as hard as tungsten carbide on the Knoop hardness scale (Gorczyca, 1987). The thermal conductivity of diamond crystals can be as high as five times that of copper at room temperature (Davis, 1995). The combination of high hardness and high thermal conductivity renders it the ultimate cutting and abrasive material (Gauthier, 1998). Diamond can be used as a cutting tool because it rapidly dissipates the heat from the cutting zone, so that thermal shock caused by sudden changes in temperature can be prevented.

Diamond tools are increasingly gaining importance as cutting and drilling materials for a wide variety of industrial applications (Tillmann, Osmanda, Yurchenko, & Theisen, 2005). Several forms of diamond are available as cutting and drilling tool materials: natural single-crystal diamonds, synthesized single-crystal diamonds, sintered polycrystalline diamonds, and chemical-vapor-deposited polycrystalline diamonds (Prelas, Popovici, & Bigelow, 1998). Polycrystalline diamond (PCD) is the main ultrahard material commercially used in the oil and gas drilling industry (Ngwenya, 2015).

Typically, polycrystalline diamond is joined to a cemented carbide substrate. For example, WC-Co is bonded to diamond to form the cemented carbide/polycrystalline diamond tip used for drill bits due to the brittleness and relatively high cost of the monolithic polycrystalline diamond (Bar-Cohen & Zacny, 2009). In these applications, the drill bits tend to fail and then the resulting failure of the drill bits greatly reduces the tool life and increases the

operational costs (Ngwenya, 2015). Therefore, the use of polycrystalline diamond drill bits is limited without adequate joining technologies that produce high quality joints with the cemented carbide. Polycrystalline diamond bonded to a tungsten carbide substrate is known as a polycrystalline diamond compact (PDC). A significant increase in cutting rate and tool life can frequently be obtained by using a polycrystalline diamond compact (PDC) drilling tool (Stephenson & Agapiou, 1997). The abrasion resistant diamond substrates disintegrate and remove the rock by shearing while the tungsten carbide substrates provide mechanical support and impact resistance (Bar-Cohen & Zacny, 2009).

The joining of materials with dissimilar atomic bonding is considerably more challenging especially if one of them is nonmetallic. Most nonmetals including polycrystalline diamond are not wet by and cannot easily be joined with conventional brazing alloys due to their chemical stability. They also typically have a much higher elastic modulus than metals. The elastic modulus mismatch can result in a high residual stress state. In addition, thermal residual stresses are another major problem that are generated due to the coefficient of thermal expansion (CTE) mismatch between the diamond and the WC-Co substrate (Jacobson & Humpston, 2005). The metal will contract more than the nonmetal during cooling from the solidus temperature of the braze alloy. The thermal residual stresses can result in the formation of interfacial cracks which then lower the shear strength of the diamond to WC-Co brazed joints (Xu, Indacochea, & Harren, 1992).

The objective of this study is to develop an active metal brazing (AMB) process to join polycrystalline diamond (PCD) to WC-Co. The experimental approach was first to analyze the effect of adding an active metal (titanium, zirconium or vanadium) to copper, silver, or a silver-copper eutectic alloy on the wettability of diamond and WC-Co substrate materials. Sessile drop

tests were utilized to compare the wettability between the liquid braze alloy and the substrate. Microstructural analysis of the diamond and WC-Co sessile drop samples was performed via scanning electron microscopy to determine the interfacial layers formed. Next, the brazing alloys and test conditions to be further studied were be determined by analyzing the combined diamond and WC-Co experimental wetting and microstructural development results. Then the research was focused on the relationships between the braze alloy composition, the braze layer thickness, the brazing thermal cycle, the microstructure developed during brazing and the mechanical properties of diamond to WC-Co brazed joints in order to optimize the brazing process. The overall aim of this study was to develop sufficient bond strength between the polycrystalline diamond (PCD) and WC-Co.

2. BACKGROUND AND LITERATURE REVIEW

2.1. Polycrystalline diamond (PCD)

Polycrystalline diamond is widely known as sintered diamond or chemical vapor deposited diamond as it is produced through high pressure, high temperature (HPHT) and chemical vapor deposition processes (Prelas, Popovici, & Bigelow, 1998). The sintered polycrystalline diamond is made by a liquid phase sintering (LPS) process which contains up to 10 volume percent of metallic phase. Nickel, cobalt and iron are primarily used as the metallic phase and they are primarily located at the crystal grain boundaries (American Welding Society, 2007). The addition of the metal phase in polycrystalline diamond sintering improves the direct bonding of the diamond grains and keeps the constituents bound together (Ngwenya, 2015). Both polycrystalline and natural diamond are used in industry. However, polycrystalline diamond has properties that can be tailored to specific applications and can be produced in large quantities so they are superior to those of most naturally formed diamonds (Boucher, 1996). Therefore, polycrystalline diamond has been used in a variety of industries.

2.2. Diamond brazing

Ceramics are inherently difficult to join to either other ceramics or to metals because of their strong ionic and covalent bonding. There are several well-established methods that can be used to join ceramics to ceramics or to metals, including direct methods such as diffusion bonding and indirect methods like brazing. At present, brazing is a ceramic joining technique that is established as a commercial process. Ceramic/ceramic and ceramic/metal joints have been produced for many years in industry.

In recent years, there has been an increase in the number of potential applications for diamonds in industry because of their unique combination of properties. In the oil and gas

drilling industry, diamond is joined to a cemented carbide to form cemented carbide/diamond tips. Joining of diamond to tungsten carbide is much more complicated compared to other ceramic joining. However, the general methods used for diamond joining are very similar to those used for brazing ceramics or cemented carbides. Brazing is currently the most reliable technique for joining diamond to tungsten carbide (American Welding Society, 2007). In this research, the brazing of diamond to tungsten carbide using active metal brazing (AMB) was studied.

2.3. Active metal brazing

The American Welding Society (AWS) definition for a brazing process is "a group of joining processes that produce the coalescence of materials by heating them to a suitable temperature and by using a filler metal having a liquidus above 450°C and below the solidus of the base metals" (AWS Committee on Definitions and Symbols, American Welding Society, American Welding Society. Technical Activities Committee, & American National Standards Institute, 2009). Brazing is a well-established commercial process and is widely used in industry because most metallic and ceramic materials can be joined by brazing (American Welding Society, 2007).

In diamond/tungsten carbide brazing, active metals are added to the braze alloy to promote reaction and wetting with the diamond and tungsten carbide substrates. The addition of active metals to the braze alloy results in increased reactivity and an improvement of the wetting behavior. The diamond and tungsten carbide wetting is improved by the formation of interfacial products that can then form a joint with the braze alloy. This brazing process is used for joining diamond to tungsten carbide and is referred to as "active metal brazing (AMB)".

In AMB, titanium is the most common active metal addition because it forms wettable layers by reaction with oxides, carbides, and nitrides. Active metal brazing requires an inert gas or a high vacuum atmosphere in order to protect the active metal braze alloys from oxidation (Jacobson & Humpston, 2005).

2.4. Wettability

When the brazing filler metal becomes molten and fills the joint space between the base materials, it is essential that the molten filler metal wets the base materials and forms a strong brazed joint. The wetting of the base materials by the molten filler metal is required to provide intimate contact with the base materials (Thwaites, 1982). Therefore, a chemical/metallurgical bond can form between the base materials.

The concept of wetting during the joining process can be illustrated by considering a liquid droplet in contact with a flat solid surface, as shown in Figure 1. The situation is based on the assumption that the spreading of the non-reactive liquid is ideal. The wetting and spreading of the molten filler alloy depends on the free energies of the various surfaces in the system. As Figure 1 illustrates, the liquid will spread over a sold surface until the three surface tensions are in balance in the horizontal direction (Jacobson & Humpston, 2005). The balance between the forces involved is expressed by the Young's equation:

$$\gamma_{SV} = \gamma_{SL} + \gamma_{LV} \cos \theta \qquad (1)$$

where θ is the contact angle between the liquid droplet and the flat solid, γ_{SV} is the surface tension between the solid and vapor, γ_{SL} is the surface tension between the solid and liquid, and γ_{LV} is the surface tension between the liquid and vapor. The Equation (1) is based on the assumption that no chemical reactions occur between the interfaces (American Welding Society, 2007).
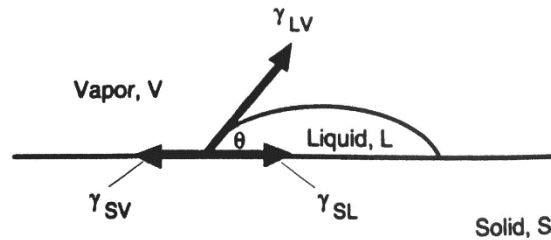
Figure 1. Surface tension forces acting when a liquid droplet wets a solid surface for sessile drop configuration.
(Jacobson & Humpston, 2005)

The contact angle θ is an important measure of the quality of wetting. In the case of nonwetting, the contact angle is greater than ninety degrees ($\theta{>}90°$). In this case, the liquid droplet cannot spread on the surface. If the contact angle is less than ninety degrees ($\theta{<}90°$), the liquid droplet can wet the soild and spread over an area of the surface. The liquid wets the solid completely and spreads freely over the surface when the contact angle is zero ($\theta{=}0°$). The area of spreading tends to increase with decreasing contact angle θ (Jacobson & Humpston, 2005). For brazing, a partial wetting condition with a contact angle of less than ninety degrees is desired.

According to Equation (1), the imbalance in surface tension ($\gamma_{SV} - \gamma_{SL}$) provides the driving force for wetting and spreading of the liquid. Wetting is improved by decreasing the contact angle θ. Accordingly, increasing γ_{SV} or decreasing γ_{SL} and γ_{LV} can improve wetting (Jacobson & Humpston, 2005). There will be a greater driving force for wetting and spreading of the liquid over the surface if the contact angle θ can be decreased. In general, the best wettability is obtained when the contact angle is less than ten degrees ($\theta{<}10°$). However, it is still possible to achieve excellent joints with much higher contact angles approaching $50°$ (Thwaites, 1982).

Table I provides examples of non-reactive wetting of different types of solid substrates such as solid metals, semiconductors, and ceramics with a partially metallic character by non-reactive liquid metals. Good wettability of WC-Co by liquid copper was confirmed by the majority of studies. The wettability of brazing copper alloys on WC based cemented carbide

surfaces was studied by Mirski et al to improve the brazing process (Mirski, & Piwowarczyk, 2011). The wetting behavior of melted Cu on WC and WC-3.5 wt% Co surfaces was investigated by Silva et al. The results indicated that a good wetting was observed in the case of the WC-Co with a final contact angle of 6° at 1080°C. The highest wettability was obtained for the WC-Co and the lowest for the WC surface. An increased concentration of Co at the interface WC-Co/Cu indicated that a probable diffusion of Co into Cu (Silva, Fernandes, & Senos, 2016).

Table I. Wetting of different types of substrates by non-reactive liquid metals.
(Dezellus & Eustathopoulos, 2010)

Type of substrate	Wetting	Examples
Solid metals	$\theta \ll 90°$	AgCu/Steel – 10-60° (Kozlova, Voytovych, Devismes, & Eustathopoulos, 2008)
Semi-conductors		Ag/SiC – 33-65° (Rado, Kalogeropoulou, & Eustathopoulos, 2000)
Ceramics with a partially metallic character		AgCu/Ti$_3$SiC$_2$ – 10° (Dezellus, Voytovych, Li, Constantin, Bosselet, & Viala, 2009)
Carbon materials	$\theta \gg 90°$	Au/C – 119-135° (Dezellus & Eustathopoulos, 1999)
Covalent ceramics		Au/BN – 135-150° (Danielli, Rosenberg, & Cadenhead, 1972)

However, non-reactive liquid metals do not wet solid substrates such as different forms of carbon materials and covalent ceramics with a high band gap such BN or AlN (Dezellus & Eustathopoulos, 2010). Non-wetting of the liquid metal on carbon materials or covalent ceramics is observed due to their bond structure which is based on covalent or ionic atomic bonds. The ability of most liquid metals to react chemically and form a strong interfacial bond on the surface is limited by the surface condition of the non-wettable substrates (American Welding Society, 2007). Therefore, the addition of a reactive metal such as titanium, zirconium, or hafnium to conventional brazing filler metals in order to obtain wetting and spreading of the braze alloys over carbon materials and covalent ceramics (Jacobson & Humpston, 2005). In this case, the wetting process is accompanied by chemical reactions between the liquid metal and substrate materials, which is also called reactive wetting.

In reactive wetting, the active braze alloy systems provide improved chemical activity with diamond and form carbides and dissolve carbon. Reactive wetting is used in brazing to activate the wetting of diamond and obtain a reliable metallurgical bond (American Welding Society. 2007). Naidich et al. demonstrated that wetting of diamond substrate can be drastically improved by adding titanium, chromium, and silicon to braze alloys such as copper, silver, gold, and tin (Naidich, 2007). Table II lists the wettability of diamond by alloys containing active metals. From the table, the alloys containing active metals on diamond exhibited good wetting behavior. Based on the improved wettability, AMB alloys were identified as the most promising brazing alloys for joining diamond to WC-Co for this study.

Table II. Diamond wetting by alloys containing active elements.
(Naidich, 1981)

Base Alloy	Active Metal Addition	Temperature (°C)	θ
Cu	12.8 at% Ti	1150	0°
Sn	0.5 at% Ti	1150	38°
Sn	2.5 at% Ti	1150	22°
Ag	0.1 at% Ti	1000	45°
Ag	0.45 at% Ti	1000	5°
Cu	0.37 at% Cr	1150	37°
Cu	6 at% Cr	1150	0°

2.5. Active brazing filler metals

In general, it is difficult to wet ceramics by conventional braze alloys. However, active metal additions to the filler metals can react with the ceramic to produce an interfacial layer that promote wetting at the ceramic surface (Akselsen, 1992). Active filler metals are used for brazing when conventional braze alloys do not wet the base materials. In active metal brazing, carbide-forming elements such as Ti, Hf, Zr, and V are commonly used as brazing alloy additions for joining ceramics, cermets, or diamonds because they react with oxides, carbides, and nitrides to form a wettable layer (Jacobson & Humpston, 2005). Active brazing alloys have been used for brazing diamond. Previous studies determined that the addition of titanium,

vanadium and chromium can improve both the wetting and bonding behavior between diamond and copper. The results indicated the migration of the added carbide-forming element to the metal/diamond interface and the presence of carbides in the case of titanium and vanadium containing alloys (Scott, Nicholas, & Dewar, 1975). The wetting of carbon by copper based alloys containing carbide forming additions has been investigated in terms of the surface energies of the substrate and the stable reaction product carbides at the metal/carbon interface (Mortimer & Nicholas, 1970).

Figure 2 presents the Gibbs standard free energy (ΔG^o) changes of formation of various carbides, as a criterion for comparing the formation tendency of these compounds. The lower the position of the line on the diagram, the more stable the carbide. Ham et al. examined the interfacial reaction behaviors of vacuum brazed joint between diamond grit and a Ni-10Sn-28Cr filler alloy. The XRD analysis determined that the carbides such as $Cr_{23}C_6$, Cr_7C_3, and Cr_3C_2 were formed at the interface. No evidence of a nickel carbide formation was observed in this study. This result was expected since there is no possibility of nickel carbide formation based on the thermodynamic data (Ham, Chung, Jung, Byoun, & Lee, 2013).

Currently, Cu-based and Ag-Cu-based braze alloy systems with additions of Ti are the most commonly used active metal brazing alloys. Other braze systems such as Ag-based braze alloys are also excellent options for joining non-metals (Fernie, Drew, & Knowles, 2009). Ti is the most commonly used active element but other elements such as Zr, Hf, V, Ni, and Cr are also used (Jacobson & Humpston, 2005).
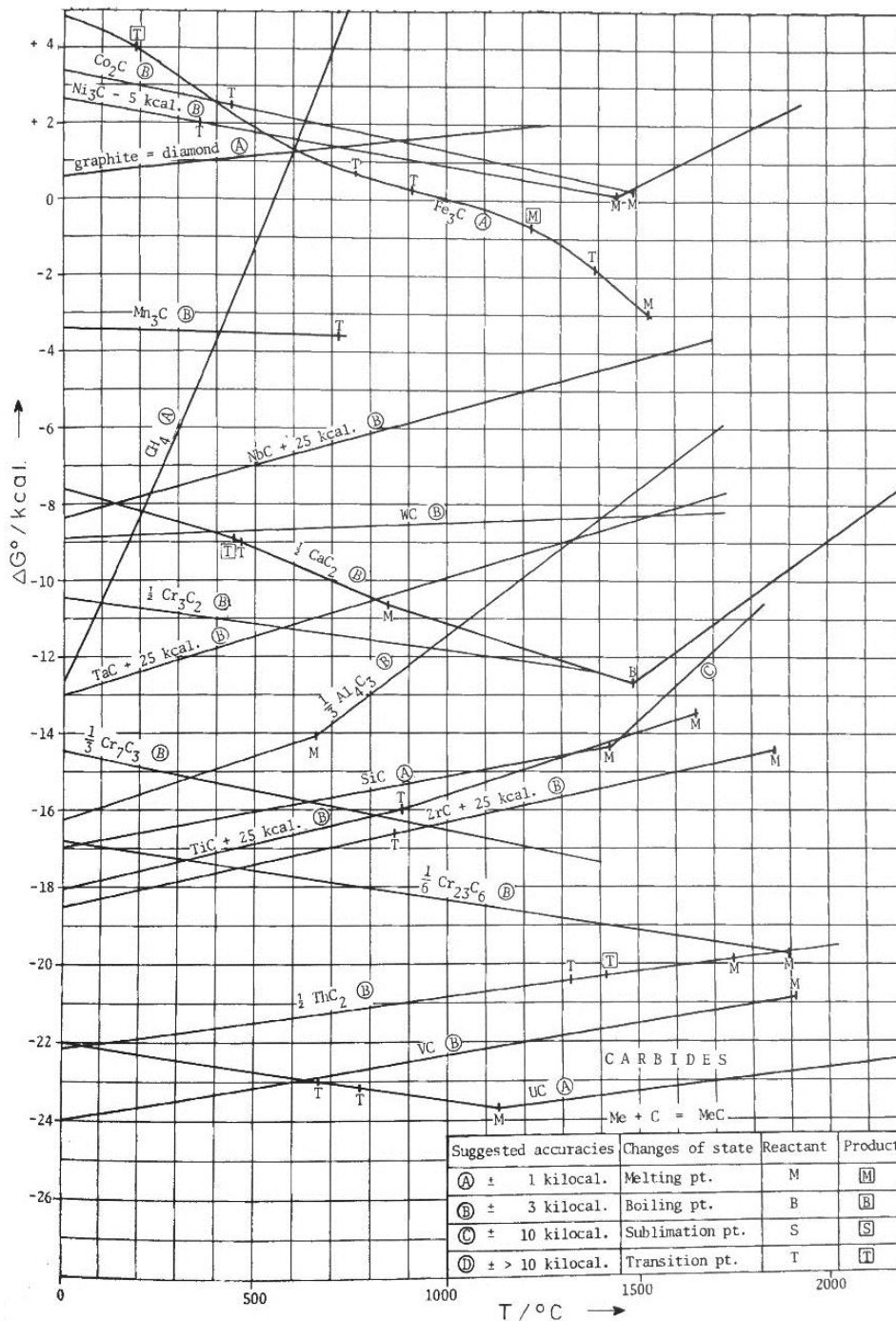
Figure 2. Gibbs standard free energy (ΔGo) of the formation of carbides at different temperatures. (Rosenqvist, 1974)

Pure copper does not wet or bond well to diamond or to other forms of carbon. However, copper-based braze alloys with additions of chromium, titanium, manganese, or vanadium can promote the wetting of diamond and other carbon substrates (Naidich & Kolesnichenko, 1964).

Scott et al. studied the wetting and bonding behavior between diamond and copper-based alloys with chromium, titanium, or vanadium additions. For Cu-Cr braze alloys, wetting occurred with Cr concentrations in excess of 0.1 at%. SEM analysis determined that carbides had formed at the braze alloy/diamond interfaces. For Cu-Ti alloys, wetting occurred only for high Ti concentrations of 15 at%. Therefore, in general the addition of chromium and titanium to the copper-based braze alloys improves the wetting behavior between diamond and the filler metals (Scott, Nicholas, & Dewar, 1975). In addition, other researchers have also shown that the braze alloy Cu-(0.3-1) wt% Cr exhibits improved wetting of diamond with contact angles of approximately 40°, while pure copper does not wet diamond. The results of this study indicated that Cu-Cr braze alloys can be used for vacuum brazing of diamond to metals, ceramics or WC-Co cemented carbides (Naidich, Kolesnichenko, Lavrinenko, & Motsak, 1977).

In addition to brazing using copper-based braze alloys, silver can also be combined with active metals such as Ti to form active metal braze alloys. Silver based filler metals with brazing temperatures from 950°C to 1050°C are the most commonly used (American Welding Society, 2007). Silver based brazing filler metals are malleable and ductile. Silver-based brazing filler metals can be used to braze copper, nickel, cobalt alloys, tool steels, and carbide tips. Ag-based braze alloys with additions of Cu have been frequently used in the active brazing. The addition of copper to silver-based alloys is effective in hardening the silver and lowering the melting point. Also titanium has much higher solubility in copper than in silver. Therefore, Ag-Cu-based braze alloys are widely used as filler metals in active brazing (Akselsen, 1992).

A eutectic Ag-Cu-based braze alloy with 28 wt% Cu is also frequently used in the brazing of ceramics and non-metals. Ag-Cu-Ti braze alloys are often used for brazing non-metals in the temperature range 800°C-900°C (Eustathopoulos, Nicholas, & Drevet, 1999). The brazed

joint exhibits good wettability at the solid/liquid interface because of the formation of interfacial Cu-Ti intermetallic layers (Shiue, Wu, Chen, & Yang, 2012). A diamond-iron compact was brazed to a cemented carbide substrate in vacuum at a temperature of 850°C with holding time of 10 minutes using an active brazing filler metal Ag-28Cu-2Ti (wt%) (American Welding Society, 2007). In all cases, Ti within the molten braze migrates at the brazing temperature to the ceramic surface to form compounds such as TiO, TiC and TiN in the form of an interfacial reaction product layer (Fernie, Drew, & Knowles, 2009). In summary, ceramics were brazed successfully with active metal braze alloy Ag-Cu-Ti. It was confirmed that the interfacial reaction layer plays an important role in the active brazing process.

2.6.   Interfacial reactions in brazed joints

In active metal brazing, mass transport occurs along the interfaces of the joint. Interfacial reaction layers are formed with properties that differ from those of the braze alloy and the non-metal substrates (Jacobson & Humpston, 2005). The formation of an interfacial reaction layer between the non-metals and active brazing filler metals results in an enhancement of the interfacial bond strength. In this case, an interfacial chemical reaction is essential to the bonding mechanism for the brazing of non-metals such as diamonds or ceramics.

Lee et al. investigated the interfacial reaction between diamond grits and a Ni-based brazing filler metal: Ni-7Cr-3Fe-3B-4Si (wt%). Chromium carbide and Ni-rich compounds were detected in the vicinity of the interface between the diamond grits and the Ni-based filler metal after vacuum brazing. In this study, chromium carbide was considered to play an important role in the high bond strength between the diamond grit and the braze alloy (Lee, Ham, Song, & Lee, 2007).

Scott et al. studied the wetting and bonding behavior between diamond substrates and copper alloyed with chromium, titanium or vanadium using the sessile drop technique. This work proposed that the diamond/copper interfaces were weak because no chemical reactions occurred and that the bonding was due to van der Waal's forces only. However, islands of carbides nucleated at favored sites on the diamond surface when the diamond made contact with the braze alloy. The interfaces were strengthened by the carbide islands because the carbides formed a chemical bridge between the diamond and the metal. A continuous interfacial layer was formed as the islands of carbide grew and contacted each other. This study also determined that the interfacial strength between the diamond substrates and the solidified sessile drops increased with increasing active alloying element concentration (Scott, Nicholas, & Dewar, 1975).

Liu et al. investigated the interfacial characteristics of brazed joints between diamond/cubic boron nitride (CBN) crystals and steel substrate using a Cu-Sn-Ti active filler powder alloy. The reliable bond strength of the brazed diamond/CBN grains to the steel substrate met the application requirements of high efficiency machining in the industrial field. The results indicated that the Ti in the Cu-Sn-Ti alloys diffused preferentially to the surface of the diamond/CBN grits to form a Ti-rich reaction layer in the brazed joints. The wetting and bonding reactions on diamond/CBN by melting Cu-Sn-Ti alloy were realized through the interfacial reaction products such as TiC, TiN, and TiB_2 compounds (Liu, Xiao, Zhang, & Duan, 2016).

2.7. Residual thermal stresses at the joint interface

The mechanical properties of brazed joints for diamond/WC-Co substrates depend on a variety of factors. Residual stress is one of the most important factors that influence the joint strength. The residual stresses are primarily due to coefficient of thermal expansion mismatch between the nonmetal and metal (Jacobson & Humpston, 2005). As illustrated in Table III,

diamond and tungsten carbide have different coefficients of thermal expansion (CTE), and both materials have lower coefficients of thermal expansion than typical metals. Therefore, the CTE mismatch can result in the development of the residual stresses during cooling from the brazing temperature. Residual stresses play an important role in the strength of the joint and life of the components in service. The residual stresses developed during the brazing process will reduce the strength of the brazed joint.

Table III. Coefficient of linear thermal expansion for selected materials.
(Cverna & ASM International, 2002)

Materials	CTE (10^{-6}/K)
Pure Silver	19
Pure Copper	17
Pure Iron	12-13
Iron carbon alloys	10-12
WC-6Co (wt%)	4.3-5.9
WC-16Co (wt%)	5.8-7.0
Diamond (Carbon)	1.2

The reduction of residual stress is mainly a matter of material selection, the design of the braze alloy when two materials are joined, and the brazing thermal cycle parameters (Galli, Botsis, & Janczak-Rusch, 2006). A ductile metal interlayer incorporated between the joining substrates can reduce the residual stresses. Brochu et al. studied that the effect of adding a copper interlayer to absorb the residual stresses developed during cooling of a silicon nitride ceramic brazed to an iron aluminide alloy. The addition of a copper interlayer was demonstrated to absorb the residual stresses developed during the cooling process resulting in sound brazed joints (Brochu, Pugh, & Drew, 2004). The residual stresses can also be minimized by the optimization of the braze material selection and the braze joint thickness. Levy investigated the effects of the filler metal work-hardening rate and the joint thickness on the levels of residual stresses developed. This study observed that the peak residual shear stress was decreased as the braze

work-hardening rate decreased and that increasing the braze thickness generally lead to higher peak residual stresses (Levy, 1991).

Buhl et al. studied that the influence of the brazing parameters on the properties of diamond/metal joints. In this work, diamonds were brazed on to a steel substrate using a Cu-Sn-based active filler alloy. Three different brazing temperatures and two different holding time were chosen as brazing parameters. The results indicated that the residual stresses in the diamond and in the filler alloy was strongly dependent on both the brazing temperature and the holding time. In conclusion, the brazing parameters must be carefully chosen in order to reduce the residual stresses (Buhl, Leinenbach, Spolenak, & Wegener, 2012).

2.8. Shear strength of brazed joints

The shear strength between the diamond and the WC-Co substrate is important for industrial applications. The shear strength of brazed joints are strongly influenced by the process parameters as well as by the choice of filler metals. The failure of brazed diamond components involves a complex mechanism that is affected by the brazing process, the properties of the diamond substrate, the filler metal, the interlayers formed during the brazing process and the residual stresses (Buhl, Leinenbach, Spolenak, & Wegener, 2010). The strength of diamond/metal joints is strongly dependent on the braze microstructure and the residual stresses in the diamond/filler alloy and filler alloy/substrate interfaces (Buhl, Leinenbach, Spolenak, & Wegener, 2012).

An interfacial reaction product layer between the diamond or WC-Co substrates and the brazing filler metals is formed by adding active elements such as Ti, Cr, V, Zr into the brazing alloy and this product layer can result in the enhancement of the interfacial bond strength (Sung, 1999). Ham et al. investigated the interfacial microstructure developed between diamond grits

and a Ni-10Sn-28Cr alloy in order to understand the bonding mechanism. The shear strength of

graphite/Ni-10Sn-28Cr filler joints brazed for 10 minutes at 1100°C indicated the maximum

value of 29.8 MPa, tends to decrease as brazing temperature increases. It was determined that the

shear strength of the brazed joints was decreased significantly from 29.8 MPa to approximately

10.6 MPa with temperature increasing from 1100°C to 1200°C due to the increases in the

thickness of brittle reaction layer and interface residual stresses. The results of this study also

proved that chromium carbides formed played an important role in the high bond strengths and

that the existing angular chromium carbides were transformed into acicular chromium carbides

with increasing brazing temperatures (Ham, Chung, Jung, Byoun, & Lee, 2013).

Chen et al. studied the microstructural evolution of the interfacial reaction products and

the shear strengths of diamond/steel joints brazed with Ag-Cu-Ti filler metals. In this study, the

thickness of TiC layer and the amount of Ti-Cu intermetallics play important roles on the shear

strength of the brazed joints. The results indicated that a layer of TiC formed on the surface of

the diamond and that the thickness of the TiC layer increased with increasing Ti additions. The

results of this study also indicated that the shear strength of the brazed joints decreased from 140

MPa to 60 MPa with Ti content increasing from 2 wt% to 7 wt%. The shear strength of the

brazed joints decreased due to the increasing thickness of the TiC layer and the formation of

intermetallic phases (Chen, Xu, Fu, & Su, 2009).

The shear strength of brazed joints strongly depends on the brazing parameters. Buhl et

al. investigated that influences of the brazing parameters on microstructure and shear strength of

diamond/metal joints. The investigations revealed that an intermetallic interlayer of Fe_2Ti formed

at the steel/filler alloy interface that increased thickness with increasing brazing temperatures and

longer holding times. The results indicated that the shear strength of the brazed joints decreased

from (321±107) MPa to (78±30) MPa at 880°C with the hold time increasing from 10 minutes to 30 minutes. A higher percentage of brittle intermetallic phases also formed with increasing brazing temperatures and holding times, and this may have also contributed to the decrease in the shear strength of the brazed joints (Buhl, Leinenbach, Spolenak, & Wegener, 2012).

3. EXPERIMENTAL METHODS AND MATERIALS

3.1. Materials

In this work, polycrystalline diamond (PCD) was brazed on to tungsten carbide substrates with 13 wt% cobalt (WC-13 wt% Co) using active metal braze alloys. The braze sample configuration is illustrated in Figure 3. The diamonds were cylinders with a diameter of 16.5 mm, and a height of 2.4 mm. The tungsten carbide with 13 wt% cobalt substrates were cylinders with a diameter of 16.5 mm, and a height of 11.5 mm.
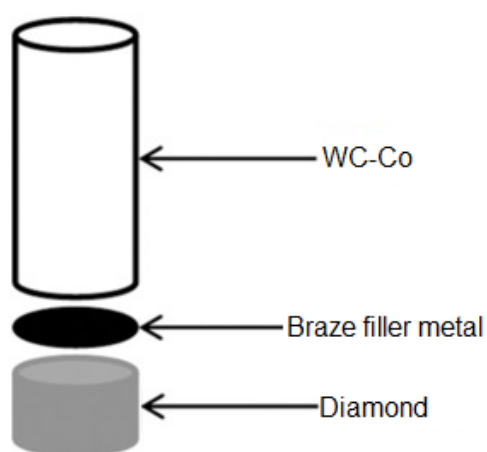
Figure 3. Braze sample configuration.

The base filler metals were copper, silver, and silver-copper eutectic foils from Lucas-Milhaupt, INC (Cudahy, WI). The copper foil was 99.99% purity and 0.254 mm thick. The silver foil was 99.9% purity and 0.0254 mm thick. The Ag-28 wt% Cu eutectic foil was 99.9% purity and 0.0254 mm thick.

The active metal additions were titanium, zirconium, and vanadium foils obtained from Alfa Aesar (Ward Hill, MA). The titanium foil was 99.94% purity and 0.0254 mm thick. The zirconium foil was 99.8% purity and 0.0254 mm thick. The vanadium foil was 99.8% purity and 0.075 mm thick. In addition, nickel and chromium alloying additions were added in foil or powder form and were also obtained from Alfa Aesar (Ward Hill, MA). The nickel foil was

greater than 99% purity and 0.127 mm thick. The chromium powder used in the brazing process had a purity of 99.8%.

3.2. Sessile drop test procedure

3.2.1. Sessile drop test matrix

A sessile drop test was used to obtain an apparent contact angle between the braze alloy and the substrate. The apparent contact angle can be compared between samples to determine their relative wettabilities. The diamond and WC-Co sessile drop test matrix for this experiment is shown in Table IV. Parallel sessile drop tests were performed on both diamond and WC-Co substrates.

Table IV. Diamond and WC-Co sessile drop test matrix.

Base Alloy	Active Metal Addition	Hold Temperature (°C)	Hold Time (min)
Cu	None	1130	30
	2 wt% Ti	1130	30
	5 wt% Ti	1130	30
	2 wt% Zr	1130	30
	1 wt% V	1200	30
Ag	None	1010	30
	2 wt% Ti	1010	30
	5 wt% Ti	1010	30
	2 wt% Zr	1010	30
Ag-28Cu (wt%)	None	810	30
	2 wt% Ti	810	30
	5 wt% Ti	810	30

3.2.2. Sample preparation

Both diamond and WC-Co sessile drop tests were performed in this study. Each metal drop consisted 0.5 grams of braze alloy. The braze alloy's mass was measured using an analytical balance and its constituent's weight percentages were based on the sessile drop test matrix. Both the substrate and the braze alloy was sonically cleaned in acetone and then ethanol for three minutes each. Then the braze alloy with the active metal was folded into a base metal "boat". The braze metal was attached to the substrate with one drop of ethyl cyanoacrylate

(Krazy Glue^{TM}). A typical WC-Co sessile drop sample prior to loading in the furnace is provided

in Figure 4. The substrate/braze metal sample was then placed into the vacuum furnace along

with a 99.95% metals basis titanium sponge from Alfa Aesar (Ward Hill, MA), which acted as

an oxygen getter.

Figure 4. WC-Co sessile drop sample prior to thermal cycle.

Figure 5. Centorr series LF vacuum furnace.

3.2.3. Experimental parameters

The furnace cycle test was performed in a Centorr Series LF vacuum furnace (Figure 5).

The first step was to lower the pressure in the vacuum furnace chamber to less than 5.0×10^{-5} torr.

After the desired vacuum was achieved, all of the samples followed the same basic thermal cycle

(Figure 6):

(1) The heating cycle started at 20°C and was held for 2 minutes (120 s).

(2) The chamber was heated to 300°C in 14 minutes (840 s).

(3) It was then held at 300°C for 30 minutes (1,800 s).

(4) After holding for 30 minutes (1,800 s), ultra-high purity (99.999%) argon gas from General Distributing Co (Butte, MT) was added at about 3 L/min (0.05 L/s) until an overpressure of about 2 psi (13,790 Pa)was achieved.

(5) At the same time, the furnace was heated to the hold temperature at a rate of 20°C/min (0.33°C/s) as the ultra-high purity argon was being added.

(6) The furnace remained at hold temperature for 30 minutes (1,800 s) once it reached the target temperature.

(7) The furnace was then cooled for 30 minutes (1,800 s) at a rate of 5°C/min (0.083°C/s).

(8) The furnace then cooled to room temperature at a rate of 10°C/min (0.167°C/s).
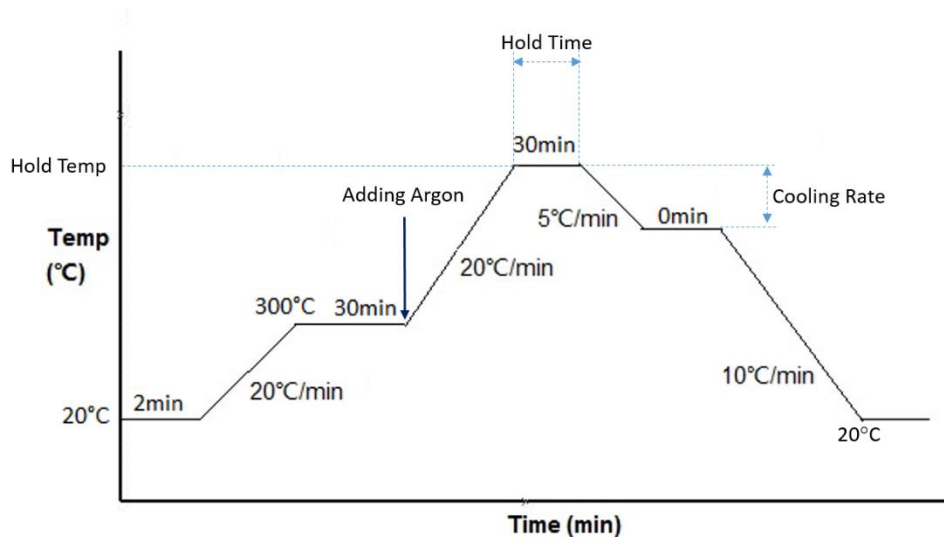
Figure 6. Schematic of basic thermal cycle.
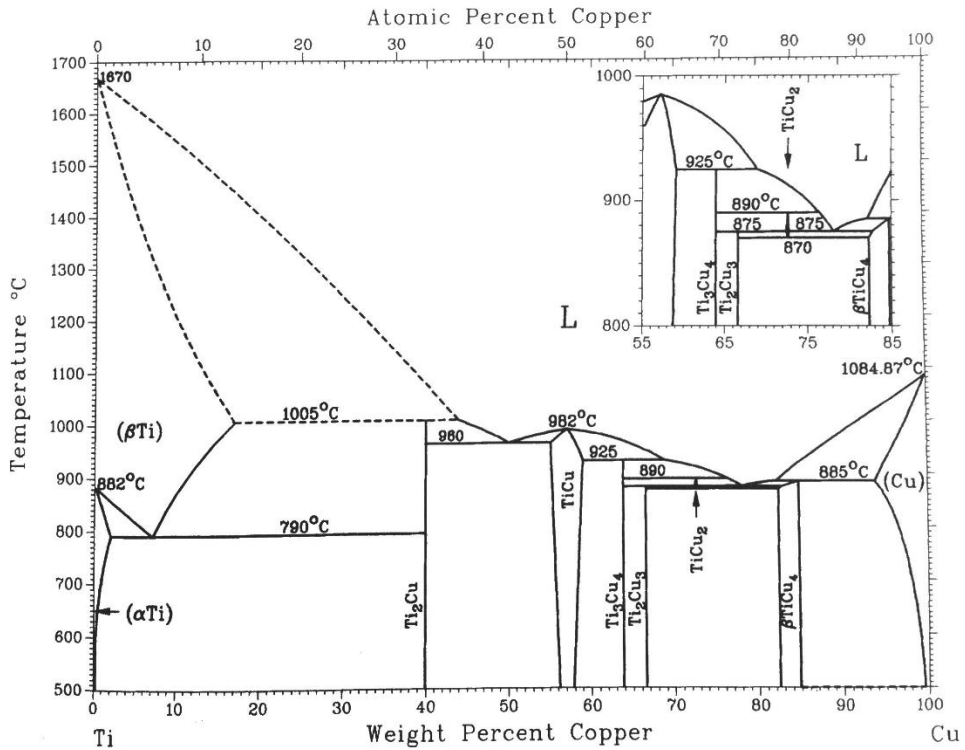
Figure 7. Ti-Cu binary phase diagram.
(Massalski, Okamoto, & ASM International, 1990)
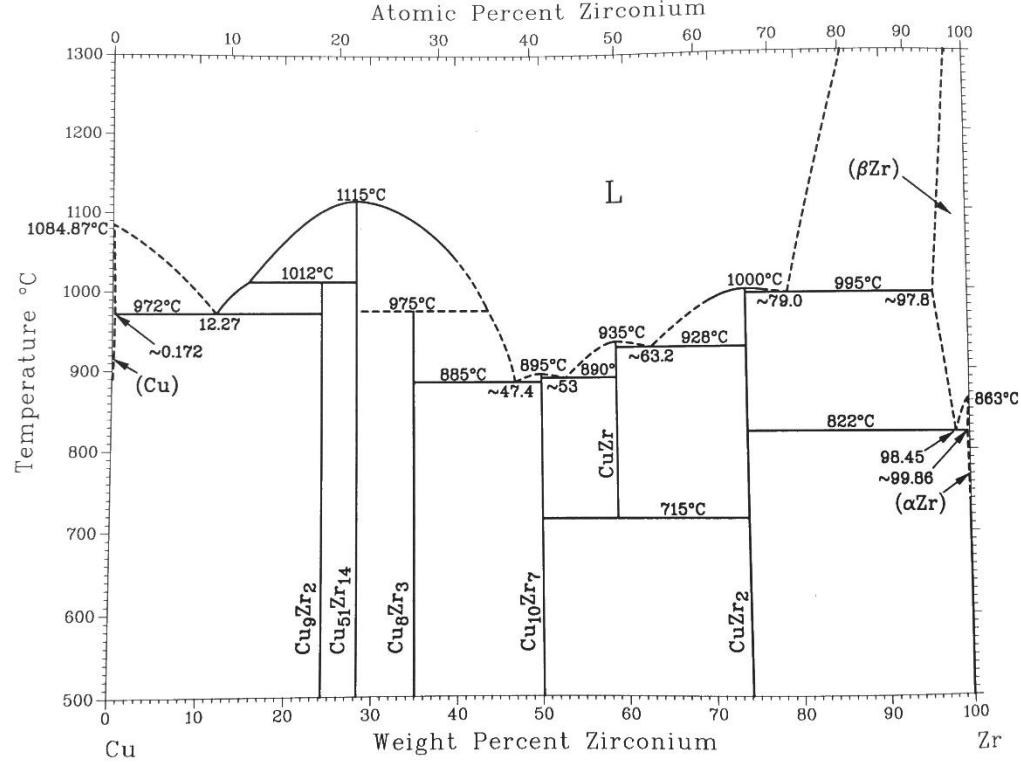
Figure 8. Cu-Zr binary phase diagram.
(Massalski, Okamoto, & ASM International, 1990)

All of the samples having a hold temperature below 1200°C are preferred to prevent graphitization of the diamond. The hold temperatures were: 1130°C for copper base braze alloys excluding the alloys with vanadium additions which was 1200°C, 1010°C for the silver base braze alloys, and 810°C for the silver-copper eutectic base braze alloys. With the exception of the vanadium addition samples, these temperatures were approximately 40-50°C above the melting temperature of the base alloy in order to guarantee complete sample melting. As illustrated in the phase diagrams (Figures 7-9), small additions of both titanium and zirconium lower the liquidus temperature of copper and silver. However, small additions of vanadium dramatically increase the liquidus temperatures so only a Cu-1 wt% V composition was evaluated and the temperature was increased to 1200°C to guarantee melting (Figure 9). The furnace was held at 300°C for 30 minutes to volatilize off any moisture or organics.
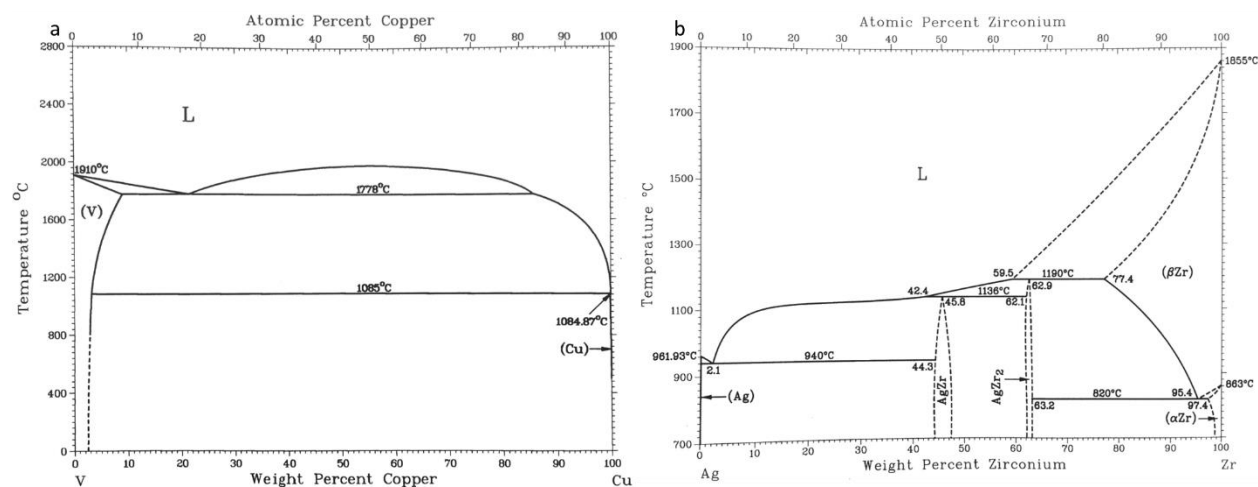
Figure 9. Binary phase diagrams: a) V-Cu, b) Ag-Zr.
(Massalski, Okamoto, & ASM International, 1990)

3.2.4. Apparent contact angle measurements

The apparent contact angle between the braze alloy and the substrate was calculated based on the relationship between the drop volume and contact radius of the braze alloy drop, assuming the dimensions of an ideal spherical cap. The volume of the braze alloy is based on the

ideal densities of its constituents and is calculated using a previously developed technique

(Meier, Gabriel, Chidambaram, & Edwards, 1995). Table V lists the ideal liquid densities of the

braze alloy constituents. The volume of the drop is estimated from:

$$V = V_1 + V_2 = \left(\frac{X_1}{\rho_1} + \frac{X_2}{\rho_2}\right) * m \qquad (2)$$

where X is the weight fraction, ρ is the density, V is the volume, m is the mass of drop, and the

subscripts 1 and 2 correspond to the constituents of the braze alloy.

Table V. Pure metal liquid densities for the braze alloy constituents.
(Iida & Guthrie, 1988)

Materials	Liquid density (g/cm³)
Copper	8.00
Silver	9.33
Titanium	4.13
Zirconium	5.93
Vanadium	5.36

The calculated volume and measured radius are then used to find the height the drop

using equation 3 (Meier, Gabriel, Chidambaram, & Edwards, 1995):

$$V = \frac{1}{2} * \pi * h * \left(r^2 + \frac{h^2}{3}\right) \qquad (3)$$

where V is the volume, r is the radius of braze alloy drop, and h is the height of braze alloy drop.

Next the height and radius is used to find the radius of curvature:

$$R = \frac{1}{2} * \left(\frac{r^2}{h} + h\right) \qquad (4)$$

where R is the radius of curvature, r is the radius of braze alloy drop, and h is the height of braze

alloy drop. Finally, the apparent contact angle can be calculated with the relationship between

the radius of curvature and the height and radius of the braze drop:

$$Tan(\theta) = \frac{r}{R - h} \qquad (5)$$

where R is the radius of curvature, r is the radius of braze alloy drop, and h is the height of braze

alloy drop, and θ is the apparent contact angle.

3.3. Brazing study

The preliminary brazing test matrix was developed by analyzing the experimental results

from the combined WC-Co and diamond sessile drop test results (Table VI). The brazed samples

were prepared based on conditions similar to the sessile drop test conditions. The samples

consisted of one WC-Co substrate, one diamond substrate and a braze alloy interlayer with an

approximate thickness of 0.2 mm. A photograph of a typical brazing sample prior to thermal

cycling is shown in Figure 10. The braze alloy was made from stacks of base alloy with the

addition of active metal foil required to obtain the desired thickness and composition. The WC-

Co substrates were placed on the top of the sample stack in order to provide a consistent brazing

load of 34.6 g. The brazing samples followed the same basic thermal cycle as the sessile drop

samples (Figure 6).

Table VI. Preliminary brazing test matrix.

Base Alloy	Active Metal Addition	Hold Temperature (°C)	Hold Time (min)	Approximate Joint Thickness (mm)
Cu	2 wt% Ti 5 wt% Ti 2 wt% Zr	1130	30	0.2
Ag	1 wt% Ti 2 wt% Ti 2 wt% Zr	1010	30	0.2
Ag-28Cu (wt%)	0.5 wt% Ti 1 wt% Ti 2 wt% Ti 5 wt% Ti	810	30	0.2

Figure 10. Brazing test sample prior to thermal cycling.

The braze thickness was studied based on two braze alloys: an Ag-Cu eutectic alloy with a 2 wt% Ti addition and Ag with a 2 wt% Ti addition. The second brazing test matrix (Table VII) was developed based on the wettability of the substrates by liquid braze alloys and the microstructural analysis of the diamond and WC-Co sessile drop samples. Five different braze alloy thicknesses (0.025, 0.05, 0.1, 0.15, and 0.2 mm) were prepared for each braze alloy. The braze samples were again prepared based on the steps previously described for the sessile drop testing. The braze procedure also followed the same basic thermal cycle as the sessile drop procedure (Figure 6). In this study, five different layers of brazing filler metal foil were placed between the diamond and WC-Co substrate. The braze thickness was used as starting thickness and was not the actual thickness of final braze joint.

Table VII. Second brazing test matrix developed for evaluation of braze layer thickness effect.

Base Alloy	Active Metal Addition	Approximate Joint Thickness (mm)	Hold Temperature (°C)	Hold Time (min)
Ag	2 wt% Ti	0.025	1010	30
		0.05		
		0.10		
		0.15		
		0.2		
Ag-28Cu (wt%)	2 wt% Ti	0.025	810	30
		0.05		
		0.10		
		0.15		
		0.2		

Based on results of the diamond and WC-Co sessile drop tests and the microstructural

analysis of the sessile drop sample cross-sections of diamond and WC-Co in the preliminary

brazing test matrix, the shear test results of the preliminary brazing test matrix, and the braze

thickness study in the second brazing test matrix, an optimized brazing test matrix was designed

with the goal of improving the shear strength of the brazed samples. The third brazing test

matrix, including test condition for the brazing thermal cycle and braze alloys, is provided in

Table VIII. The test variables used for braze alloy system optimization were hold time, cooling

rate and composition. The braze samples were prepared using Ag-Cu eutectic alloy with 2 wt%

Ti addition and Ag with 2 wt% Ti addition. As illustrated in Table VIII, the braze samples have

been studied in a hold time range of 2-50 minutes and a cooling rate range of 2-10 °C/min using

a Ag-Cu eutectic alloy with a 2 wt% Ti addition.

Table VIII. The third brazing test matrix.

Base Alloy	Active Metal Addition	Additional Alloy	Hold Temp (°C)	Hold Time (min)	Cooling Rate (°C /min)	Approximate Joint thickness (mm)
Ag-28Cu (wt%)	2% wt Ti	–	810	2	5	0.2
				10		
				30		
				50		
Ag-28Cu (wt%)	2% wt Ti	–	810	30	2	0.2
					8	
					10	
					25	
Ag	2% wt Ti	2% wt Ni	1080	30	5	0.2
		2% wt Cr				

In addition, alloying elements (Ni and Cr) were added in an attempt to improve the

mechanical properties of the brazed samples for Ag with a 2 wt% Ti addition. The effects of the

Ni and Cr additions on the mechanical properties of the brazed samples were studied based on

conditions similar to the sessile drop test conditions. The hold temperature was 1080°C for Ag-2

wt% Ti with additions of Ni or Cr instead of the 810°C hold temperature used for the Ag with 2

wt% Ti addition brazed samples. In this study, a braze temperature of less than the graphitization temperature of polycrystalline diamond (PCD) was set as an additional requirement. As illustrated in Cr-Ag, Ni-Ag, and Ti-Ag phase diagrams (Figures 11 and 12), small additions of Cr or Ni dramatically increase the liquidus temperature of silver so that Ag-2 wt% Ti with additions of Ni or Cr performed at 1080°C. The braze samples were prepared using the same procedure as the preliminary brazing test matrix. The samples consisted of one WC-Co substrate, one diamond substrate and a braze alloy interlayer with an approximate thickness of 0.2 mm. The braze alloy was made from stacks of Ag-2 wt% Ti with additions of 2 wt% Ni or 2 wt% Cr to obtain the desired composition. The brazing samples followed the same basic thermal cycle as the previous braze test matrices (Figure 6).
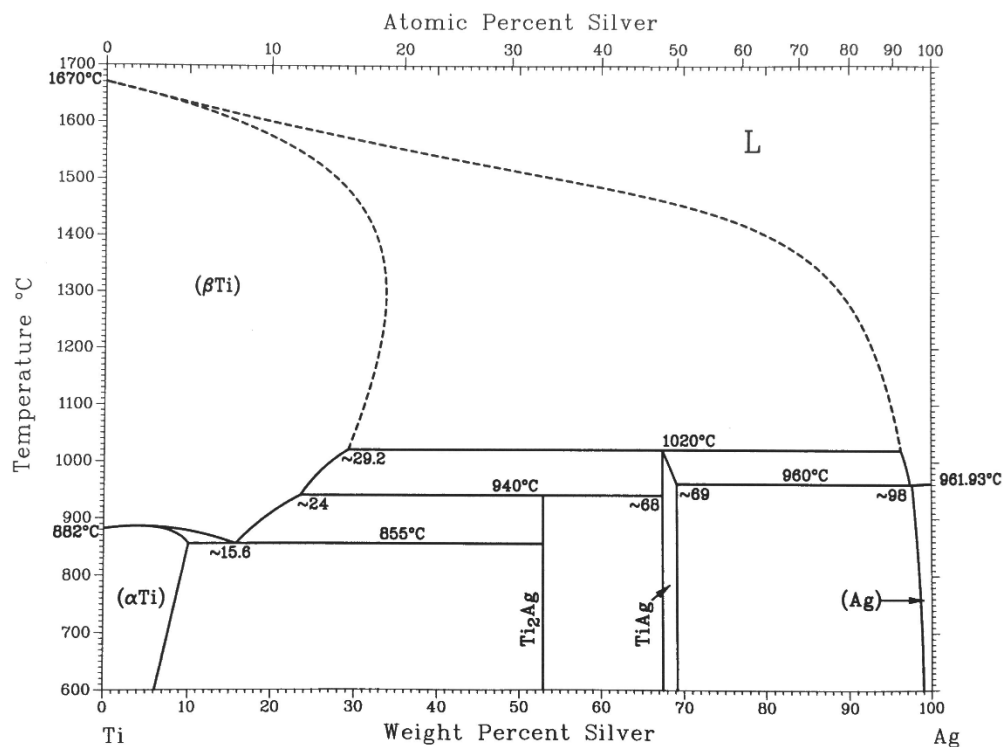
Figure 11. Ti-Ag binary phase diagram.
(Massalski, Okamoto, & ASM International, 1990)
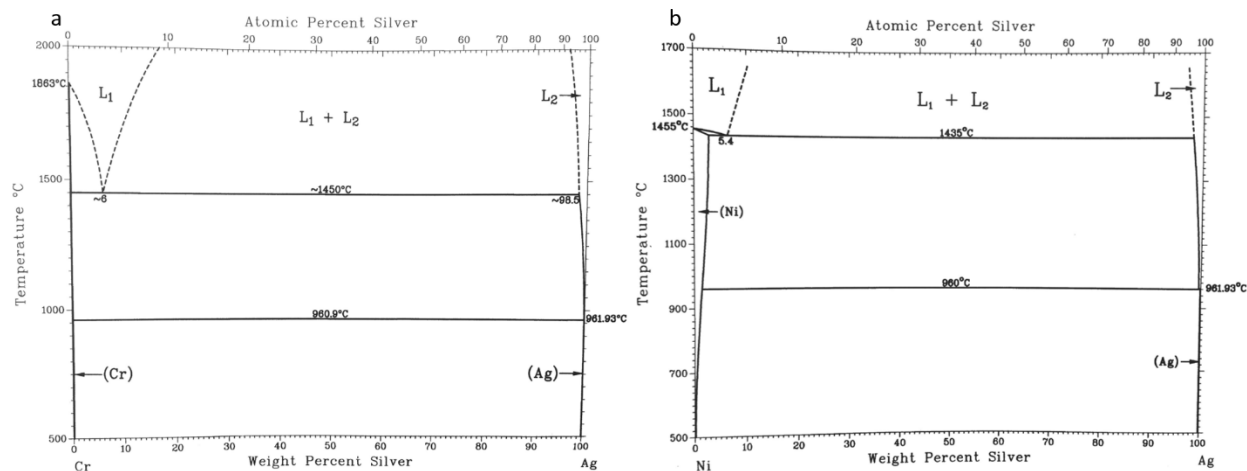
Figure 12. Binary phase diagrams: a) Cr-Ag, b) Ni-Ag.
(Massalski, Okamoto, & ASM International, 1990)

3.4. Microstructural analysis

The WC-Co sessile drop samples were sectioned, ground, and polished prior to SEM analysis. The sessile drop samples were cross-sectioned along the center of the brazed cylinder with a diamond saw blade and then mounted in Bakelite™. The cross-sectioned samples were successively ground on 60, 120, 240, 400, and 600 grit sand paper. The samples were then successively polished using 6, 1, and 0.25 micron diamond paste.

The diamond sessile drop and braze samples were very difficult to prepare for microstructural analysis because of its very high hardness and brittleness. Sample preparation for microstructural analysis is a very time-consuming process in this study.

The diamond sessile drop samples were also cross-sectioned along the center of the brazed alloy. The sectioned samples were first rough ground on Norton grinding wheel obtained from Saint-Gobain Abrasives Inc (Worcester, MA). The ground samples were then successively polished using 6, 1, and 0.25 micron diamond paste. The diamond sessile drop samples were not

mounted. All twelve WC-Co and diamond sessile drop samples in the sessile drop test matrix were evaluated in this study.

The brazed samples were sectioned, ground and polished prior to SEM analysis. The brazed diamond/WC-Co samples were cross-sectioned in a direction perpendicular to the joint interface. The sectioned samples were first rough ground and were successively hand polished using 30, 15, 6, 1, and 0.25 micron diamond paste. The braze samples were also not mounted. For the brazed joints, six samples were selected in the hold time range of 10-50 minutes and cooling rate range of 5-25 °C/min using the silver-copper eutectic alloy with 2 wt% Ti addition.

The microstructures were analyzed using a LEO 1430VP Scanning Electron Microscope (SEM), which was used in conjunction with EDX (Energy-Dispersive X-ray spectroscopy). Small pieces of double sided carbon conductive tape were applied on the end of each sample to minimize sample charging.

Figure 13. MTS Landmark servohydraulic test systems.

3.5. Shear testing

The strength of the diamond to WC-Co joints was evaluated by means of shear fracture tests. Shear tests were performed at room temperature using a MTS Landmark servohydraulic testing machine (Figure 13). The shear test fixture is shown in Figure 14 and the entire test configuration is given in Figure 15. The crosshead speed was 2.54 mm/min for all of the shear tests.
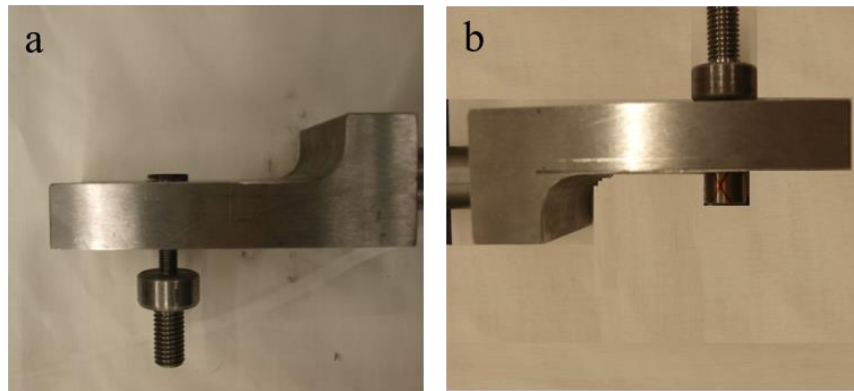
Figure 14. Shear test fixture: a) WC-Co side, b) diamond side.

Figure 15. The shear test configuration.

4. RESULTS AND DISCUSSION

4.1. Wetting and reactivity of WC-Co and diamond substrate

4.1.1. WC-Co wetting and reactivity

4.1.1.1. Sessile drop test results

The sessile drop results are divided into three sections based on the base metal alloy (Cu, Ag, or Ag-Cu). The reported contact angles are apparent contact angles and there is significant error in these result (± 5 to 10°) especially for small contact angles since the drops are relatively small. Also, for several conditions, the drop spread to the edge of the substrate. In this case, the contact angle could not be determined but it was less than 8°.

4.1.1.1.1. Copper based alloys

The apparent contact angles for the copper-based alloys are presented in Table IX. The copper based systems had apparent contact angles that varied from less than 8° to 60°. For the pure copper alloy, the drop spread to the edge of the substrate. In this case, the apparent contact angle was less than 8°. Similarly, the copper with a 1 wt% V addition had an apparent contact angle of less than 8°. Addition of titanium and zirconium actually had the tendency to increase the apparent contact angle but all test conditions exhibited a wetting contact angle. The solidified sessile drops for the copper-based braze alloys are presented in Figure 16.

Table IX. Apparent contact angles for copper-based alloy sessile drops on WC-Co substrates.

Base Alloy	Active Metal Addition	Hold Temperature (°C)	Hold Time (min)	Apparent Contact Angle	Observations
Cu	None	1130	30	<8°	Alloy reached edge of sample
Cu	2 wt% Ti	1130	30	43°	
Cu	5 wt% Ti	1130	30	60°	
Cu	2 wt% Zr	1130	30	51°	
Cu	1 wt% V	1200	30	<8°	Alloy reached edge of sample
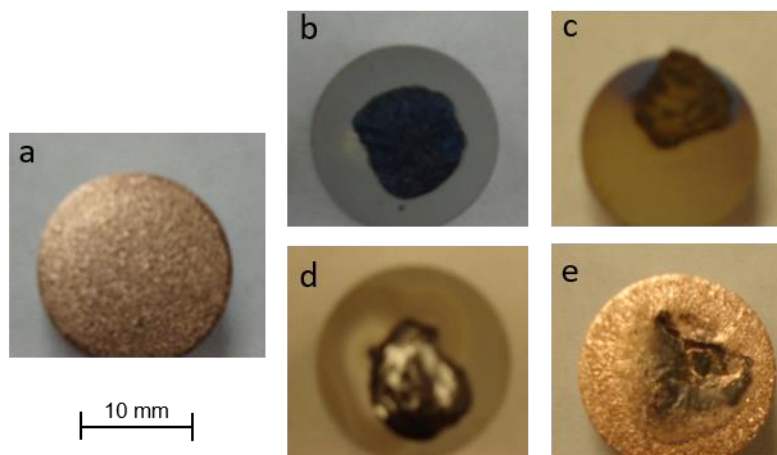
Figure 16. WC-Co sessile drop test samples for copper based alloys: a) Cu with no active metal addition, b) 2 wt% Ti addition, c) 5 wt% Ti addition, d) 2 wt% Zr addition, e) 1 wt% V addition.

4.1.1.1.2. Silver based alloys

Table X lists the apparent contact angles for the silver-based braze alloys on WC-Co substrates. The silver based alloys exhibited excellent wetting under all conditions and had apparent contact angles that ranged from 8° to 29°. The apparent contact angle of pure silver on the WC-Co substrate was 16°. The titanium additions increased the apparent contact angle and the zirconium additions decreased the contact angle. For silver with titanium additions, the apparent contact angle increased from 19° to 29° with increasing Ti content from 2 wt% to 5 wt%. Figure 17 provides photographs of the solidified sessile drops for the silver-based braze alloys.

Table X. Apparent contact angles for silver-based alloy sessile drops on WC-Co substrates.

Base Alloy	Active Metal Addition	Hold Temperature (°C)	Hold Time (min)	Apparent Contact Angle
Ag	None	1010	30	16°
Ag	2 wt% Ti	1010	30	19°
Ag	5 wt% Ti	1010	30	29°
Ag	2 wt% Zr	1010	30	8°
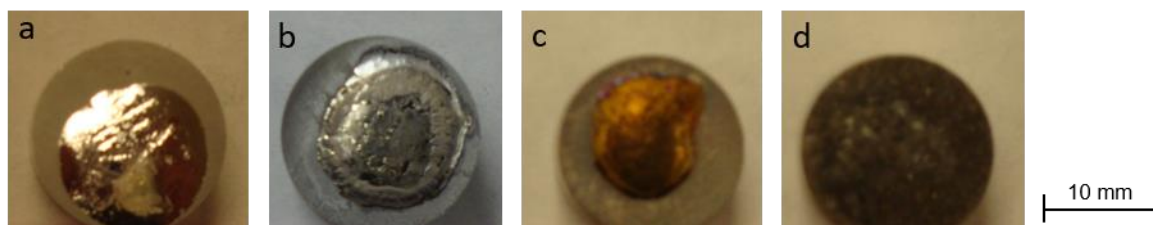
Figure 17. WC-Co sessile drop test samples for silver based alloys: a) Ag with no active metal addition, b) 2 wt% Ti addition, c) 5 wt% Ti addition, d) 2 wt% Zr addition.

4.1.1.1.3.   Silver-copper based alloys

The apparent contact angles for the silver-based braze alloys are listed in Table XI. The silver-copper based systems had apparent contact angles that varied from less than 8° to 36°. For the silver-copper condition, the apparent contact was 36°. In contrast to the copper and silver based alloys the silver-copper alloy's apparent contact angle decreased with the addition of titanium. For the silver-copper eutectic alloy with a 5 wt% Ti addition, the apparent contact angle was less than 8° and the drop had spread to the edge of the substrate. The solidified sessile drops for the silver-copper eutectic-based braze alloys are presented in Figure 18.

Table XI. Apparent contact angles for silver-copper eutectic-based alloy sessile drops on WC-Co substrates.

Base Alloy	Active Metal Addition	Hold Temperature (°C)	Hold Time (min)	Apparent Contact Angle	Observations
Ag-28Cu (wt%)	None	810	30	36°	
Ag-28Cu (wt%)	2 wt% Ti	810	30	9°	
Ag-28Cu (wt%)	5 wt% Ti	810	30	<8°	**Alloy reached edge of sample**
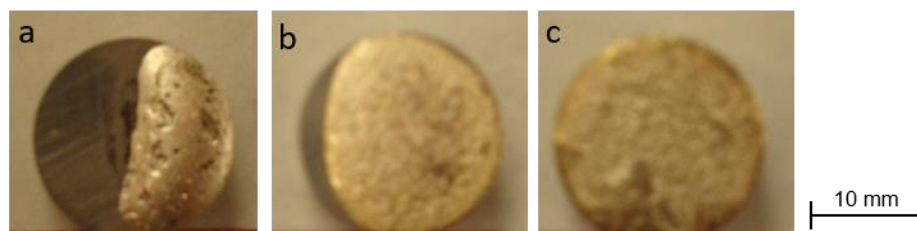
Figure 18. WC-Co sessile drop test samples for silver-copper eutectic-based alloys: a) Ag-Cu with no active metal addition, b) 2 wt% Ti addition, c) 5 wt% Ti addition.

4.1.1.1.4.   Summary for WC-Co substrate sessile drop tests

Based on the contact angle results provided in Tables IX-XI, it was concluded that the pure copper, pure silver, and silver-copper eutectic alloys all exhibited good wetting behavior on WC-Co substrates. The addition of the active metals resulted in different wetting behavior trends depending on the initial base alloy.

For the copper based alloys, the addition of titanium or zirconium significantly increased the apparent contact angle (Table IX). The addition of vanadium to copper caused minimal change in the apparent contact angle. It is possible that this lack of change was caused by the higher melting point of vanadium that might have resulted in the drop not completely melting (Figure 16e).

For the silver based alloys, pure silver on the WC-Co substrate exhibited good wettability. Table X illustrates that the silver alloys were similar to the copper alloys in that the addition of titanium increased the apparent contact angle. The addition of zirconium decreased the apparent contact angle, as indicated in Table X and Figure 17d.

Based on the contact angle results listed in Table XI, it was observed that the silver-copper eutectic based alloys exhibited the opposite wetting trends relative to the copper and silver based alloys. The addition of titanium decreased the apparent contact angle for the silver-

copper eutectic system. For all three alloy systems evaluated, the sessile drop conditions were always wetting.

4.1.1.2. Sessile drop microstructures

A microstructural analysis was performed for all of the WC-Co sessile drop test conditions. The microstructures are not all presented at the same magnification. A single example of each microstructure is presented for each test condition. The magnification was chosen to highlight the major reaction zone for each sample and therefore lower magnifications were used for thicker reaction zones. All compositional information for the metallic elements are weight percentages from an EDS semi-quantitative analysis. The weight percentages are only given for general comparisons and are not considered reliable. The EDS semi-quantitative analysis technique is not considered reliable for thin layers or for complex multi-phase microstructures.

4.1.1.2.1. Copper based alloys

Typical cross-sectional microstructures for the copper-based alloy sessile drops are given in Figures 19-23. Figure 19 is a cross-section for pure copper. Based on EDS analysis, the topmost section of the image is a Cu-rich layer with about 95 wt% Cu and 5 wt% Co. The Co and Cu rich zone is about 80 wt% Co and 20 wt% Cu and has medium thickness (10-30 microns). The W rich section is about 95 wt% W and 5 wt% Cu and it is very thick (100-150 microns). All three zones indicate dissolution reactions: the top zone is Co in Cu, the Co and Cu zone is Cu in Co, and the W zone is Cu in W.

Figure 19. SEM micrograph of pure Cu/WC-Co sessile drop interface.

Figure 20 is a cross-section for Cu with a 2 wt% Ti addition. Based on the EDS analysis, the top section is about 99 wt% Cu and 1 wt% Ti. The middle section (Ti and Cu rich) is about 85 wt% Ti and 15 wt% Cu and it is very thin (2-5 microns). The top layer's high Cu and relatively low Ti content indicates a dissolution reaction with the Ti in the Cu or the formation of an intermetallic layer. The Ti and Cu rich layer's higher Ti and lower Cu suggests the possibility that a reduction reaction has taken place between the Ti and C from the substrate. The presence of Cu and the break in the middle layer could be a result of polishing damage.
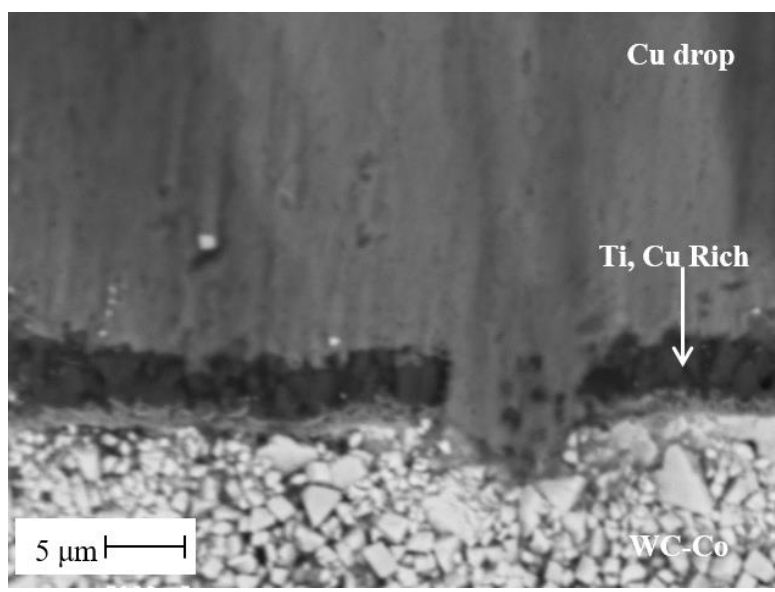
Figure 20. SEM micrograph of Cu-2 wt% Ti/WC-Co sessile drop interface.

Figure 21 is a Cu with a 5 wt% Ti addition sessile drop cross-section. The top layer is about 4 wt% Ti and 96 wt% Cu. The Cu, Ti, and W rich layer is about 10 wt% W, 11 wt% Ti, and 78 wt% Cu and it is thin (1-10 microns). Both layers exhibit evidence of dissolution reactions. The top layer is Ti in Cu and the Cu, Ti, and W rich layer is Ti and W in Cu.
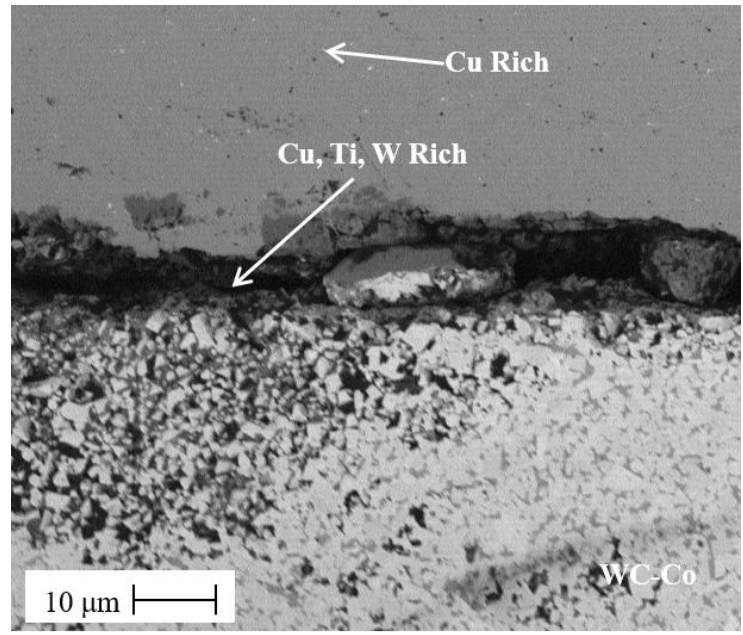
Figure 21. SEM micrograph of Cu-5 wt% Ti/WC-Co sessile drop interface.

Figure 22 is a Cu with a 2 wt% Zr addition sessile drop cross-section. Based on the EDS analysis, the Cu and Zr rich zone is about 13 wt% Zr and 87 wt% Cu, which is discontinuous and very thick (about 50 microns). The Zr and Cu rich zone is about 8 wt% W, 26 wt% Cu, and 66 wt% Zr and it is very thin (about 2 microns). The Cu and Zr rich zone exhibits evidence of a possible dissolution reactions. The Zr and Cu rich zone's higher Zr and lower Cu suggests the possibility that a reduction reaction has taken place between the Zr and C from the substrate. The top layer is Zr in Cu and the Zr and Cu layer is Cu and W in Zr.
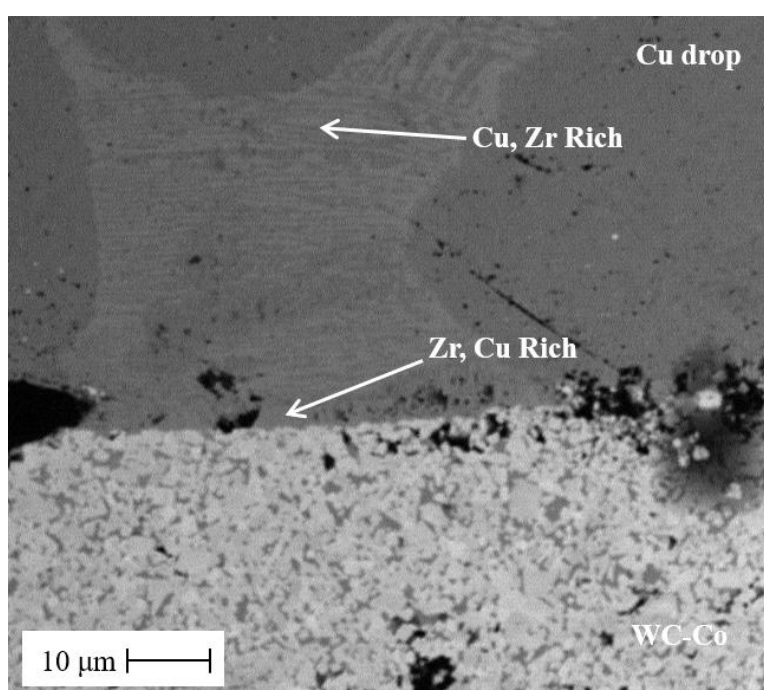
Figure 22. SEM micrograph of Cu-2 wt% Zr/WC-Co sessile drop interface.

Figure 23 is a Cu with a 1 wt% V sessile drop cross-section. Based on EDS analysis, the top layer is close to 7 wt% Co and 92 wt% Cu. The Co and Cu rich layer is about 14 wt% Cu and 86 wt% Co and it is thick (25-30 microns). The Co, Cu, and V rich layer is about 2 wt% V, 12 wt% Cu, and 85 wt% Co and it is thin (2-7 microns). The V, Co, and Cu rich layer is about 6 wt% W, 10 wt% Cu, 37 wt% Co, and 46 wt% V and it is thin (2-7 microns). All layers exhibit

evidence of dissolution reactions. The top layer is Co in Cu, the Co and Cu rich layer Cu in Co,

the Co, Cu, and V rich layer is V and Cu in Co, and the V, Co, and Cu layer is W, Cu, Co in V.
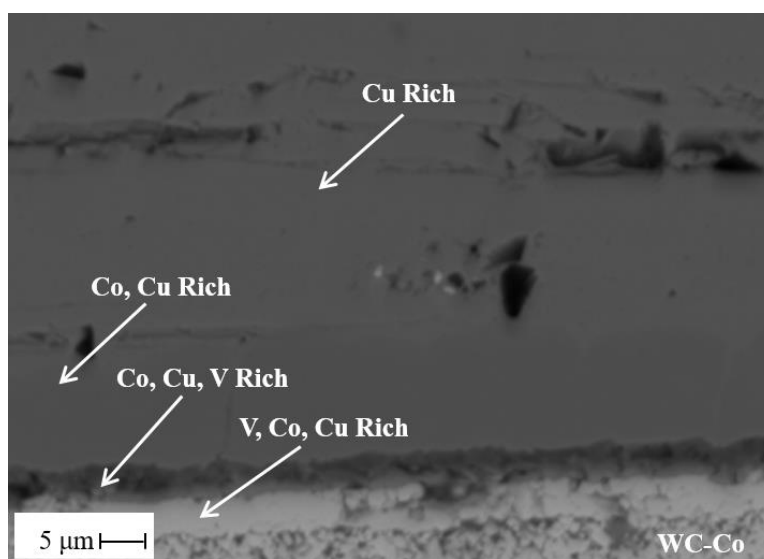
Figure 23. SEM micrograph of Cu-1 wt% V/WC-Co sessile drop interface.

4.1.1.2.2. Silver based alloys

Figures 24-27 are typical cross-sectional microstructures for the silver-based alloy sessile

drops. The silver-based alloys were difficult to polish and significant smearing of the silver

phase was observed for all of the samples. This indicates that the silver layer is very soft and that

these alloys would have the potential for relatively low shear strengths. Figure 24 is a cross-

section for pure silver. The Ag rich layer is about 3 wt% W and 97 wt% Ag and it is very thin (1-

5 microns). This layer provides evidence to support a dissolution reaction of W in Ag.
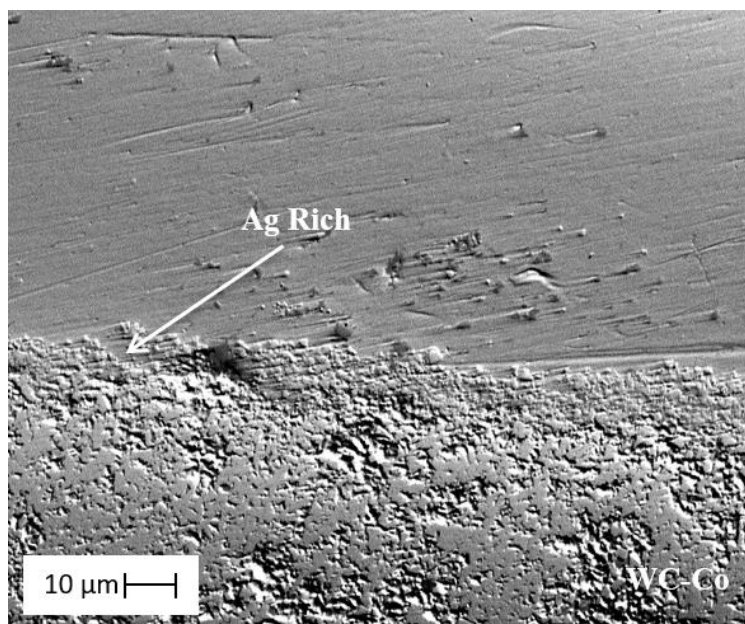
Figure 24. SEM micrograph of pure Ag/WC-Co sessile drop interface.
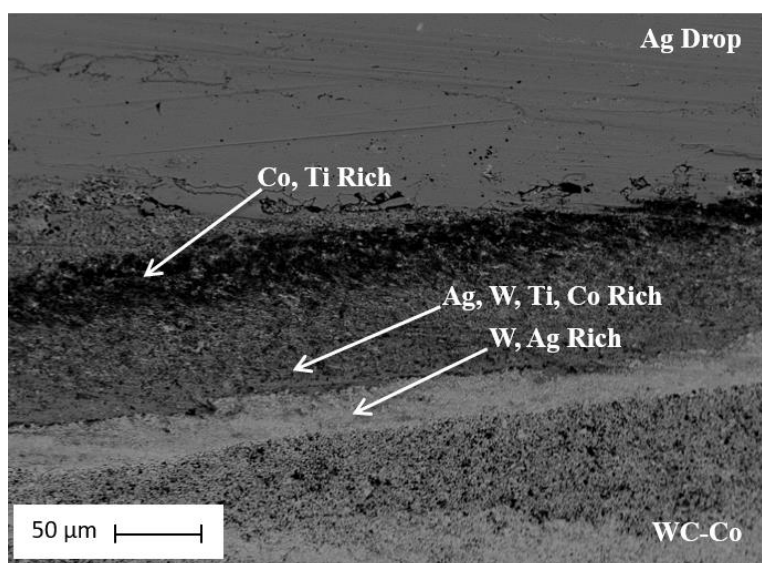
Figure 25. SEM micrograph of Ag-2 wt% Ti/WC-Co sessile drop interface.

Figure 25 is a cross-section for Ag with a 2 wt% Ti addition. Based on the EDS analysis, the Co and Ti rich layer is about 2 wt% W, 45 wt% Ti, and 53 wt% Co and is thick (30-70 microns). The Ag, W, Ti, and Co rich layer is about 14 wt% Co, 21 wt% Ti, 28 wt% W, and 34 wt% Ag and it is very thick (80-140 microns). The W and Ag rich layer is close to 2 wt% Ti, 34

wt% Ag, and 64 wt% W and it is thick (20-40 microns). The Co and Ti rich layer is possibly a dissolution of W in Co-Ti intermetallic. The other two layers also provide evidence for dissolution reactions. The Ag, W, Ti, and Co rich layer is Co, Ti, and W in Ag and the W and Ag rich layer is Ti and Ag in W.
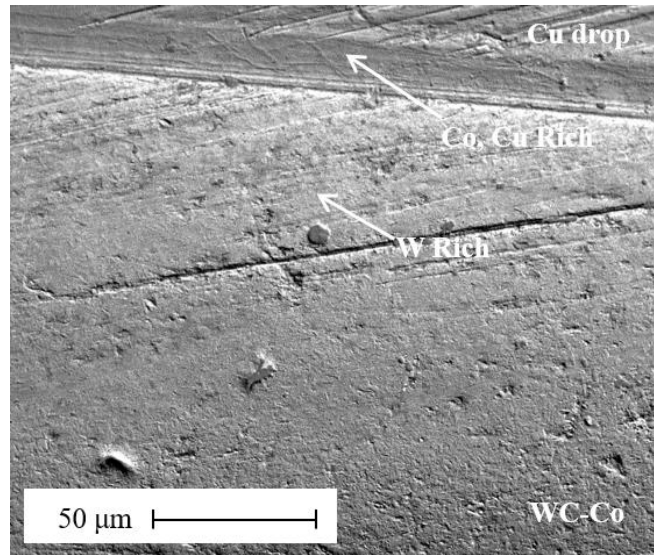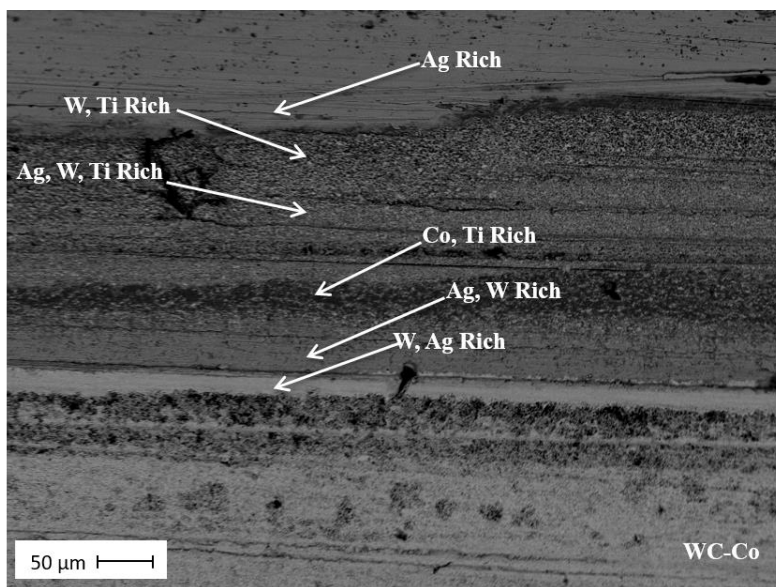

Figure 26. SEM micrograph of Ag-5 wt% Ti/WC-Co sessile drop interface.

Figure 26 is a cross-section for Ag with a 5 wt% Ti addition. Based on the EDS analysis, the top layer is close to 1 wt% Ti and 99 wt% Ag. The W and Ti rich layer is about 2 wt% Co, 5 wt% Ag, 41 wt% Ti, and 51 wt% W and it is very thick (50-100 microns). The Ag, W, and Ti rich layer is 12 wt% Co, 13 wt% Ti, 17 wt% W, and 58 wt% Ag and it is thick (40-80 microns). The Co and Ti rich layer is about 12 wt% W, 42 wt% Ti, and 45 wt% Co and it is thick (30-60 microns). The Ag and W rich layer is close to 9 wt% Ti, 13 wt% W, and 78 wt% Ag and it is thick (40-80 microns). The W and Ag rich layer is about 2 wt% Co, 10 wt% Ag, and 88 wt% W and it is thin (10-20 microns). All of the layers exhibit evidence of dissolution reaction of the smaller additions into the larger additions or the formation of intermetallic phase.

Figure 27 is a Ag with a 2 wt% Zr sessile drop cross-section. The Ag rich layer is close to 96 wt% Ag and 4 wt% Zr and it is thin (2-8 microns), which is most likely a dissolution reaction of Zr in Ag or possibly the formation of an Ag-Zr intermetallic.
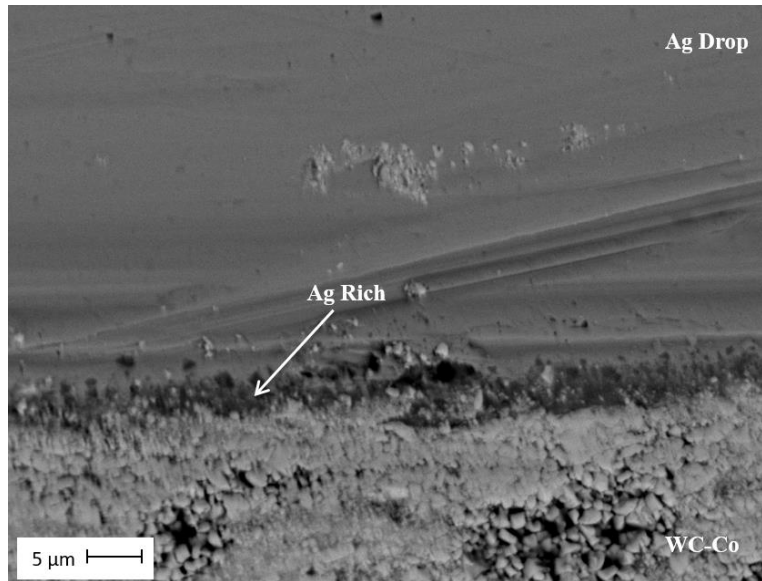
Figure 27. SEM micrograph of Ag-2 wt% Zr/WC-Co sessile drop interface.

4.1.1.2.3. Silver-copper based alloys

Figures 28-30 are typical cross-sectional microstructures for the silver-copper eutectic based alloy sessile drops. Figure 28 shows the Ag-Cu alloy sessile drop cross-section. The sessile drop microstructure at the top of the sample is a very good example of a typical microstructure of Ag-Cu eutectic alloy (Callister & Rethwisch, 2010). Based on the EDS analysis, the W rich layer is close to 4 wt% Cu, 14 wt% Co, and 81 wt% W. The reaction zone is thin (2-5 microns) and there is evidence of a dissolution reaction of Co and Cu in W.
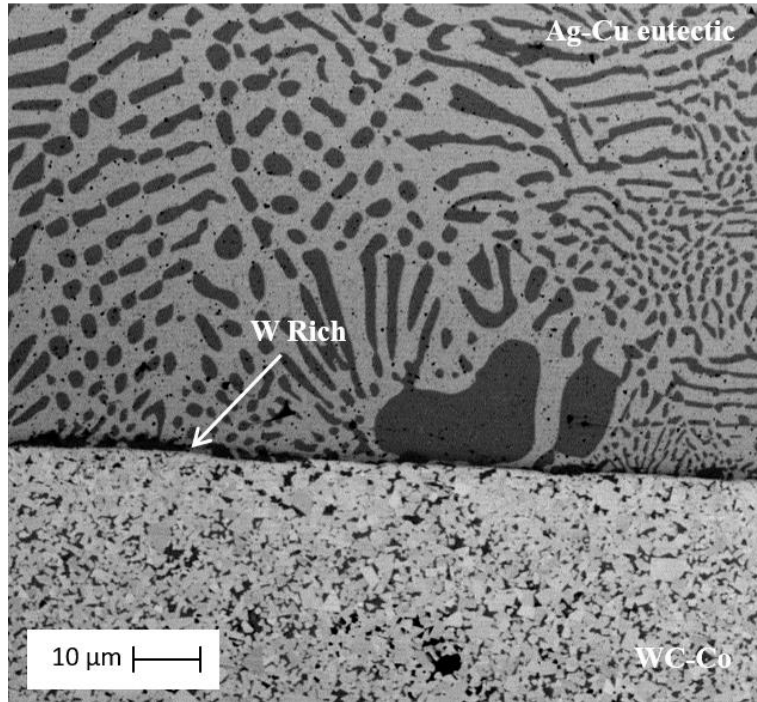
Figure 28. SEM micrograph of Ag-28Cu (wt%) eutectic/WC-Co sessile drop interface.
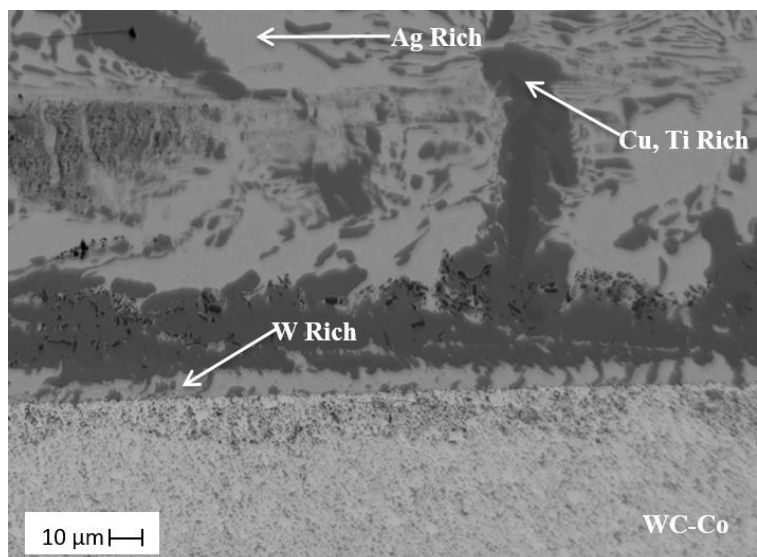
Figure 29. SEM/EDS analysis of Ag-28Cu (wt%) eutectic-2 wt% Ti/WC-Co interface.

Figure 29 is a cross-section for Ag-Cu eutectic alloy with a 2 wt% Ti addition. Based on the EDS analysis, the Ag rich region has about 12 wt% Cu and 88 wt% Ag. The Cu and Ti rich layer is close to 3 wt% Ag, 32 wt% Ti, and 65 wt% Cu and it varies greatly in thickness (25-100

microns), which is approximately 60 mol% Cu, 38 mol% Ti, and 2 mol% Ag. It is predicted that

an intermetallic Cu-Ti formed at the interface during cooling of the sessile drop. The W rich

layer is 100 wt% W and it is thin (5-14 microns). The Cu and Ti rich layer is possibly a

dissolution of Ag in an intermetallic Cu-Ti.
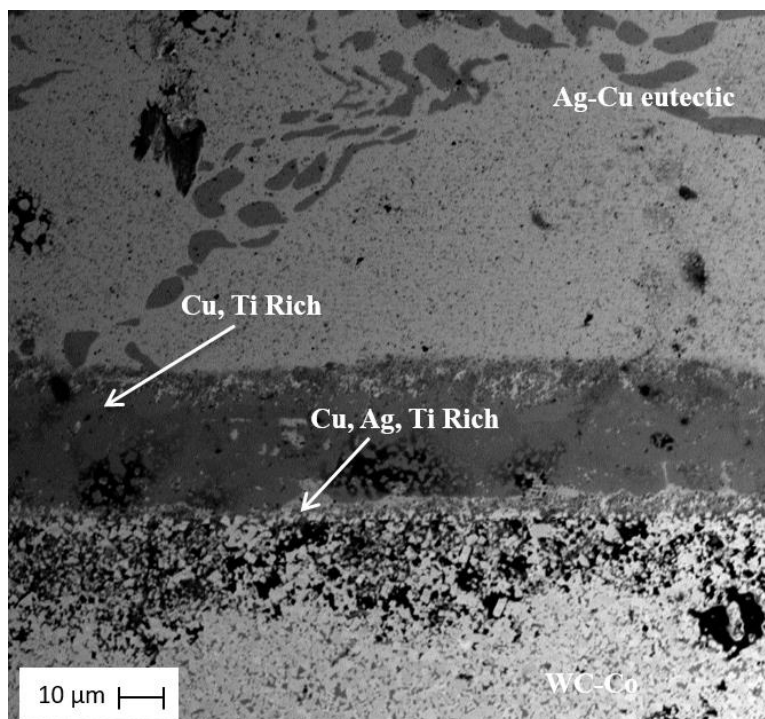
Figure 30. SEM micrograph of Ag-28Cu (wt%) eutectic-5 wt% Ti/WC-Co sessile drop interface

Figure 30 is a cross-section for Ag-Cu eutectic alloy with a 5 wt% Ti addition. Based on

the EDS analysis, the Cu and Ti rich layer is about 29 wt% Ti and 68 wt% Cu and it is thick (20-

40 microns). It is predicted that Ti-Cu intermetallic products formed at the interface during

cooling of the sessile drop. The Cu, Ag, and Ti rich layer is about 22 wt% Ti, 25 wt% Ag, and 53

wt% Cu and it is very thin (1-5 microns). It is proposed that the Cu, Ag, and Ti rich layer is a

second intermetallic solidification product formed at the interface during cooling. All of the

layers exhibit evidence of dissolution reactions and the Cu and Ti rich layer is possibly

intermetallic phases Cu-Ti. The Cu, Ag, and Ti rich layer is also possibly an intermetallic.

Two different types of interfacial reactions were observed between the braze alloy sessile

drops and the WC-Co substrates: reduction and dissolution. Reduction reactions occurred when

the active metal addition was reduced by the carbon from the tungsten carbide to form a new

carbide (e.g. TiC). Specific reduction reactions were difficult to verify because the SEM/EDS

analysis techniques have limitations on quantifying carbon because of its low atomic weight and

due to limitations of semi-quantitative analysis for analyzing thin layers and mixed

microstructures. A reduction reaction was observed at the interface for the Cu sessile drops with

2 wt% Ti and 2 wt% Zr additions on the WC-Co substrates (Figures 20 and 22). Dissolution

reactions occurred when two or more different metals dissolved together. Dissolution reaction

zones were identified as regions with two or more different metals mixed together. Dissolution

reactions were observed at the interfaces in Figures 19-30 for all of the samples.

4.1.2. Diamond wetting and reactivity

4.1.2.1.   Sessile drop test results

The sessile drop results are again divided into sections based on the base metal system

(Cu, Ag, or Ag-Cu). Parallel braze alloy compositions and test conditions were run for the

diamond substrates so that direct comparisons could be made with WC-Co substrate wetting

data.

4.1.2.1.1.   Copper based alloys

The copper based systems had apparent contact angles that ranged from 49° to 106°

(Table XII). For the pure copper alloy, the apparent contact angle was 106°, indicating a non-

wetting condition. The addition of titanium, vanadium, or zirconium had the tendency to

decrease the apparent contact angle and all additions resulted in wetting conditions. For copper

with titanium additions on the diamond substrates, the apparent contact angle decreased from 64°

to 49° with increasing the titanium content from 2 wt% Ti to 5 wt% Ti. The final sessile drops

for the copper-based braze alloys are presented in Figure 31.

Table XII. Apparent contact angles for copper-based alloy sessile drops on diamond substrates.

Base Alloy	Active Metal Addition	Hold Temperature (°C)	Hold Time (min)	Apparent Contact Angle
Cu	None	1130	30	106°
Cu	2 wt% Ti	1130	30	64°
Cu	5 wt% Ti	1130	30	49°
Cu	2 wt% Zr	1130	30	70°
Cu	1 wt% V	1200	30	84°
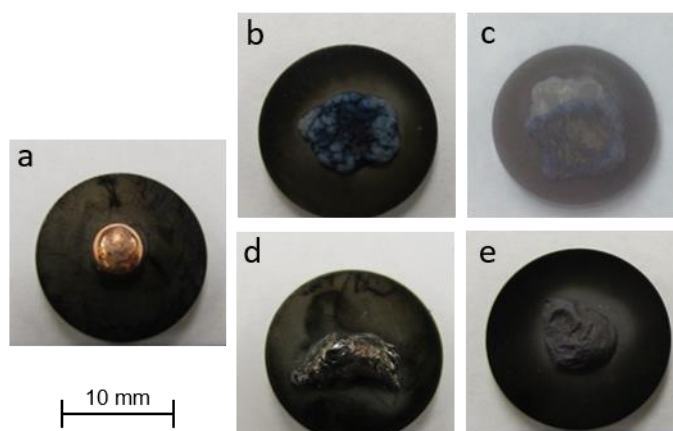
Figure 31. Diamond sessile drop test samples for copper based alloys: a) Cu with no active metal addition, b) 2 wt% Ti addition, c) 5 wt% Ti addition, d) 2 wt% Zr addition, e) 1 wt% V addition.

4.1.2.1.2. Silver based alloys

The silver based systems had apparent contact angles that varied from 29° to 116° (Table

XIII). The apparent contact angle for pure silver on a diamond substrate was 116°, indicating a

non-wetting condition. The titanium and zirconium additions decreased the apparent contact

angle. For silver with titanium additions on the diamond substrates, the apparent contact angle

decreased from 72° to 29° with increasing titanium content from 2 wt% to 5 wt%. Figure 32

provides photographs of the final solidified sessile drops for the silver-based braze alloys.

Table XIII. Apparent contact angles for silver-based alloy sessile drops on diamond substrates.

Base Alloy	Active Metal Addition	Hold Temperature (°C)	Hold Time (min)	Apparent Contact Angle
Ag	None	1010	30	116°
Ag	2 wt% Ti	1010	30	72°
Ag	5 wt% Ti	1010	30	29°
Ag	2 wt% Zr	1010	30	46°
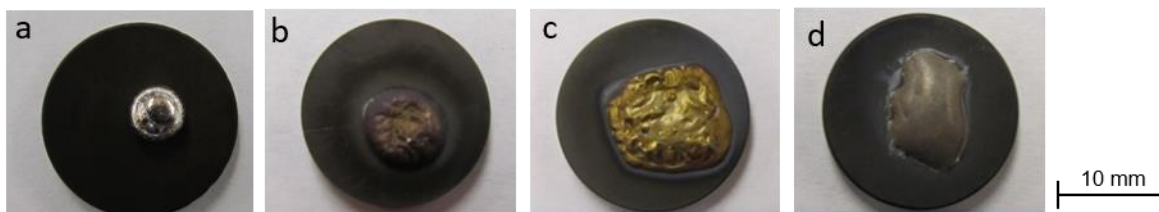
Figure 32. Diamond sessile drop test samples for silver based alloys: a) Ag with no active metal addition, b) 2 wt% Ti addition, c) 5 wt% Ti addition, d) 2 wt% Zr addition.

4.1.2.1.3. Silver-copper based alloys

The silver-copper based systems with titanium addition had apparent contact angles less than 8° (Table XIV). The silver-copper eutectic braze alloy exhibited an apparent contact angle greater than 90° indicating that it was non-wetting. Similar to the copper and silver based alloys the silver-copper alloy's apparent contact angles decreased with the addition of Ti. For the silver-copper eutectic alloy with titanium additions on the diamond substrates, the drop spread to the edge of the substrate. In this case, the apparent contact angle was less than 8°. The silver-copper alloy's apparent contact angle decreased with addition of titanium. The final sessile drops for the silver-copper eutectic-based braze alloys are presented in Figure 33.

Table XIV. Apparent contact angles for silver-copper eutectic-based alloy sessile drops on diamond substrates.

Base Alloy	Active Metal Addition	Hold Temperature (°C)	Hold Time (min)	Apparent Contact Angle	Observations
Ag-28Cu (wt%)	None	810	30	111°	
Ag-28Cu (wt%)	2 wt% Ti	810	30	<8°	**Alloy reached edge of sample**
Ag-28Cu (wt%)	5 wt% Ti	810	30	<8°	**Alloy reached edge of sample**

Figure 33. Diamond sessile test samples for silver-copper eutectic-based alloys: a) Ag-Cu with no active metal addition, b) 2 wt% Ti addition, c) 5 wt% Ti addition.

4.1.2.1.4.   Summary for diamond substrate sessile drop tests

Pure copper, pure silver, and copper-silver eutectic alloys all exhibited non-wetting behavior on the diamond substrates. The wettability of the diamond substrates was improved by adding an active metal to the copper, silver, and silver-copper eutectic alloys. The addition of the active metals resulted in different wetting behavior trends depending on the initial base alloy.

For the copper based alloys, the addition of titanium, vanadium, and zirconium decreased the apparent contact angle on diamond substrates (Table XII). The copper with a 5 wt% Ti addition had the lowest apparent contact angle (49°). The apparent contact angle decreased from 106° to 49° with a 5 wt% Ti addition to copper. The addition of vanadium to copper caused the smallest change in the wettability (from 106° to 84°) but it still transitioned from a non-wetting condition to a wetting condition.

For the silver based alloys, a pure silver sessile drop on a diamond substrate exhibited low wettability (116°). Table XIII indicates that the silver based systems were similar to copper in that the addition of titanium and zirconium decreased the apparent contact angle. The differences between the systems are in the relative degrees of apparent contact angle decrease. The silver with a 5 wt% Ti addition had the lowest apparent contact angle (29°). The apparent contact angle decreased from 116° to 29° with a 5 wt% Ti addition to silver. The addition of zirconium to silver had a major effect on the apparent contact angle (Table XIII).

For the silver-copper eutectic based systems, the pure silver-copper eutectic on the diamond substrate exhibited low wettability (111°). Table XIV indicates that the silver-copper alloys with titanium additions had apparent contact angles less than 8°. The drops with titanium additions spread to the edge of the substrate indicating high wettability. The apparent contact angle for the silver-copper alloys decreased with the addition of titanium. The silver-copper eutectic with titanium addition had the lowest apparent contact angle (<8°). For all three alloy systems studied, without active metal additions, the base metal alloys were non-wetting on diamond substrates. However, an active metal addition improved the wettability for all three base alloy systems.

4.1.2.2. Sessile drop microstructures

A microstructural analysis was performed for all of the diamond sessile drop test conditions. A single example of each microstructure is also presented for each test condition. All compositional information for the metallic elements are weight percentages from an EDS semi-quantitative analysis.

4.1.2.2.1. Copper based alloys

Figure 34 is a pure copper sessile drop on diamond substrate cross-section. Within the resolution of the SEM, neither a reaction zone nor an interfacial product layer was identified at the interface.
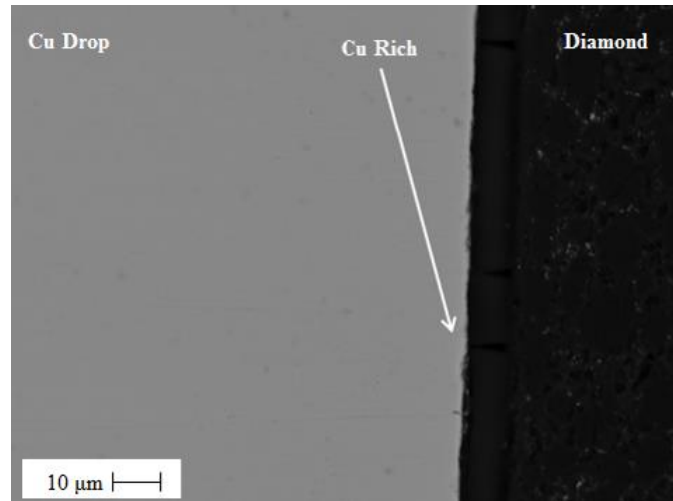
Figure 34. SEM micrograph of pure Cu/diamond sessile drop interface.

The cross-section for the center of the Cu sessile drop with a 2 wt% Ti addition is

presented in Figure 35. No titanium carbide reaction layers or solidification product layers were

resolved under the SEM. EDS line scans are illustrated in Figure 35b for the Cu sessile drop with

a 2 wt% Ti addition. The EDS line scan analysis of the braze alloy region indicated the presence

of copper and titanium. The titanium content increased moving from the braze alloy region into

the diamond substrate while the copper content decreased at the interface near the diamond

substrate.

Figure 35. SEM/EDS analysis of Cu-2 wt% Ti/diamond sessile drop interface: a) SEM micrograph, b) EDS line scans.

Figure 36 is a cross-section for the Cu sessile drop with a 5 wt% Ti addition. Within the resolution of the SEM, neither a reaction zone nor an interfacial product layer was identified at the interface. Figure 36b is the EDS line analysis performed on the sessile drop Cu with a 5 wt% Ti addition. The EDS line scan analysis of the braze alloy region revealed the presence of copper and titanium. The results indicated that the area along the interface from the braze alloy region into the diamond substrate have a high copper content while the titanium content is low. The titanium content increased moving from the braze alloy region into the diamond substrate while the copper content decreased at the interface near the diamond substrate.

Figure 36. SEM/EDS analysis of Cu-5 wt% Ti/diamond sessile drop interface: a) SEM micrograph, b) EDS line scans.

Figure 37 is a Cu with a 2 wt% Zr addition sessile drop cress-section. No reaction products or interfacial products were identified within the resolution of SEM/EDS analysis. EDS line scans are given in Figure 37b for the Cu sessile drop with a 2 wt% Zr addition. EDS analysis revealed the presence of copper. However, zirconium was not observed at the interface within the resolution of SEM/EDS analysis. The copper content at the interface is constant and does not vary moving from the braze alloy region into the diamond substrate.
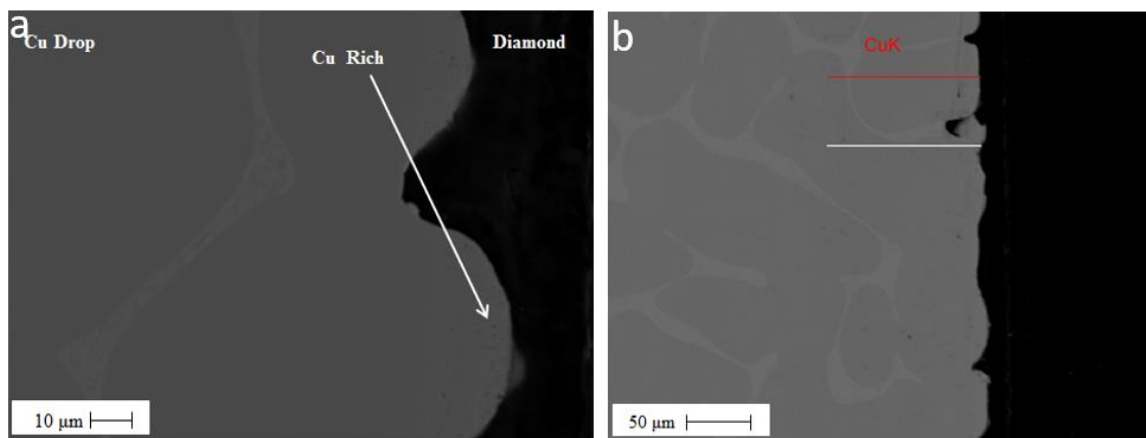
Figure 37. SEM/EDS analysis of Cu-2 wt% Zr/diamond sessile drop interface: a) SEM micrograph, b) EDS line scans.

Figure 38 is a Cu with a 1 wt% V sessile drop cross-section. EDS line scans are presented in Figure 38b for the Cu sessile drop with a 1 wt% V addition. The EDS line scan analysis of the braze alloy region indicated the presence of copper and vanadium. There is a reduction reaction product layer observed at the interface. The EDS analysis indicated the joint was mainly composed of a V-rich reduction reaction product layer. The EDS analysis also determined that the area along the interface moving from the braze alloy region into the diamond substrate has a high copper content. The vanadium content increased moving from the braze alloy region into the diamond substrate while the copper content decreased at the interface near the diamond substrate. Then the copper and vanadium content at the V rich region remained nearly constant. A vanadium rich layer was possibly formed at the interface between the braze alloy and the diamond. The reaction layer's high vanadium and low copper content suggests that it is possible that a reduction reaction occurred between the vanadium in the braze alloy and carbon from the diamond substrate. As illustrated in Figure 38, this V rich layer was relatively thin (8-9 microns). The mean thickness and standard deviation of the V rich layer were 9 microns and 1 micron (based on 5 measurements), respectively.
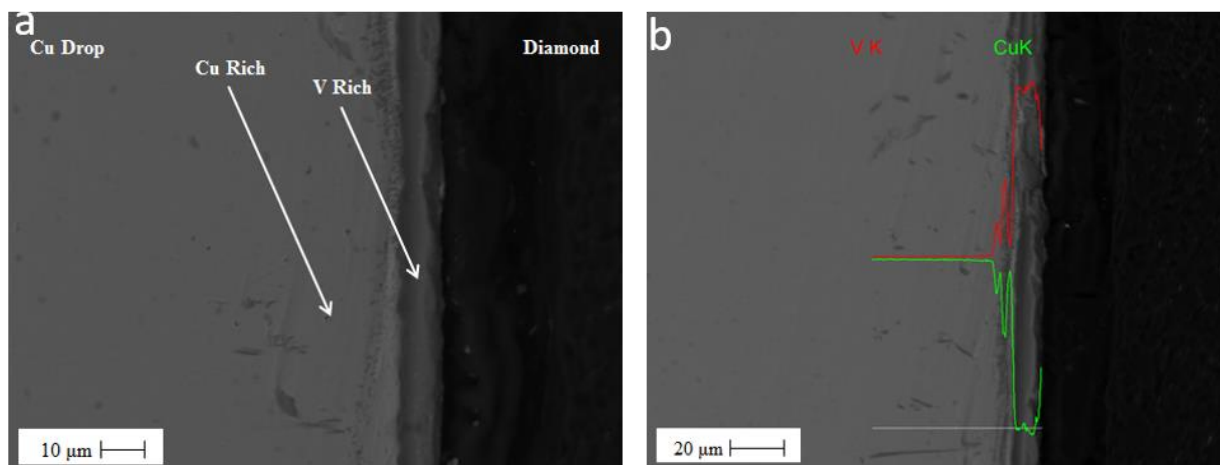
Figure 38. SEM/EDS analysis of Cu-1 wt% V/diamond sessile drop interface: a) SEM micrograph, b) EDS line scans.

4.1.2.2.2. Silver based alloys

Figure 39 is a pure Ag sessile drop and diamond substrate cross-section. Within the resolution of the SEM, neither a reaction zone nor an interfacial product layer was identified at the interface.
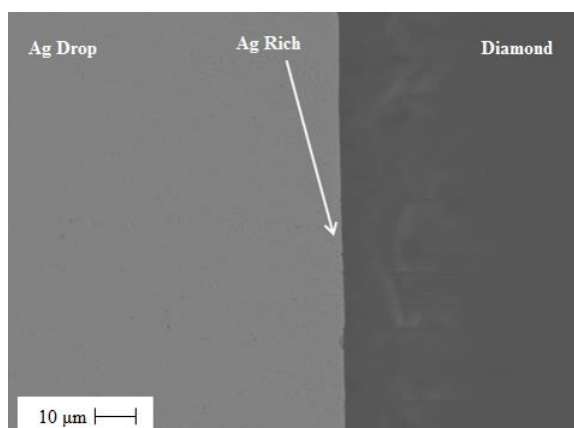
Figure 39. SEM micrograph of pure Ag/diamond sessile drop interface.

Figure 40 is a cross-section for the center of a Ag sessile drop with a 2 wt% Ti addition. No titanium carbide reaction layer or product layers were resolved under the SEM. EDS line scans are presented in Figure 40b for the silver sessile drop with a 2 wt% Ti addition. The EDS line scan analysis of the braze alloy region indicated the presence of silver and titanium. The titanium content increased moving from the braze alloy region into the diamond substrate while

the silver content decreased at the interface near the diamond substrate. The EDS point scan indicated that the dark phase at the interface was rich in silicon while the braze alloy region at the interface was rich in silver. The presence of silicon in this region could be due to contamination during the sample preparation.
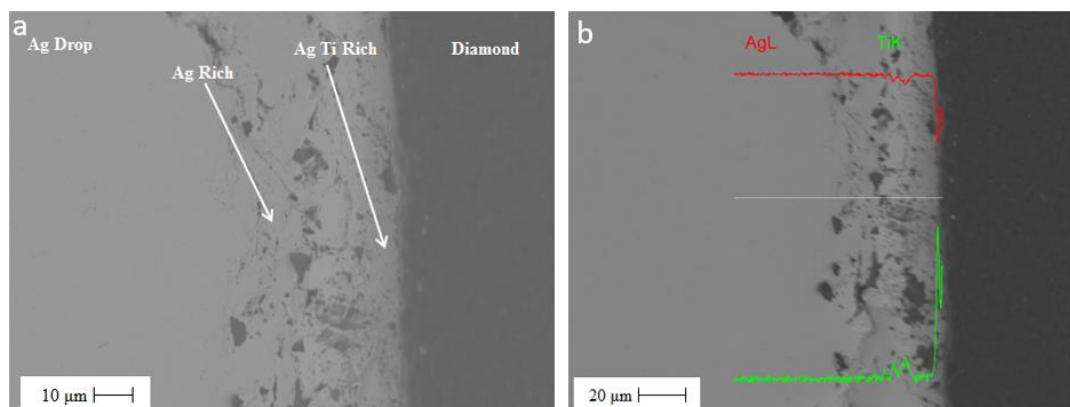
Figure 40. SEM/EDS analysis of Ag-2 wt% Ti/diamond sessile drop interface: a) SEM micrograph, b) EDS line scans.
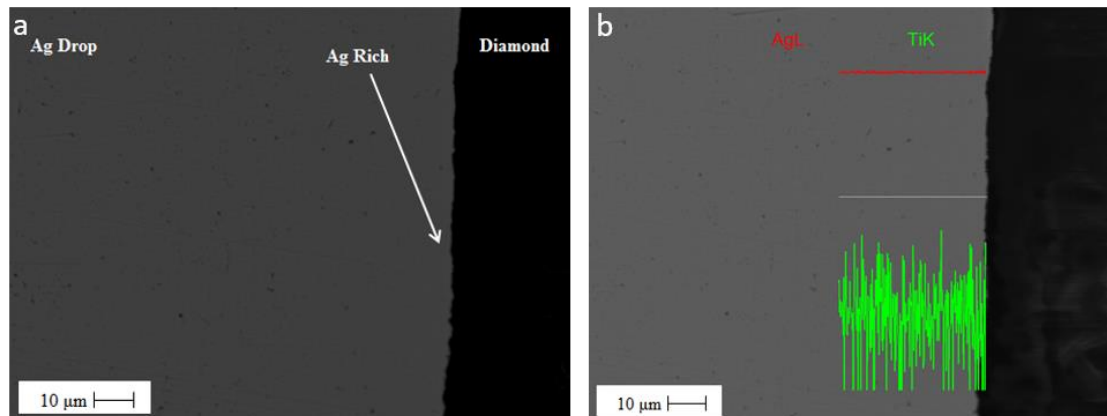
Figure 41. SEM/EDS analysis of Ag-5 wt% Ti/diamond sessile drop interface: a) SEM micrograph, b) EDS line scans.

The cross-section for the Ag with a 5 wt% Ti addition is presented in Figure 41. Within the resolution of the SEM, neither a reaction zone nor an interfacial product layer was identified at the interface. Figure 41b is the EDS line scan analysis performed on the Ag sessile drop with a 5 wt% Ti addition. The EDS line scan analysis indicated the presence of silver and titanium. The

results also indicated that the area along the interface from the braze alloy region into the diamond substrate has a high silver content while the titanium content is relatively low. The silver content at the interface is nearly constant moving from the braze alloy region into the diamond substrate while the titanium content is relatively low and does not vary significantly with position.
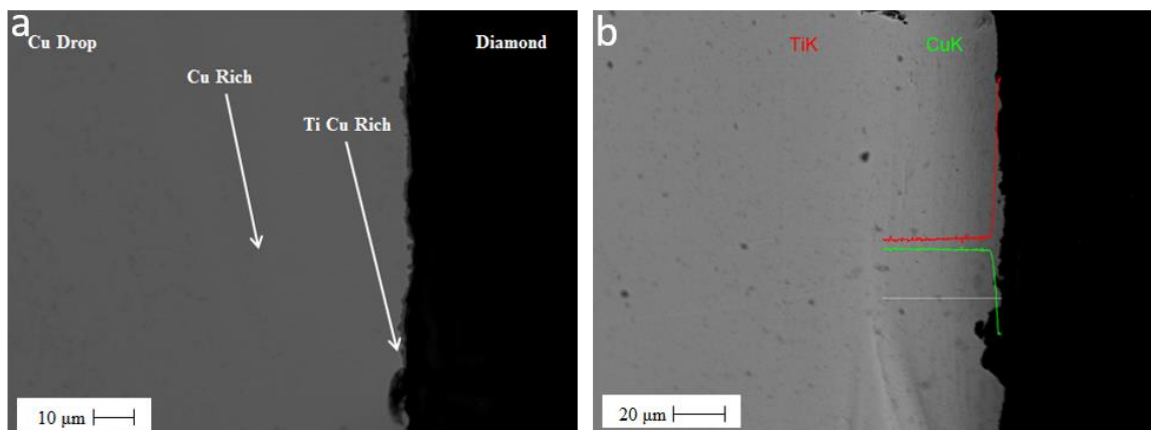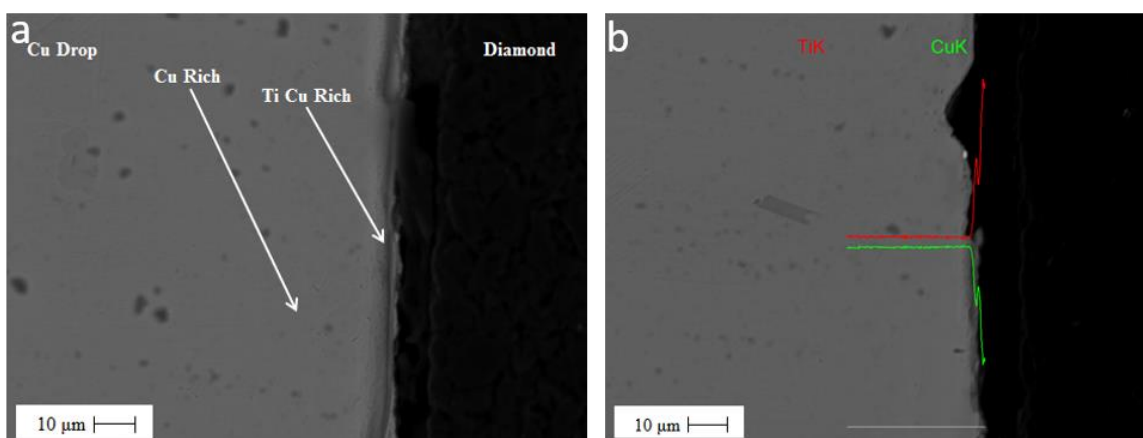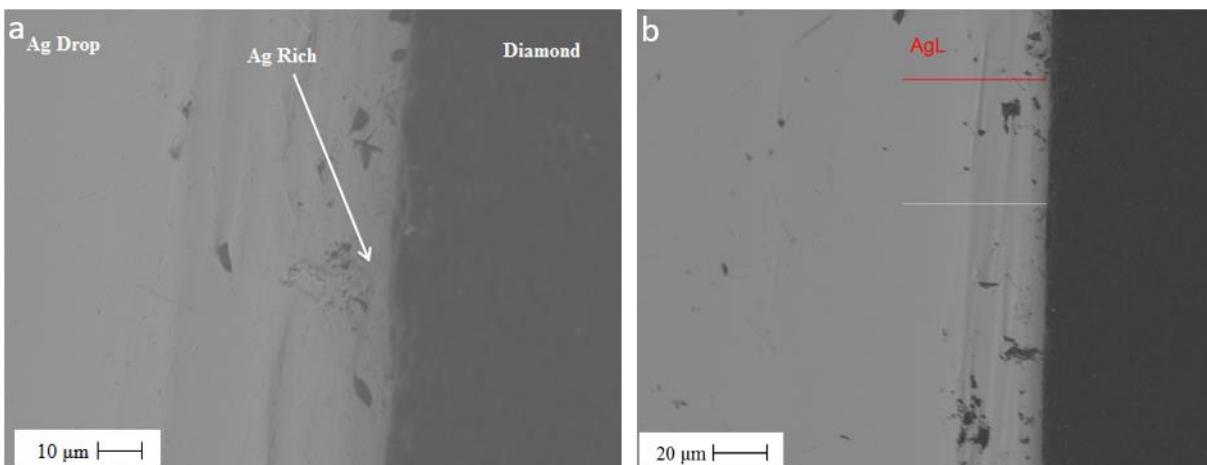

Figure 42. SEM/EDS analysis of Ag-2 wt% Zr/diamond sessile drop interface: a) SEM micrograph, b) EDS line scans.

Figure 42 is a Ag with a 2 wt% Zr sessile drop cross-section. No reaction products or interfacial products were identified within the resolution of SEM/EDS. EDS line scans are presented in Figure 42b for Ag the sessile drop with a 2 wt% Zr addition. The EDS analysis revealed the presence of silver. However, zirconium was not observed in the same region within the resolution of SEM/EDS. The silver content at the interface was constant and did not vary moving from the braze alloy region into the diamond substrate.

### 4.1.2.2.3.   Silver-copper based alloys

Figure 43 is a cross-section for the Ag-Cu alloy sessile drop. Within the resolution of the SEM, neither a reaction zone nor an interfacial product layer was identified at the interface.
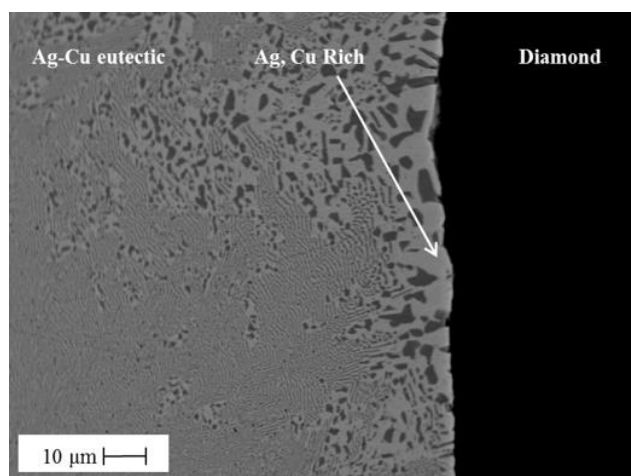
Figure 43. SEM micrograph of Ag-28Cu (wt%) eutectic/diamond sessile drop interface.

Figure 44 is a cross-section for the center of sessile drop Ag-Cu eutectic alloy with a 2 wt% Ti addition. EDS line scans are presented in Figure 44b for the Ag-Cu sessile drop with a 2 wt% Ti addition. The variation in chemical composition is presented using EDS line scans. EDS line scan analysis of the braze alloy region indicated the presence of Ag, Cu, and Ti. There were no reaction product layers observed at the interface. The EDS analysis indicated the joint was mainly composed of a Cu rich product layer. The Ti and Cu content increased moving from the braze alloy region into the Cu rich region while the Ag content decreased at the interface between the braze alloy and the Cu rich region. Then the Cu, Ti, and Ag content were nearly constant in the Cu-Ti rich region. A Cu-Ti rich product layer was formed at the interface between the diamond and the braze alloy. Cu-Ti solid compounds were formed upon solidification of the Ag-Cu-2%Ti brazing alloy. The Cu and Ti rich layer is approximately 63 wt% Cu, 32 wt% Ti, and 4 wt% Ag, which is approximately 58 mol% Cu, 39 mol% Ti, and 4 mol% Ag (Figure 45). In conclusion, the addition of the active metal (2 wt% Ti) is proposed to have resulted in an intermetallic solidification product Cu-Ti forming at the interface.
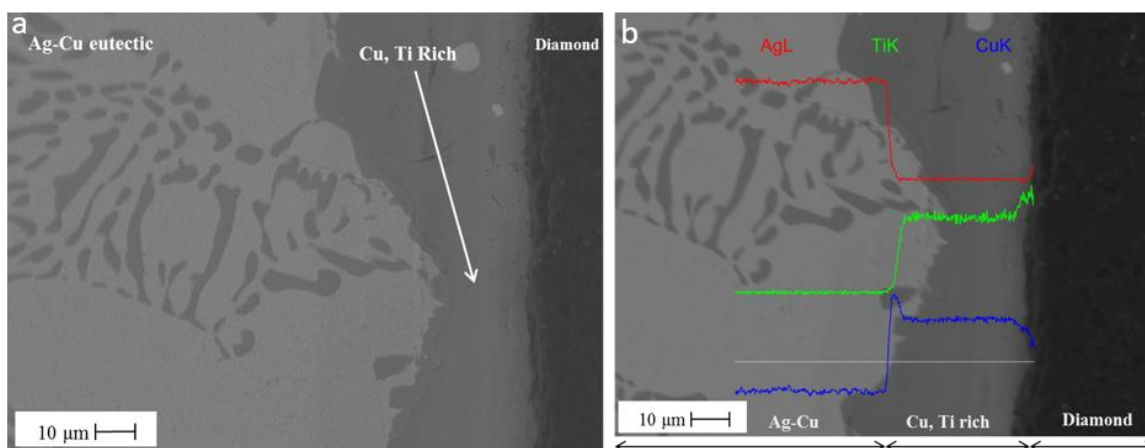
Figure 44. SEM/EDS analysis of Ag-28Cu (wt%) eutectic-2 wt% Ti/diamond sessile drop interface: a) SEM micrograph, b) EDS line scans.
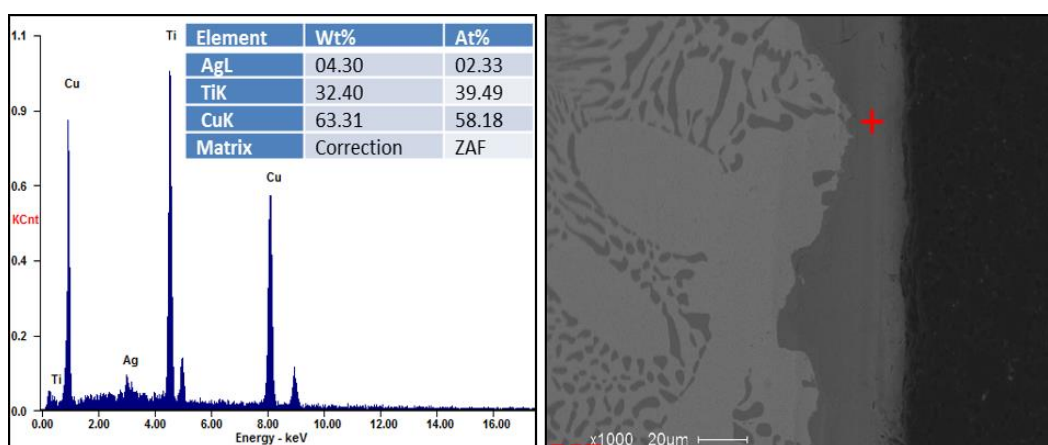
Figure 45. EDS point scan of Ag-28Cu (wt%) eutectic -2 wt% Ti/diamond sessile drop interface.

The cross-section for the Ag-Cu eutectic alloy with a 5 wt% Ti addition is presented in Figure 46. EDS line scans are presented in Figure 46b for the Ag-Cu sessile drop with a 5 wt% Ti addition. EDS line scan analysis of the alloy side indicated the presence of silver, copper, and titanium. There are still no reaction layers observed at the interface. The EDS analysis indicates the joint is mainly composed of two product layers: a Cu-rich product layer and a Ag-rich product layer.

The Cu and Ti content initially increased moving from the braze alloy region into the Cu rich region while the Ag content decreased at the interface between the braze alloy and the Cu

rich region. Then the Cu, Ti, and Ag content were nearly constant in the Cu rich region. A Cu-Ti

rich product layer was formed at the interface between the diamond and the Ag-Cu sessile drop

with a 5 wt% titanium addition. The Cu and Ti rich layer is approximately 61 wt% Cu, 35 wt%

Ti, and 4 wt% Ag, which is approximately 56 mol% Cu, 42 mol% Ti, and 2 mol% Ag (Figure

47a). It is again proposed that the Cu-Ti rich product formed at the interface is an intermetallic

solidification product.

There is a Ag rich layer at the interface between the Cu rich region and the diamond

substrate. The Ag content increased moving from the Cu rich region into the diamond substrate

while the Cu and Ti content decreased at the interface between the Cu rich region and the Ag

rich region. The Ag-rich layer is approximately 65 wt% Ag, 23 wt% Cu, and 13 wt% Ti, which

is approximately 49 mol% Ag, 29 mol% Cu, and 22 mol% Ti (Figure 47b). It is proposed that

the Ag rich product is a second intermetallic solidification product formed at the interface during

cooling.
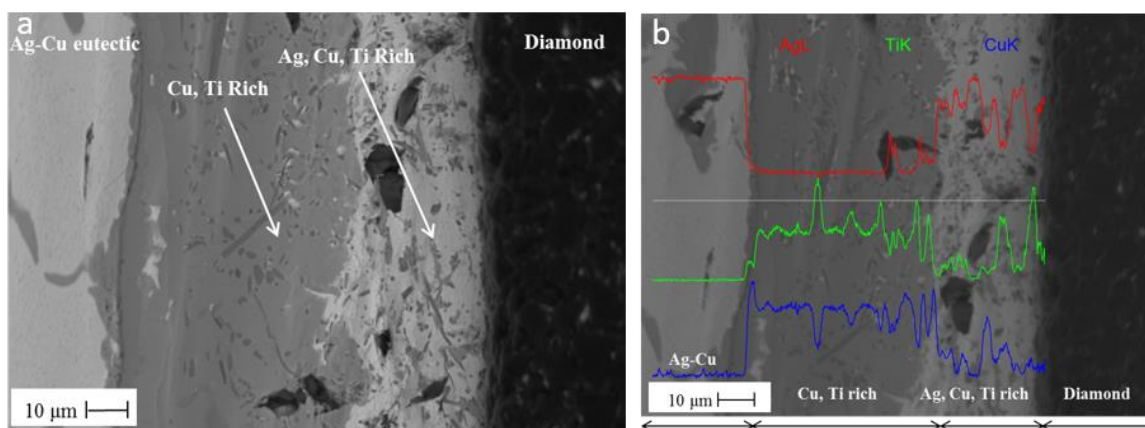
Figure 46. SEM/EDS analysis of Ag-28Cu (wt%) eutectic-5 wt% Ti/diamond sessile drop interface: a) SEM micrograph, b) EDS line scans.

Element	Wt%	At%
AgL	03.47	01.86
TiK	35.25	42.48
CuK	61.28	55.66
Matrix	Correction	ZAF

Element	Wt%	At%
AgL	64.93	49.40
TiK	12.56	21.53
CuK	22.51	29.07
Matrix	Correction	ZAF
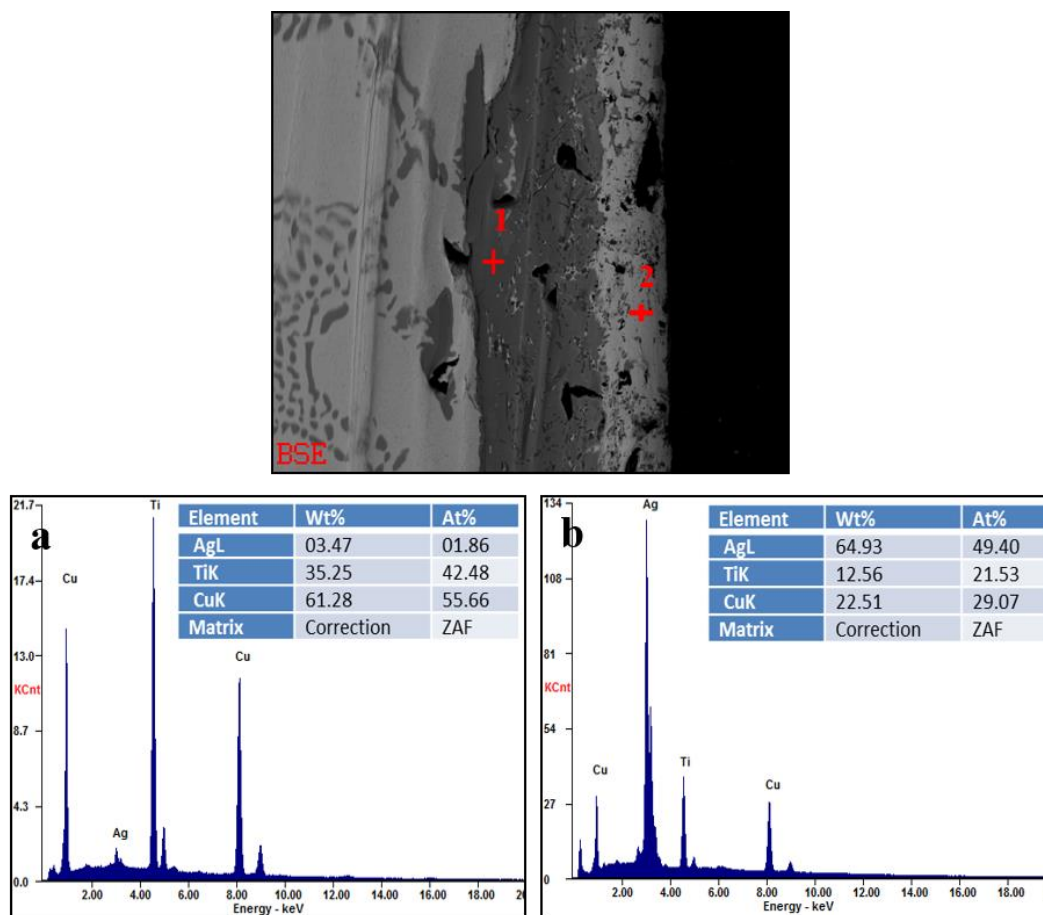
Figure 47. EDS point scans of Ag-28Cu (wt%) eutectic -5 wt% Ti/diamond sessile drop interface: a) EDS spectrum of point 1, b) EDS spectrum of point 2.

In summary, the only reduction reaction was observed at the interface for the copper sessile drop with a 1 wt% V addition on diamond substrates. No reaction products or interfacial products were identified within the resolution of SEM/EDS analysis for the copper sessile drop with additions of Ti (2 or 5 wt%) or 2 wt% Zr on the diamond substrates.

For the silver based alloys, within the resolution of the SEM, neither a reaction zone nor an interfacial product layer was identified at the interface. For the silver-copper eutectic based systems, SEM/EDS analysis revealed that no titanium carbide reaction product layers are identified at the interface within the resolutions of the SEM/EDS. Intermetallic solidification products were formed at the interface with increasing titanium content.

4.1.3. Overall summary for sessile drop testing

4.1.3.1. Comparison of WC-Co and diamond sessile drop test results

Table XV lists the combined WC-Co and diamond sessile drop test apparent contact angle results. For the copper based braze alloys, pure copper on a WC-Co substrate exhibited good wetting ($\theta < 8°$), but pure copper on a diamond substrate exhibited low wettability ($\theta = 106°$). The addition of Ti and Zr increased the apparent contact angle on the WC-Co substrates and all conditions were wetting. For diamond substrates, the addition of Ti, Zr, or V all decreased the apparent contact angle. The wettability was better for the WC-Co substrates with no active metal additions while the addition of an active metal is crucial for the wetting of the diamond substrates.

For the silver based braze alloys, the apparent contact angle of pure silver on a diamond substrate was 116°, indicating a non-wetting condition. However, pure silver on a WC-Co substrate exhibited good wettability ($\theta = 16°$). The addition of Ti and Zr decreased the apparent contact angle on the diamond substrates. For the WC-Co substrates, the addition of Ti increased the apparent contact angle while the addition of Zr resulted in improved wettability. Similar to the copper based alloys, the wettability is improved for WC-Co substrates for silver with no active metal additions while the addition of an active metal is crucial for the wetting of the diamond substrates by silver based alloys.

For the silver-copper eutectic based braze alloys, silver-copper eutectic alloys (Ag-28 wt% Cu) on WC-Co substrates exhibited good wettability ($\theta = 36°$) while silver-copper eutectic alloys on diamond substrates exhibited poor wettability ($\theta = 111°$). The addition of Ti to the silver-copper eutectic alloy decreased the apparent contact angle on both the WC-Co and diamond substrates. For both the WC-Co and diamond substrates, the addition of Ti resulted in improved wettability.

Table XV. Summary of apparent contact angles for WC-Co and diamond sessile drops.

Base Alloy	Active Metal Addition	Hold Temperature (°C)	Hold Time (min)	Apparent Contact Angle (WC-Co)	Apparent Contact Angle (Diamond)
Cu	None	1130	30	<8°	106°
	2 wt% Ti	1130	30	43°	64°
	5 wt% Ti	1130	30	60°	49°
	2 wt% Zr	1130	30	51°	70°
	1 wt% V	1200	30	<8°	84°
Ag	None	1010	30	16°	116°
	2 wt% Ti	1010	30	19°	72°
	5 wt% Ti	1010	30	29°	29°
	2 wt% Zr	1010	30	8°	46°
Ag-28Cu (wt%)	None	810	30	36°	111°
	2 wt% Ti	810	30	9°	<8°
	5 wt% Ti	810	30	<8°	<8°

Pure copper, pure silver, and silver-copper eutectic alloys on diamond substrate exhibited poor wetting when compared with the same alloys on WC-Co substrates. For the WC-Co substrates, cobalt provided wetting of braze alloy with no active metal addition (Ag, Cu, and Ag-Cu) via dissolution reactions. However, there was no mechanism for wetting of diamond substrates without the reduction reaction facilitated by the active metal addition. Therefore, while the addition of an active metal is needed for the wetting of the diamond substrates, the wettability is actually better for the WC-Co substrates with no active metal additions.

4.1.3.2. Comparison of WC-Co and diamond sessile drop microstructures

For the copper based braze alloys, two different types of reactions were observed between the braze alloys and the WC-Co substrates: reduction and dissolution reactions. The reduction reactions were observed at the interface for the Cu sessile drop with a 2 wt% Ti and a 2 wt% Zr on WC-Co substrates (Figures 20 and 22). Dissolution reactions were identified for all of the copper based alloy sessile drops on WC-Co substrates. For the diamond substrates, the only reduction reaction was observed at the interface for the copper alloy sessile drop with a 1 wt% V

addition (Figure 38). No reaction products or interfacial products were identified within the resolution of SEM/EDS analysis for the copper sessile drop with additions of Ti or Zr.

For the silver based braze alloys, dissolution reactions were also identified for all of the alloy sessile drops on WC-Co substrates, as illustrated in Figures 24-27. For the diamond substrates, within the resolution of the SEM, neither a reaction zone nor an interfacial product layer was identified at the interface.

For the silver-copper eutectic based braze alloys, SEM/EDS analysis revealed that no titanium carbide reaction product layers were formed at the diamond substrate interface within the resolutions of the SEM/EDS. Intermetallic solidification products were formed at the interface between the braze alloy and the diamond substrate with increasing Ti content (Figures 44 and 46). There is a change from one to two solidification product layers at the interface with increasing the titanium content from 2 wt% to 5 wt%. For the WC-Co substrates, the silver-copper eutectic based alloy systems were similar to the silver based alloy systems in that the dissolution reactions were also for all of the silver-copper eutectic based alloy sessile drops (Figures 28-30).

4.2. Shear strength and microstructure of brazed joints

Brazed samples for all three brazing test matrices were evaluated for shear strength (Tables VI-VIII). Selected braze sample microstructure were also evaluated. The shear test results and microstructural analysis are presented in the following sections.

4.2.1. Shear test results of initial test matrix

The goal of this phase of the research was to obtain shear strength data for brazed samples prepared using thermal cycles corresponding to the sessile drop test conditions. Table VI is the initial brazing test matrix. A total of 5-6 samples were tested at each condition. The error bars represent the standard deviation for the 5-6 repeat samples.

Table XVI lists the shear test results for diamond/WC-Co brazed with Cu-2 wt% Zr braze alloys. The average shear strength of copper with 2 wt% Zr was 31MPa and the standard deviation was 7 MPa. For copper with a 2 wt% Zr addition, there was no visible cracking on the surface region of diamond substrates. Two additional test conditions were also evaluated: copper with 2 wt% and 5 wt% Ti additions. For the copper with 2 wt% and 5 wt% Ti additions, the diamond and WC-Co substrates did not bond and it was observed that the two substrates were not wet by either of the two braze alloys.

Table XVI. Shear test results for the copper based braze alloys.

Base Alloy	Active Metal Addition	Shear Strength (MPa)						Average Shear Strength (MPa)	Standard Deviation (MPa)
Cu	2 wt% Zr	27.03	28.96	21.59	34.79	30.61	41.06	31	7
Cu	2 wt% Ti	*						N/A	N/A
Cu	5 wt% Ti	**						N/A	N/A

* Braze samples were attempted but no bond was formed for four samples.
** Braze sample were attempted but no bond was formed for the six samples.

Braze specimens were prepared with silver with additions of Ti (1 wt% and 2 wt%) and 2 wt% Zr. Table XVII lists the shear test results for diamond/WC-Co brazed with silver based braze alloys. The average shear strengths for the three braze alloy: silver with Ti (1 wt% or 2

wt%) or 2 wt% Zr are plotted in Figure 48. The average shear strength were 45, 54, and 55 MPa

for three braze samples respectively. The average shear strength for silver increased from 45

MPa to 54 MPa with the Ti content increasing from 1 wt% to 2 wt%. The difference between the

average shear strengths was 9 MPa which was relatively small. It is proposed that the average

shear strength of the silver with Ti additions was relatively low because the failure occurs in the

silver and the pure silver has a very low shear strength. The standard deviations for two braze

sample conditions (1 wt% and 2 wt% Ti additions) were relatively small and this correlated the

observation that there was no visible interfacial cracking observed in the diamond for these

samples. The average shear strengths for silver with 2 wt% Ti and 2 wt% Zr were approximately

equal. However, the standard deviation of silver with 2 wt% Zr was relatively large (17 MPa).
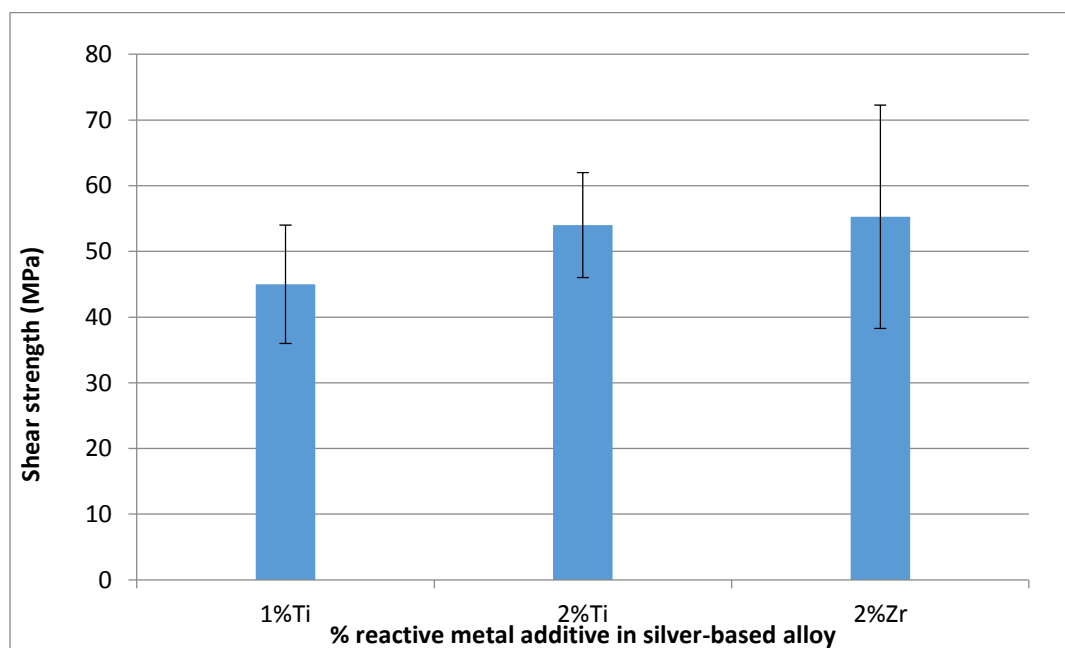
Figure 48. The average shear strength for the silver-based braze alloys.

Table XVII. Shear test results for the silver based braze alloys.

Base Alloy	Active Metal Addition	Shear Strength (MPa)						Average Shear Strength (MPa)	Standard Deviation (MPa)
Ag	1 wt% Ti	58.39	40.45	34.94	45.74	52.75	39.26	45	9
Ag	2 wt% Ti	49.1	44.08	66.72	61.06	52.96	51.07	54	8
Ag	2 wt% Zr	73.84	44.96	51.15	34.81	71.65	*	55	17

* The sample was not well aligned and the shear test could not be performed.

Braze specimens were fabricated with silver-copper eutectic braze alloys with additions of Ti (0.5, 1, 2, and 5 wt%). The silver-copper eutectic alloy had a final thickness of 0.2 mm. Table XVIII lists the shear test results for diamond/WC-Co brazed with silver-copper eutectic braze alloys. The average shear strengths were 36, 35, 95, and 75 MPa for the four braze alloy conditions, respectively. The average shear strengths for the four braze alloy conditions (silver-copper eutectic alloys with 0.5, 1, 2, and 5 wt% Ti additions) are plotted in Figure 49. The silver-copper eutectic alloy with a 2 wt% Ti addition had the highest average shear strength of 95 MPa. The average shear strength for silver-copper eutectic alloy increased from 36 MPa to 95 MPa with the Ti content increasing from 0.5 wt% to 2 wt%. The standard deviation increased along with strength for the higher Ti contents. The standard deviation increased from 11 MPa to 48 MPa with the Ti content increasing from 0.5 wt% to 5 wt%. The standard deviation of two braze sample conditions (0.5 wt% and 1 wt% Ti additions) were relatively small which correlated with no visible interfacial cracking in the diamond for the majority of the samples. However, more and large visible cracking was observed on the surface region of the diamond substrates for the silver-copper eutectic alloy with additions of 2 wt% and 5 wt% Ti.

Table XVIII. Shear test results for the silver-copper eutectic-based braze alloys.

Base Alloy (wt%)	Active Metal Addition	Shear Strength (MPa)						Average Shear Strength (MPa)	Standard Deviation (MPa)
Ag-28Cu	0.5 wt% Ti	23.75	46.52	25.2	45.85	45.83	30.15	36	11
Ag-28Cu	1 wt% Ti	22.3	26.54	33.51	27.76	38.33	61.31	35	14
Ag-28Cu	2 wt% Ti	59.3	75.05	154.26	120.33	64.44	-	95	41
Ag-28Cu	5 wt% Ti	45.24	150.61	93.56	50.53	32.86	-	75	48
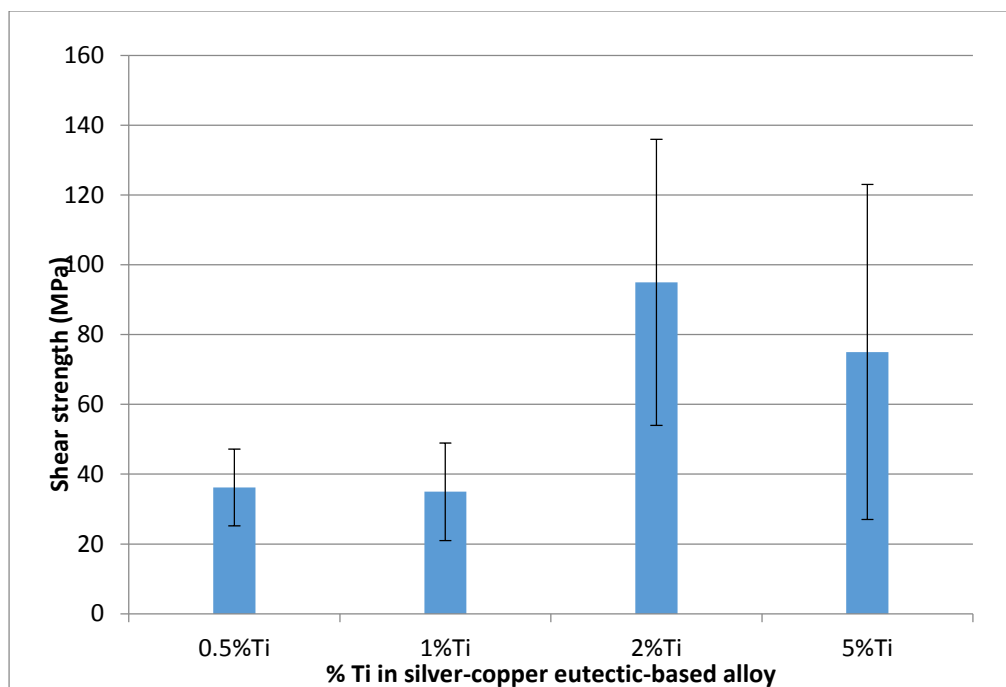
Figure 49. The average shear strength for the silver-copper eutectic-based braze alloys.

4.2.2. Effect of braze thickness on shear strength

The goal of this phase of the research was to study the effect of braze thickness on the braze shear strength. The highest average shear strength was obtained for the silver-copper eutectic alloy with a 2 wt% Ti addition (Tables XVI-XVIII). Therefore, the silver-copper eutectic alloy with a 2 wt% Ti addition was the first braze alloy system chosen for the thickness study. The other filler metal alloy that exhibited promising results was the silver alloys with a 2 wt% Ti addition. Considering the smaller standard deviation and the observation that the Ag-2 wt% Ti brazed samples did not exhibit any cracking after brazing, the Ag-2 wt% Ti alloy was the second braze alloy system chosen for the thickness study. As illustrated in Figure 6, all of the samples followed the same basic thermal cycle. Table VII is a braze thickness test matrix. A total of 5-6 samples were tested at each condition. The error bars represent the standard deviation for 5-6 repeat samples.

4.2.2.1.   Silver based braze alloy

Braze specimens were fabricated using stacks of silver with the addition of 2 wt% Ti. Five different braze thicknesses were studied. Table XIX lists the shear test results for the five braze thickness conditions. The average shear strengths for the five braze thickness conditions (0.025, 0.05, 0.1, 0.15 and 0.2 mm) are plotted in Figure 50 for the Ag-2 wt% Ti alloy.

As illustrated in Figure 50, the average shear strength for the Ag-2 wt% Ti alloy increased from 9 MPa to 54 MPa with the braze thickness increasing from 0.025 mm to 0.2 mm. For the silver braze alloy with a 2 wt% Ti addition, the braze thickness of 0.2 mm had the highest average shear strength of 54 MPa. However, within the reproducibility error, the average shear strength was approximately constant in the braze thickness range of 0.1 mm to 0.2 mm. The shear strengths of the brazed samples were very consistent at each braze thickness condition and no visible cracks was observed in any of the samples.
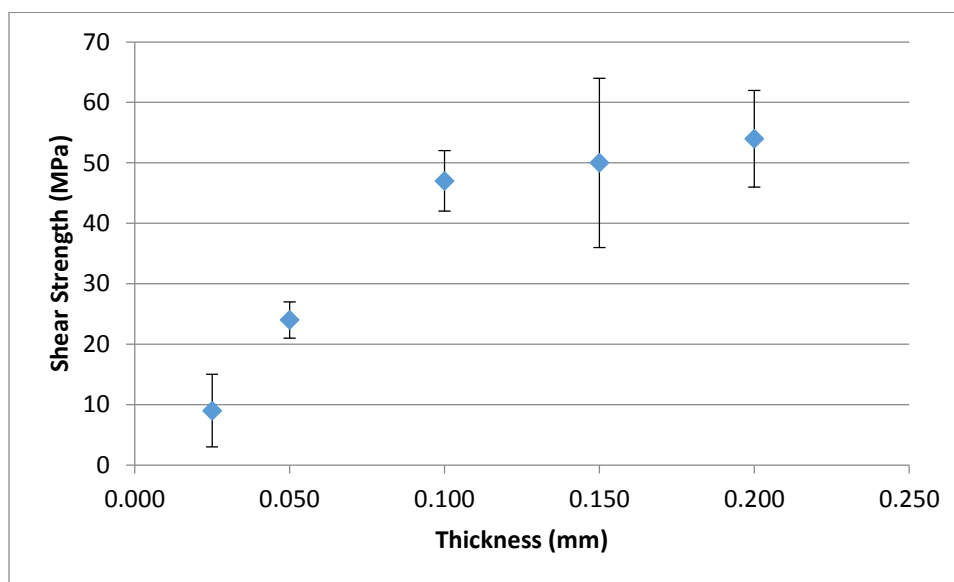
Figure 50. The average shear strength in function of braze thickness for the Ag-2 wt% Ti alloy condition.

Table XIX. Shear test results for the Ag-2 wt% Ti braze alloys with various braze thicknesses.

Approximate Joint Thickness (mm)	Shear Strength (MPa)						Average Shear Strength (MPa)	Standard Deviation (MPa)
0.025	2.4	12.9	0*	12.4	11.9	13.6	9	6
0.050	23	24.6	25.3	19.8	29.4	22.6	24	3
0.10	54.2	39.1	48.7	47.6	45.2	44.9	47	5
0.15	33.8	36.3	68	60.4	55.4	45	50	14
0.2	49	44	66.7	61.1	53	51	54	8

* The values of shear strength described as 0 are for samples that failed during loading into the shear test fixture.

4.2.2.2. Silver-copper eutectic based braze alloy

Braze specimens were also fabricated using a silver-copper eutectic alloy with the addition of 2 wt% Ti. Five different braze thicknesses were also evaluated for this braze alloy condition. Table XX lists the shear test results for the five braze thickness conditions. The average shear strengths for the five braze thickness conditions (0.025, 0.05, 0.1, 0.15 and 0.2 mm) are plotted in Figure 51 for the Ag-Cu-2 wt% Ti alloy. For this braze alloy, the highest average shear strength was obtained for a joint thickness of 0.2 mm. Within the reproducibility error, the average shear strengths did not change significantly in the thickness range of 0.1 to 0.15 mm. There were no visible cracks in any of the samples. The standard deviation was smaller and the strengths were more consistent for the samples with a thickness less than 0.2 mm.

Table XX. Shear test results for the Ag-Cu-2 wt% Ti braze alloys with various braze thicknesses.

Approximate Joint Thickness (mm)	Shear Strength (MPa)						Average Shear Strength (MPa)	Standard Deviation (MPa)
0.025	0*	33.6	38.8	26.8	33.6	0*	22	18
0.050	47.5	58.3	46	59.3	37.7	48	50	8
0.10	57	69	75	67.32	88.4	71.6	71	10
0.15	57.3	38.2	50	58	70	58.5	59	12
0.2	59.3	75.05	154.26	120.33	64.44	-	95	41

* The values of shear strength described as 0 are for samples that failed during loading into the shear test fixture.
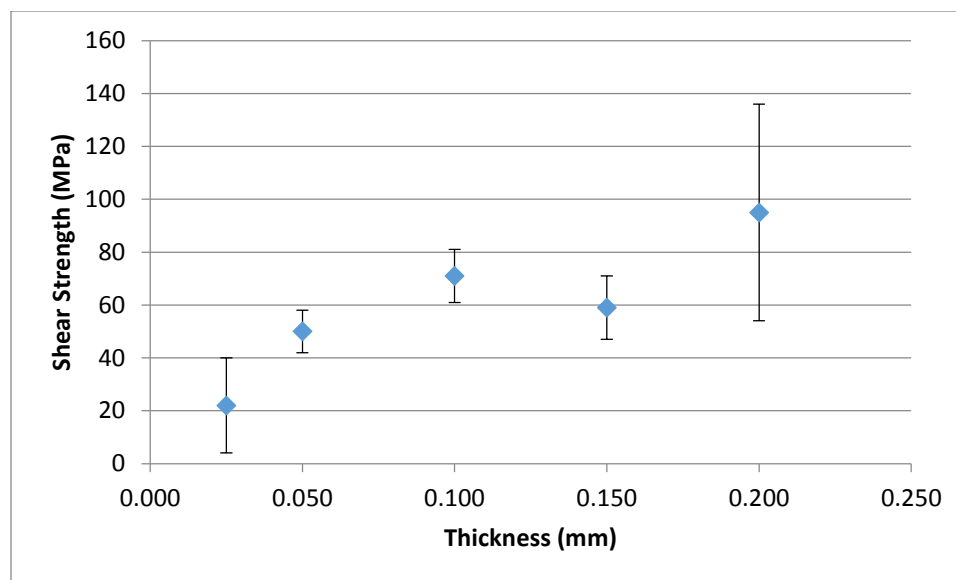
Figure 51. The average shear strength in function of braze thickness for the Ag-Cu-2 wt% Ti braze alloys.

4.2.2.3. Summary

For the Ag-2 wt% Ti braze alloys, it was observed that the samples failed in the silver braze layer as opposed to fracture occurring along the braze alloy/diamond interface. It was observed that the Ag-2 wt% Ti/diamond interface was always stronger than the silver interlayer itself. Pure silver is softer and more ductile than the substrate materials. Saxton et al. indicated that the maximum shear stress in a material can withstand prior to plastic instability was $\sigma_{UTS}/2$ if it is assumed that no triaxial stress is developed (Saxton, West, & Barrett, 1971). The typical tensile strength for pure silver is approximately 125 MPa which sets the upper limit of the shear strength of the joint at approximately 62.5 MPa (ASM International Handbook Committee, 1998). It is proposed that the approximately constant shear strength (47 to 54 MPa) in the thickness range of 0.1 to 0.2 mm is due to the shearing of the ductile silver interlayer. For the thinner joints, it is hypothesized that the shear strength of the joint decreases due to microscopic flaws dominating the failure behavior (Saxton, West, & Barrett, 1971).

For the Ag-Cu-2 wt% Ti alloys, the average shear strength trend is similar for the Ag-2 wt% Ti braze alloys. However, the values of the average shear strength were higher compared to the braze alloys prepared using the Ag-2 wt% Ti alloys. It is proposed that the relatively flat region obtained at higher thickness values indicated that lack of the development of a triaxial stress state. The decrease in average shear strength for thinner joints indicated that the shear strength was controlled by microscopic defects (Saxton, West, & Barrett, 1971).

4.2.3. Shear test results and microstructures for optimized test matrix

The goal of this phase of the research was to obtain shear strength data for braze alloy process optimization. Based on the preliminary and second brazing test matrices, braze alloys were identified as Ag-Cu-2 wt% Ti and Ag-2 wt% Ti. The Ag-Cu-2 wt% Ti braze alloy had the highest average shear strength and the shear strengths for the Ag-2 wt% Ti alloys were the most consistent. The test variables evaluated for the braze alloy system optimization were hold time, cooling rate, and composition. As illustrated in Table VIII, the braze samples were studied in a hold time range of 2-50 minutes and a cooling rate range of 2-10 °C/min using the Ag-Cu eutectic alloy with 2 wt% Ti addition. Alloying elements (Ni and Cr) were added in an attempt to improve the mechanical properties of the braze alloys starting with Ag with a 2 wt% Ti addition. A total of 5-6 samples were tested at each condition. The error bars represent the standard deviation for 5-6 repeat samples.

4.2.3.1. Shear test results for optimized test matrix

4.2.3.1.1. Silver based braze alloy systems

Braze specimens were prepared starting with silver with the addition of 2 wt% Ti. Ni or Cr were added into the filler metal in an effort to increase the shear strength of the braze filler metal layer. The shear test results are listed in Table XXI. The average shear strengths for the

three braze alloy: Ag-2% Ti, Ag-2% Ti-2% Ni, and Ag-2% Ti-2% Cr (wt%) are plotted in Figure 52.

The average shear strengths of Ag-2% Ti-2% Ni and Ag-2% Ti-2% Cr (wt%) were 34 MPa and 20 MPa, respectively. Therefore, the additions of Ni or Cr into the filler metal actually lowered the shear strengths relative to the Ag-2 wt% Ti braze alloy. The standard deviation of three braze sample conditions were relatively small which correlates with no visible interfacial cracking observed near the diamond substrate.

Table XXI. Shear test results for the Ag-2 wt% Ti alloy condition with additions of Ni or Cr.

Sample Condition (wt%)	Shear Strength (MPa)						Average Shear Strength (MPa)	Standard Deviation (MPa)
Ag-2%Ti	49.1	44.08	66.72	61.06	52.96	51.07	54	9
Ag-2%Ti-2%Ni	41.25	34.24	35.86	30.74	33.72	30.24	34	4
Ag-2%Ti-2%Cr	19.24	28.98	28.72	14.86	12.38	17.9	20	7
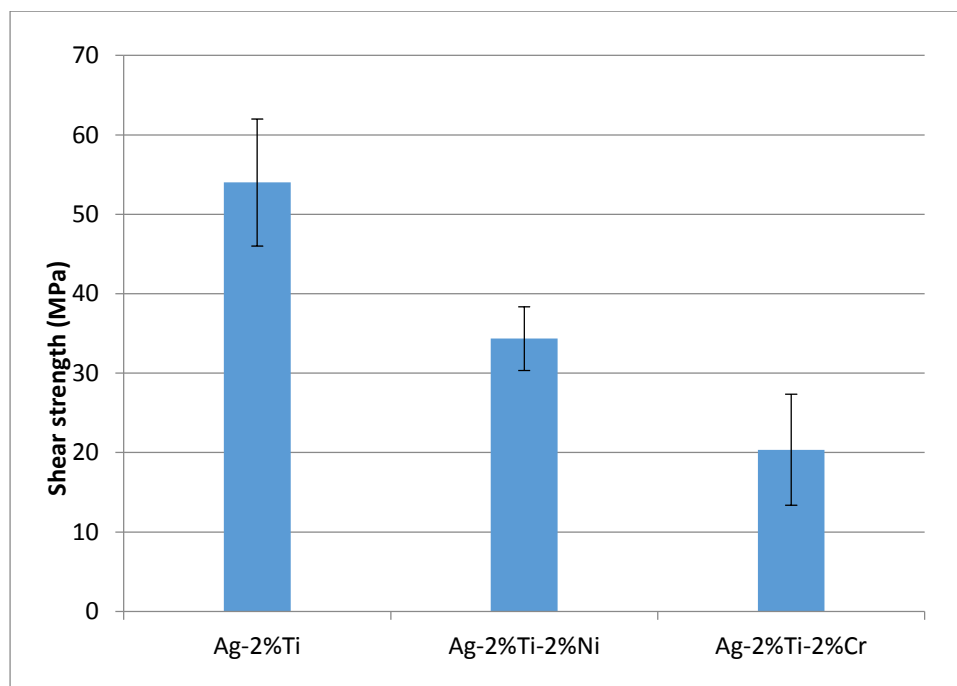
Figure 52. The average shear strength for three Ag-Ti based braze alloy compositions.

4.2.3.1.2.   Silver-copper based systems

The effect of hold time and cooling rate on the shear strength of the brazed samples is presented in this phase. The shear strength of braze samples were studied in the hold time range of 2-50 minutes (120-3,000 s) and cooling rate range of 2-10 °C/min (0.033-0.167 °C/s) using the silver-copper eutectic alloy with 2 wt% Ti addition. The braze specimens were silver-copper eutectic alloys with the addition of 2 wt% Ti. The silver-copper eutectic alloy had a thickness of 0.2 mm.

Figure 53. Diamond/WC-Co samples brazed with a silver-copper eutectic alloy with a 2% wt Ti addition for hold times of a) 2 mins, b) 10 mins, c) 30 mins, d) 50 mins.

4.2.3.1.2.1.   Effect of hold time on shear strength

The brazed samples for the four different hold times are shown in Figure 53. It was observed that the braze alloy flowed upward out of the joints into the surrounding WC-Co substrates (Figure 53a-d). Table XXII lists the shear test results for the four different hold times. The average shear strengths for the four different hold time conditions (2, 10, 30, and 50 minutes) are plotted in Figure 54. The silver-copper eutectic alloy with 2 wt% Ti has the highest average shear strength (95 MPa) when the hold time was 30 minutes. However, more cracking was observed on the surface region of diamond substrates with a hold time of 30 minutes. It is

possible that thermal stresses generated from the coefficient of thermal expansion (CTE) mismatch resulted in the formation of interfacial cracks.

Table XXII. Shear test results for the Ag-Cu-2 wt% Ti braze alloy with different hold times.

Sample Condition (wt%)	Holding Time (min)	Shear Strength (MPa)						Average Shear Strength (MPa)	Standard Deviation (MPa)
Ag-Cu-2%Ti	2	62.09	78.62	67.69	55.37	102.12	-	73	18
	10	54.53	39.53	39.13	60.83	47.88	40.75	47	9
	30	59.3	75.05	154.26	120.33	64.44	-	95	41
	50	48.41	61.88	57.09	55.23	96.48	-	64	19

The average shear strength for silver-copper eutectic alloy with a 2 wt% Ti addition increased from 47 to 95 MPa with an increase in hold time from 10 to 30 minutes. However, the standard deviation also increased from 9 to 41 MPa when the hold time was from 10 to 30 minutes. The standard deviation of the two hold time conditions of 10 and 50 minutes were 9 and 19 MPa, respectively which were relatively small and which correlates with no visible interfacial cracking in the diamond for the majority of the samples.
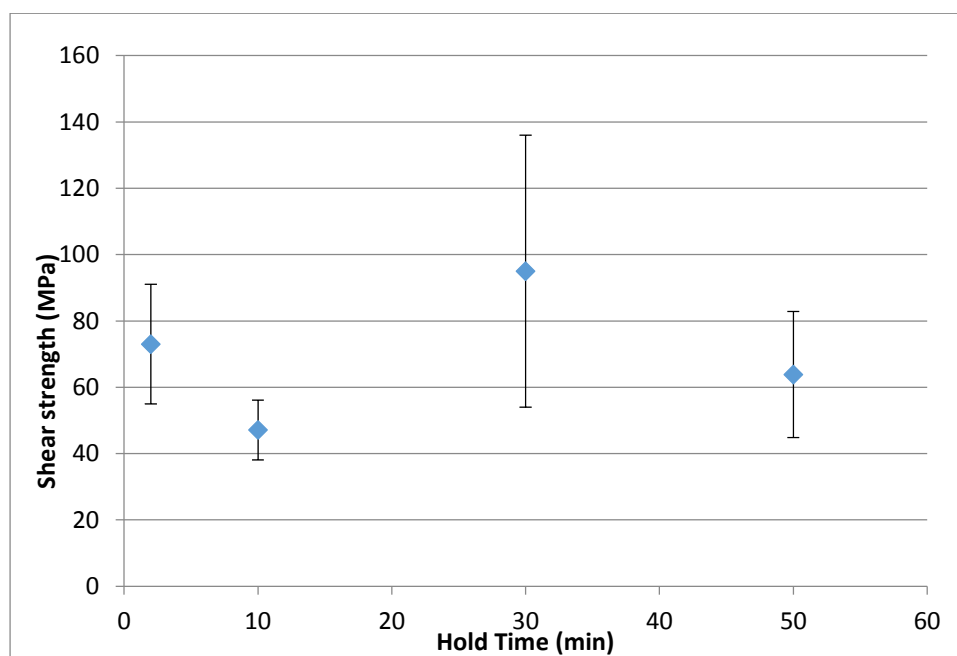
Figure 54. The average shear strength for the Ag-Cu-2 wt% Ti braze alloy with different hold times.

4.2.3.1.2.2. Effect of cooling rate on shear strength

The brazed samples for the four different cooling rate conditions are shown in Figure 55. It was also observed that the braze alloy flowed upward out of the joints into the surrounding WC-Co substrates (Figure 55a-d).Table XXIII lists the shear test results for the four different cooling rate. The average shear strengths for the four different cooling rate conditions (2, 5, 8, and 10 °C/min) are plotted in Figure 56.
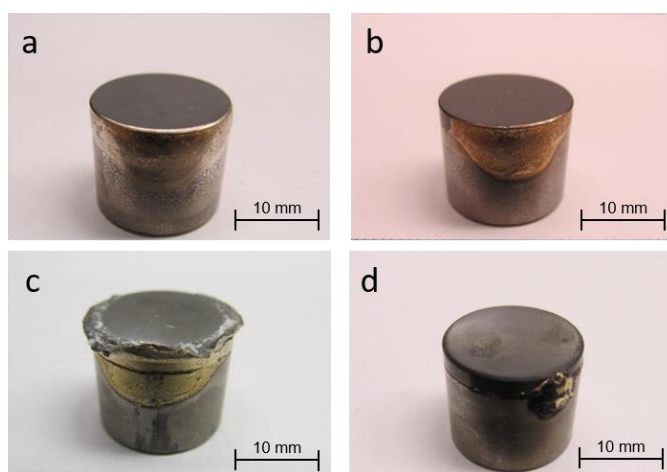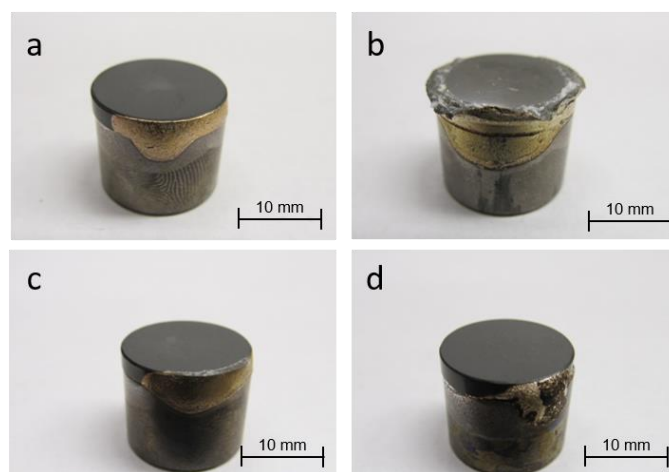

Figure 55. Diamond/WC-Co samples brazed with a silver-copper eutectic alloy with a 2% wt Ti addition for a cooling rates of a) 2 °C/min, b) 5 °C/min, c) 8 °C/min, d) 10 °C/min.

The average shear strength for silver-copper eutectic alloy with 2 wt% Ti addition increased from 45 MPa to 95 MPa with a decrease in cooling rate from 10 °C/min to 5 °C/min. With the increasing cooling rate, the average shear strength of the joints initially increases and then gradually decreases. The silver-copper eutectic alloy with a 2 wt% Ti addition had the highest average shear strength of 95 MPa when the cooling rate was 5 °C/min. The standard deviation increased from 14 MPa to 41 MPa with the cooling rate conditions of 2 and 10 °C/min. The standard deviation for the two cooling rate conditions of 2 and 10 °C/min were relatively small which again correlated with no visible interfacial cracking in the diamond. Based on the above analysis, for all conditions examined, the maximum average shear strength of 95 MPa was

obtained for a brazed joint heated to 810°C for a hold time of 30 minutes and a cooling rate of 5

°C/min with a Ag-Cu eutectic-2 wt% Ti alloy.

Table XXIII. Shear test results for the Ag-Cu-2 wt% Ti braze alloy with different cooling rates.

Sample Condition (wt%)	Cooling Rate (°C/min)	Shear Strength (MPa)					Average Shear Strength (MPa)	Standard Deviation (MPa)
Ag-Cu-2%Ti	**2**	76.08	37.73	61.88	73.75	83.09	67	18
	5	59.3	75.05	154.26	120.33	64.44	95	41
	8	105.25	31.01	41.86	41.92	-	55	34
	10	43.83	37.58	65.46	51.62	28.58	45	14
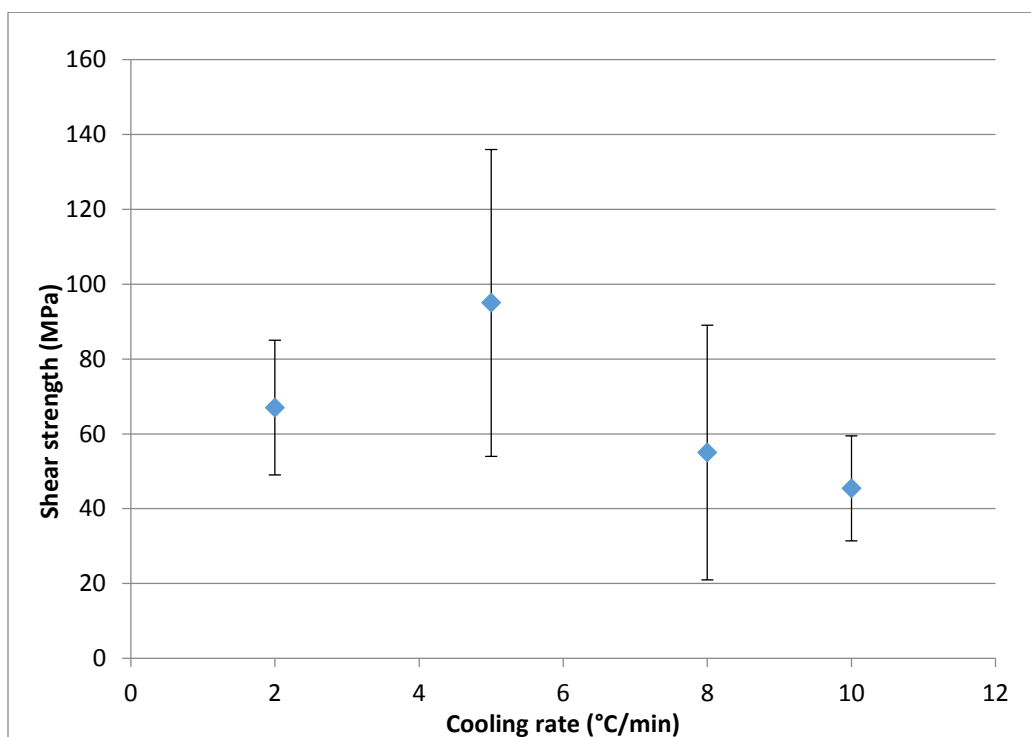
Figure 56. The average shear strength for for the Ag-Cu-2 wt% Ti braze alloy with different cooling rates.

4.2.3.2. Brazed joint microstructures for optimized test matrix

A braze cross-sectioned microstructural analysis was performed for the silver-copper

eutectic braze alloys. For the brazed joints, six samples were selected in the hold time range of

10-50 minutes and cooling rate range of 5-25 °C/min using the silver-copper eutectic alloy with a

2 wt% Ti addition. An example of each microstructure is presented for each test condition. The

metallic element compositional profiles were obtained from an EDS semi-quantitative analysis. The relative percentages are only provided for general comparisons and are not considered highly reliable. The EDS semi-quantitative analysis technique is not considered reliable for thin layers or complicated multiphase microstructures.

4.2.3.2.1.   Effect of hold time on microstructural development

Figure 57a is a cross-section of the center of the brazed diamond/WC-Co sample for a hold time of 10 minutes. No titanium carbide reaction layer or other product layers were observed under the SEM. Micro-cracks were observed in tungsten carbide near the joint interface. EDS line scans are presented in Figure 57b. The variation in chemical composition is presented using EDS line scans. EDS line scan analysis of the joint region indicated that there were no reaction layers or other product layers at the interfaces. The Ti content was nearly constant in the joint region. At the interface between the braze alloy and diamond substrate, neither a reaction zone nor an interfacial product layer was identified.

Figure 57. SEM/EDS analysis of WC-Co/ Ag-28Cu (wt%) eutectic-2 wt% Ti /diamond interface for a hold time of 10 minutes: a) SEM micrograph, b) EDS line scans.

Figure 58a is a cross-section of the center of the brazed diamond/WC-Co sample for a hold time of 30 minutes. No micro-cracks were observed in this cross-section. EDS line scans

are presented in Figure 58b. At the interface between the braze alloy region and the substrates for

a hold time of 30 minutes, Cu rich and Ag rich products formed at the interfaces. However, it

was very difficult to accurately analyze the Cu or Ag rich product layers because the layers were

too thin. It was also observed that large precipitates were uniformly dispersed in the braze alloy

region.

The EDS analysis of the interface between the braze alloy and WC-Co substrate indicated

the joint was mainly composed of a Cu-Ti rich product layer. However, this Cu-Ti rich product

layer was thin and not clearly visible. The Ti, Co, and Cu content in the regions increased

moving from the braze alloy region into the diamond substrate while the Ag content decreased in

the braze alloy region. As observed in Figure 58b, Cu-Ti-Co rich precipitates with large irregular

shapes were dispersed in the braze alloy region. At the interface between the braze alloy region

and diamond substrate, a thin Ag rich layer (~3 microns thick) formed.

Figure 58. SEM/EDS analysis of WC-Co/ Ag-28Cu (wt%) eutectic-2 wt% Ti /diamond interface for a hold time of 30 minutes: a) SEM micrograph, b) EDS line scans.

Figure 59a is a cross-section for the center of the brazed diamond/WC-Co sample for a

hold time of 50 minutes. Within the resolution of the SEM, neither a reaction zone nor an

interfacial product layer was identified at either of the joint interfaces. A large number of micro-

cracks were observed in the WC-Co substrate near the joint interface. EDS line scans are presented in Figure 59b. The Ti content at the joint interface was nearly constant moving from the WC-Co substrate through the braze alloy into the diamond substrate.

For the different hold time conditions, SEM/EDS analysis revealed that no titanium carbide reaction product layers could be identified at the interface within the resolutions of the SEM. Micro-cracks were observed in the WC-Co substrate near the joint interface when the told times were 10 or 50 minutes. No micro-cracks were observed in the cross-section with a hold time of 30 minutes. As a result, the silver-copper eutectic alloy with a 2 wt% Ti has the highest average shear strength of 95 MPa when the hold time was 30 minutes.

Previous investigators observed that a TiC layer forms at the diamond interface and that the thickness of the TiC layer depends on the brazing conditions (Chen, Xu, Fu, & Su, 2009). However, no reaction product were resolved within the SEM resolution this study.
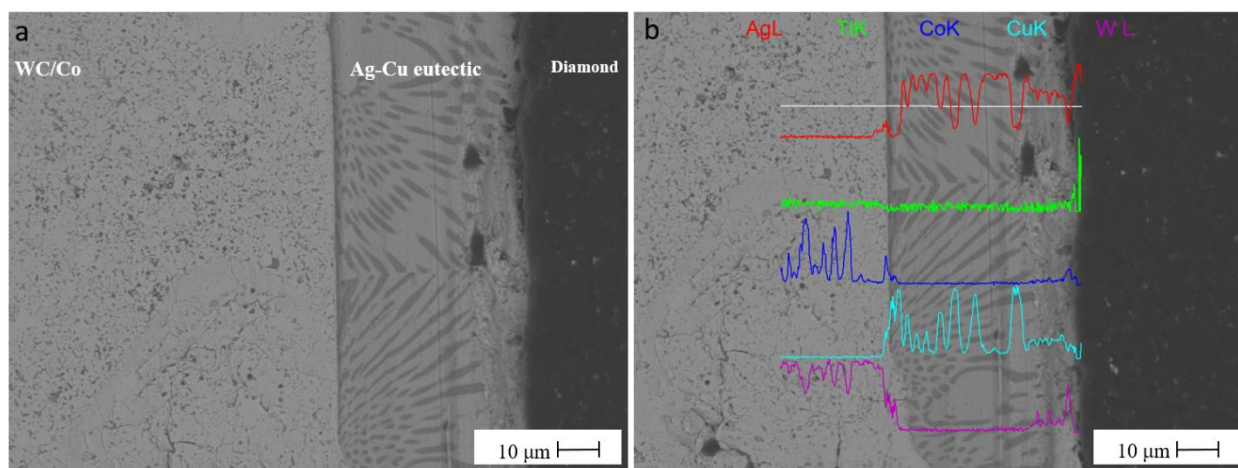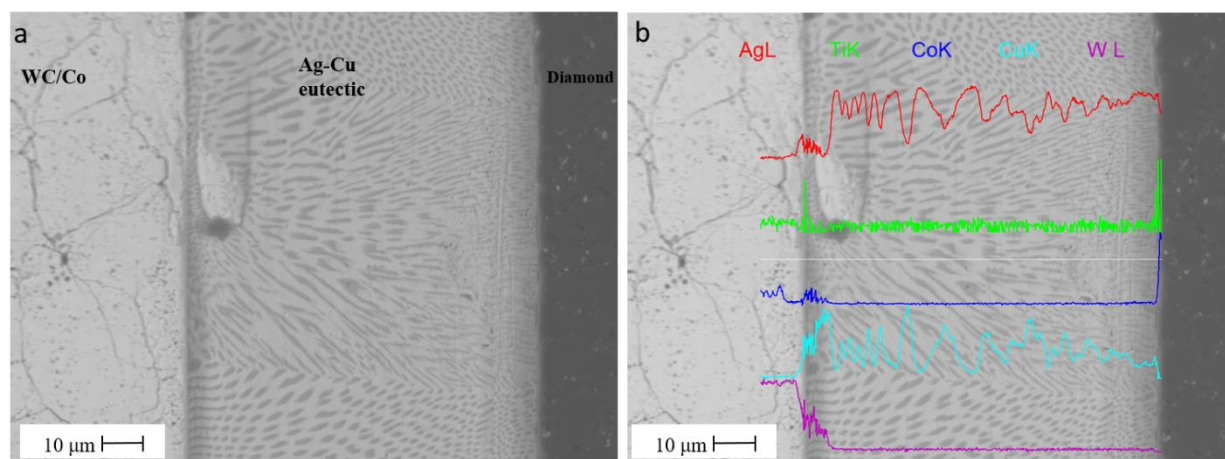

Figure 59. SEM/EDS analysis of WC-Co/ Ag-28Cu (wt%) eutectic-2 wt% Ti /diamond interface for a hold time of 50 minutes: a) SEM micrograph, b) EDS line scans.

4.2.3.2.2. Effect of cooling rate on microstructural development

Figure 60a is a cross-section for the center of the brazed diamond/WC-Co sample for a cooling rate of 8°C/min. No micro-cracks were observed in this cross-section. EDS line scans are

presented in Figure 60b. The EDS line scan analysis of the interface between the braze alloy and WC-Co substrate indicated that a thin Cu-Ti rich product layer was formed at the interface. The Ti, Co, and Cu content in the regions increased moving from the braze alloy region into the diamond substrate while the Ag content decreased at the braze alloy region. In addition, a large number of Cu-Ti-Co rich precipitates of irregular shapes were also dispersed in the braze alloy region (Figure 60a). At the interface between the braze alloy and the diamond substrate, a Ag rich layer (~3 microns thick) formed. It was very difficult to accurately analyze this Ag-Cu-Ti rich product layer because it was very thin.
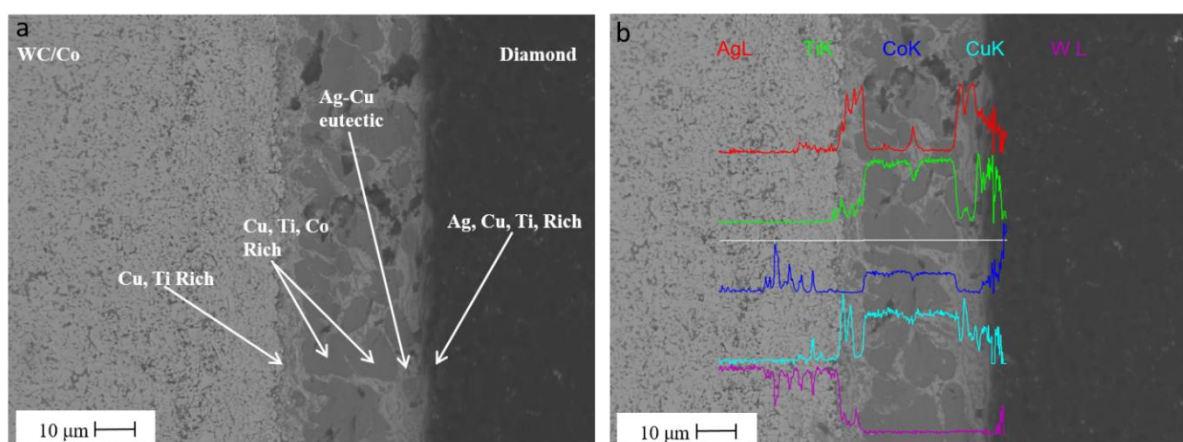
Figure 60. SEM/EDS analysis of WC-Co/ Ag-28Cu (wt%) eutectic-2 wt% Ti /diamond interface for a cooling rate of 8 °C/min: a) SEM micrograph, b) EDS line scans.

Figure 61a is a cross-section for the center of the brazed diamond/WC-Co sample for a cooling rate of 10 °C/min. No titanium carbide reaction layer or other product layers were resolved using the SEM. Micro-cracks were observed in the WC-Co substrate near the joint interface. EDS line scans are presented in Figure 61b. The Ti content at the interface is nearly constant moving from the WC-Co substrate into the diamond substrate. However, the W and Co content in this region increased moving from the braze alloy into the diamond substrate while the Ag and Cu content decreased at the braze alloy region. W, Co rich zones were also observed at the braze alloy region.
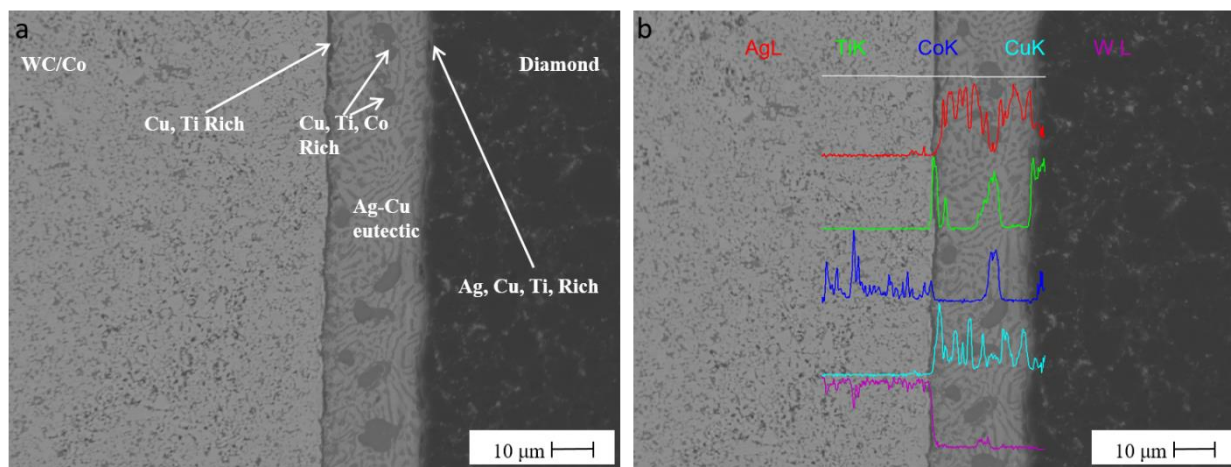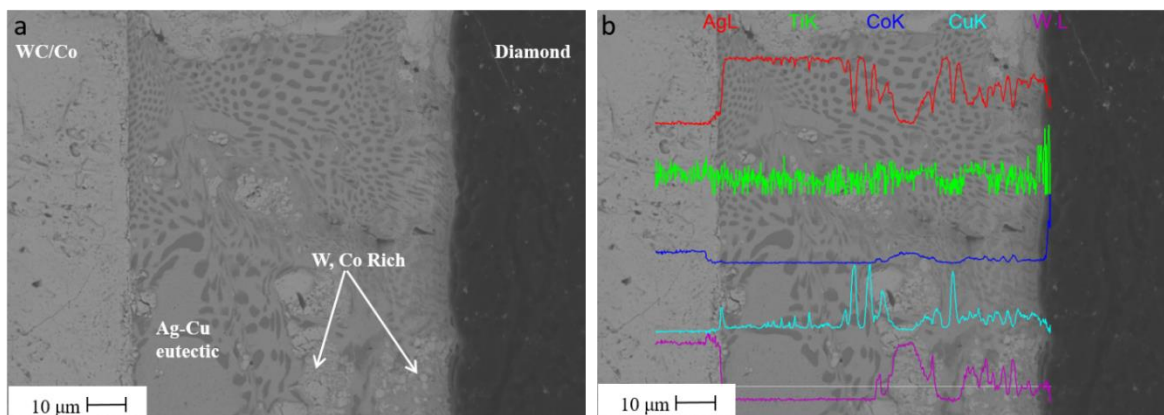
Figure 61. SEM/EDS analysis of WC-Co/ Ag-28Cu (wt%) eutectic-2 wt% Ti /diamond interface for a cooling rate of 10 °C/min: a) SEM micrograph, b) EDS line scans.

Figure 62 is a cross-section through the center of the brazed diamond/WC-Co sample for

a cooling rate of 10 °C/min. No titanium carbide reaction layer or product layers were resolved

under the SEM. As illustrated in Figure 62, large cracks were observed in diamond near the joint

interface. The braze alloy flowed into the crack filling the crack before it solidified. W-Co rich

zones were again observed at the braze alloy region.
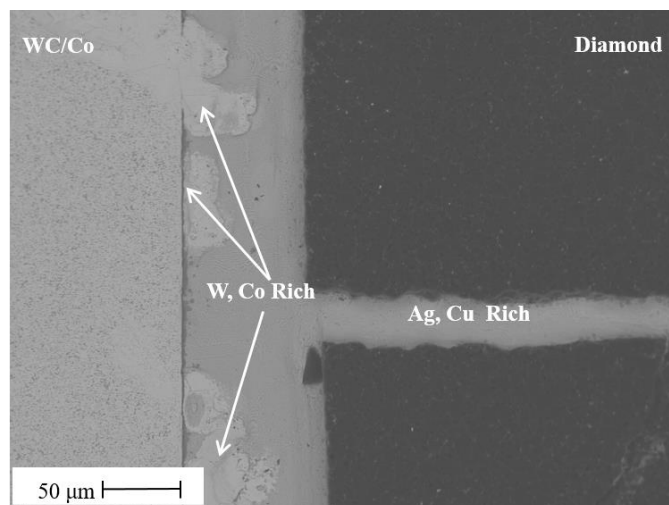
Figure 62. SEM micrograph of WC-Co/ Ag-28Cu (wt%) eutectic-2 wt% Ti /diamond interface for a cooling rate of 25 °C/min.

For the different cooling rate conditions, no reaction zone was identified at the interface

within the resolution of the SEM/EDS analysis. Micro-cracks were observed in the WC-Co

substrate near the joint interface when the cooling rate was 10 °C/min. Large cracks were

observed in diamond near the joint interface with a cooling rate of 25 °C/min. Therefore, a high cooling rate correlates with cracking in substrates. As a result, the average shear strength for the brazed joints decreased with increase in cooling rate from 5 °C/min to 10 °C/min. W-Co rich zones were identified at the braze alloy region with increasing the cooling rate.

For a cooling rate of 5 °C/min, Cu-Ti-Co rich precipitates were observed at the braze alloy region (Figure 58). A large number of Cu-Ti-Co rich precipitates of irregular shapes were identified at the braze alloy region when the cooling rate increased from 5 °C/min to 8 °C/min. However, no precipitates had been observed at the joint interface with a cooling rate of 10 °C/min and 25 °C/min. The brazed joints had the highest average shear strength of 95 MPa when the cooling rate was 5 °C/min (Table XXIII). As the cooling rate increased from 5 °C/min to 8 °C/min, the average shear strength decreased. It was concluded that the large amount of precipitation may result in harmful effects on the shear strength of joints. At the interface between the braze alloy region and the substrates, thin Ag rich and Cu rich layers formed.

4.3. Discussion

For the preliminary brazing test matrix, only the diamond and WC-Co substrates did not

bond when brazed using copper with additions of 2 wt% and 5 wt% Ti. Table XV lists the

apparent contact angles on the WC-Co and diamond substrates using copper with additions of 2

wt% and 5 wt% Ti ranged from 43° to 64° and both conditions were still wetting. As previously

mentioned, reaction product layers were identified at the interface for the copper sessile drop

with additions of 2 wt% and 5 wt% Ti on WC-Co substrates. However, SEM/EDS analysis

revealed that no reaction products or interfacial products were observed within the resolution of

the SEM/EDS for the copper sessile drops with additions of 2 wt% and 5 wt% Ti on diamond

substrates. This result agrees with a previous study that concluded the interface between the

copper and diamond was weak because no reaction products or interfacial products observed and

bonding was due to van der Waal's forces only (Scott, Nicholas, & Dewar, 1975).
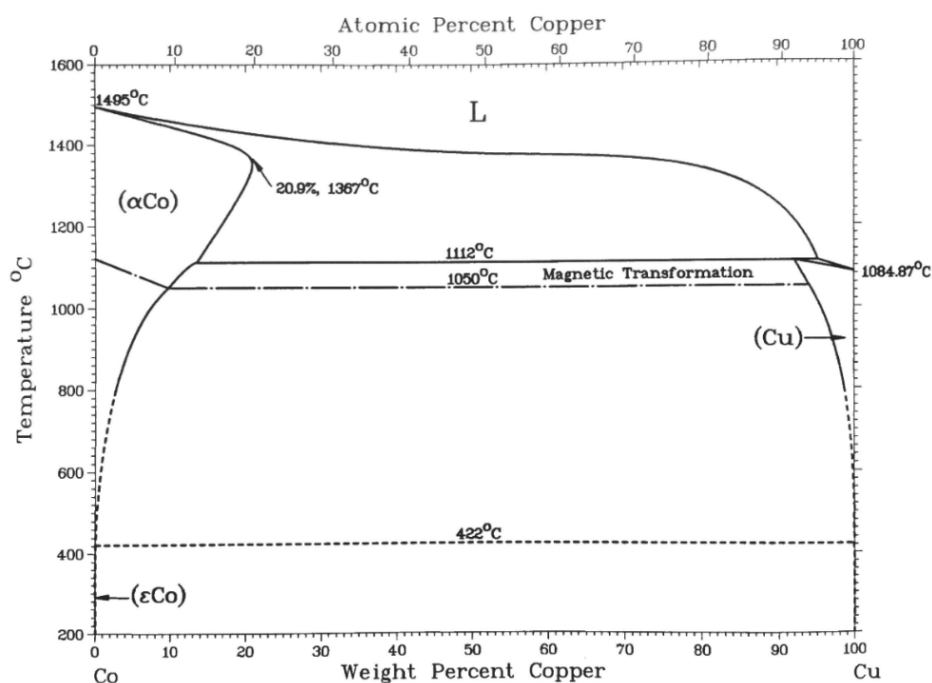
Figure 63. Co-Cu binary phase diagram.
(Massalski, Okamoto, & ASM International, 1990)

Table XV provides the apparent contact angle values obtained using copper based alloys on WC-Co and diamond substrates. Pure copper on a WC-Co substrate exhibited excellent wetting (θ<8°). However, the addition of Ti and Zr increased the apparent contact angle on the WC-Co substrates. The wettability was better for the WC-Co substrates with no active metal addition. WC-Co is relatively easily wet by molten brazing alloys. The higher the percentage of cobalt, the easier it is to wet the tungsten carbide (Roberts, 2013). Pure copper on a WC-13 wt% Co substrate exhibited excellent wetting because the addition of Co to the tungsten carbide improves the wettability. As illustrated in Figure 19, there were also reaction product layers observed between the pure copper and the WC-Co substrate. A Co and Cu rich zone was observed at the interface. Based on the Co-Cu phase diagram (Figure 63), an increased concentration of Co at the interface WC-Co/Cu indicated diffusion of Co into Cu (Silva, Fernandes, & Senos, 2016). The additions of 2 wt% and 5 wt% Ti increased the apparent contact angles on the WC-Co substrates. It is possible that the reaction product layer formed at the interface hinders the diffusion of Co into Cu and therefore the extent of the dissolution reaction will tend to be smaller. As observed in Figures 20 and 21, the Ti and Cu rich reaction layer was thin. A reduction reaction was observed at the interface for Cu sessile drops with 2 wt% Ti and for a 2 wt% Zr on WC-Co substrate (Figures 20 and 22). It is proposed that TiC and ZrC reaction products formed at the interface, respectively. Figure 2 provides the Gibbs free energies of formation for carbides as a function of temperature presented as Ellingham plots. Kubaschewski et al. reported the Gibbs free energy of formation of ZrC corresponding to the reaction (Kubaschewski, Evans, & Alcock, 1967):

$$Zr + C \rightarrow ZrC \tag{6}$$

The Gibbs free energy of ZrC formation is represented in the temperature range of 25-1947°C:

$$\Delta G^0(TiC)(kj/mol) = -184.5 + 0.009T \tag{7}$$

Based on the Gibbs free energies of formation for ZrC, the formation of ZrC at the inferface is thermodynamically predicted.

The Gibbs free energy of formation of TiC corresponding to the reaction in Equation 8 was first reported by Richardson (Richardson, 1953):

$$Ti + C \rightarrow TiC \tag{8}$$

The Gibbs free energies of TiC formation are represented in the temperature range of 25-877°C as:

$$\Delta G^0(TiC)(kj/mol) = -183.05 + 0.01T \tag{9}$$

At higher temperatures (877-1727°C), the Gibbs free energy of TiC formation is:

$$\Delta G^0(TiC)(kj/mol) = -186.31 + 0.013T \tag{10}$$

Based on these equations, the formation of TiC is likely to occur at the WC-Co/braze alloy during the sessile drop process.

For the diamond substrates, the addition of Ti, Zr, and V decreased the apparent contact angle, which improved both the wetting and bonding behavior between copper alloy and diamond substrate (Table XV). Active metals are used in brazing to improve the wetting of diamond substrate and form a reliable metallurgical bond. However, no reaction products or interfacial products were identified within the resolution of SEM/EDS analysis.

A TiC reaction product is predicted for the liquid Cu-Ti alloys on diamond substrates but no reaction products were observed within the resolution of the SEM/EDS. The Gibbs free energies of formation for carbides as a function of temperature were presented as Ellingham plots in Figure 2. Based on the equations (8)-(10), the free energy for formation of TiC is

negative at the brazing temperature, which means that the formation of TiC is thermodynamically favored at the diamond/braze alloy interface during the sessile drop process.

In a previous study, it was observed that islands of carbide nucleate at favored sites on the diamond surface when a diamond is contacted with an alloy. More and larger carbide islands form with increasing concentrations of the reactive element in the alloy. The islands of carbides grow, contact each other and form a continuous interfacial layer as the concentration of the carbide former is increased. Therefore, the interface between the alloy and diamond substrate become stronger. However, the interfaces cease to strengthen and may weaken as the carbide thickens due to the development of flaws after this point is reached (Scott, Nicholas, & Dewar, 1975).

For the silver based systems in the preliminary brazing test matrix, the average shear strengths were 45, 54, and 55 MPa for three sets of braze samples which were prepared using silver with additions of Ti (1 and 2 wt%) and 2 wt% Zr. The differences in average shear strength of the three brazed samples was relatively small. Table XV indicates that the silver based sessile drops on WC-Co substrates exhibited good wetting under all conditions. The pure silver alloy on a diamond substrate exhibited a non-wetting condition while the additions of Ti and Zr resulted in high wettability. As illustrated in Figures 25-27, dissolution reactions were identified between the silver alloys and the WC-Co substrates. Within the resolution of the SEM, neither a reaction zone nor an interfacial product layer was observed at the interface between the silver alloys and the diamond substrates. It is possible that thin product layers formed at the interface because the diamond and WC-Co substrates did bond. As illustrated in Ti-Ag phase diagram (Figure 11), it is predicted that the intermetallic product formed at the interface was TiAg. However, it was very difficult to accurately analyze the thin product layers. The interfacial

reactions of diamond with silver based filler alloys have been studied and the formation of a titanium carbide layer on the diamond surface has been observed (Yamazaki & Suzumura, 2000). Klotz et al. verified the formation of a titanium carbide layer at the diamond interface, whose thickness depends on the brazing conditions (Klotz, Liu, Khalid, & Elsener, 2008). However, Buhl et al. observed a TiC layer that was very thin and that could not be resolved in their micrographs (Buhl, Leinenbach, Spolenak, & Wegener, 2010).

The silver-copper eutectic alloy with 2 wt% Ti from the preliminary brazing test matrix had the highest average shear strength (95 MPa). Table XV indicates that the silver-copper eutectic alloy with additions of 2 wt% and 5 wt% Ti on WC-Co and diamond substrate also exhibited excellent wettability. Reaction layers were observed at the interface of the WC-Co substrates for the silver-copper eutectic sessile drops with additions of 2 wt% and 5 wt% Ti. It is proposed that intermetallic phases were formed at the interface for the silver-copper eutectic sessile drops on diamond substrates with additions of 2 wt% and 5 wt% Ti. A Cu rich region was observed at the interface between the WC-Co and the Ag-Cu eutectic-2 wt% Ti sessile drop. EDS point scan analysis determines that the approximate mole ratio for Cu:Ti is 3:2. As illustrated in Ti-Cu phase diagram (Figure 7), it is proposed that Cu_3Ti_2 is the intermetallic solidification product formed at the interface during cooling of the sessile drop. For the silver-copper eutectic sessile drops with an addition of 5 wt% Ti on WC-Co substrates, the EDS analysis indicated that the joint is mainly composed of two different Cu rich product layers: a Cu-Ti rich product layer and a Cu-Ag-Ti rich product layer. A Cu-Ti rich product layer was formed at the interface between the WC-Co and the Ag-Cu eutectic-5 wt% Ti sessile drop. EDS point scan analysis determined that the approximate mole ratio for Cu:Ti is 16:9. As illustrated in Ti-Cu phase diagram (Figure 7), it is predicted that Cu_3Ti_2 and Cu_2Ti are the possible

intermetallic products formed at the interface during cooling of the sessile drop. EDS point scan analysis also determined that there was a Cu-Ti-Ag rich product layer with approximately 55 at% Cu, 30 at% Ti, and 15 at% Ag. The Cu:Ti:Ag mole ratio is approximately 11:6:3. Based on the vertical Cu-Ti-Ag section of the Ag-Cu-Ti system (Figure 64), it is predicted that the final phases of the Ag-28 wt% Cu- 5 wt% Ti braze alloy are Cu_4Ti, Ag and Cu solid solutions.

Similar to the sessile drops on WC-Co substrates, a Cu-Ti rich product layer was formed at the interface between diamond and the Ag-Cu eutectic-2 wt% Ti sessile drop. EDS point scan analysis determined that the approximate mole ratio for Cu:Ti is 3:2. As illustrated in Ti-Cu phase diagram (Figure 7), it is proposed that Cu_3Ti_2 is the intermetallic solidification product formed at the interface during cooling of the sessile drop. For the silver-copper eutectic sessile drop with additions of 5 wt% Ti on diamond substrates, the EDS analysis indicated that the joint is mainly composed of two product layers: a Cu-rich product layer and a Ag-rich product layer. EDS point scan analysis determined that the Cu-Ti rich product layer was approximately 56 at% Cu, 42 at% Ti, and 2 at% Ag. The approximate mole ratio for Cu:Ti is 4:3. As illustrated in Ti-Cu phase diagram (Figure 7), it is predicted that the intermetallic solidification product formed at the interface is Cu_4Ti_3. EDS point scan analysis revealed that there was a Ag-rich product layer with approximately 49 at% Ag, 29 at% Cu, and 22 at% Ti. The Ag:Cu:Ti mole ratio is approximately 2:1:1. The silver-copper eutectic sessile drop with an addition of a 5 wt% Ti was regarded as a eutectic 72Ag-28Cu (wt%) with a low concentration of Ti. A vertical Cu-Ti-(60 at% Ag) section of the Ag-Cu-Ti system is illustrated in Figure 64 (Hirnyj & Indacochea, 2008). Because the content of Ti was relatively low, it is predicted that the final phases of the Ag-28 wt% Cu- 5 wt% Ti braze alloy are Cu_4Ti, Ag and Cu solid solutions. It is proposed that the Cu_4Ti is intermetallic solidification product formed at the interface during cooling.
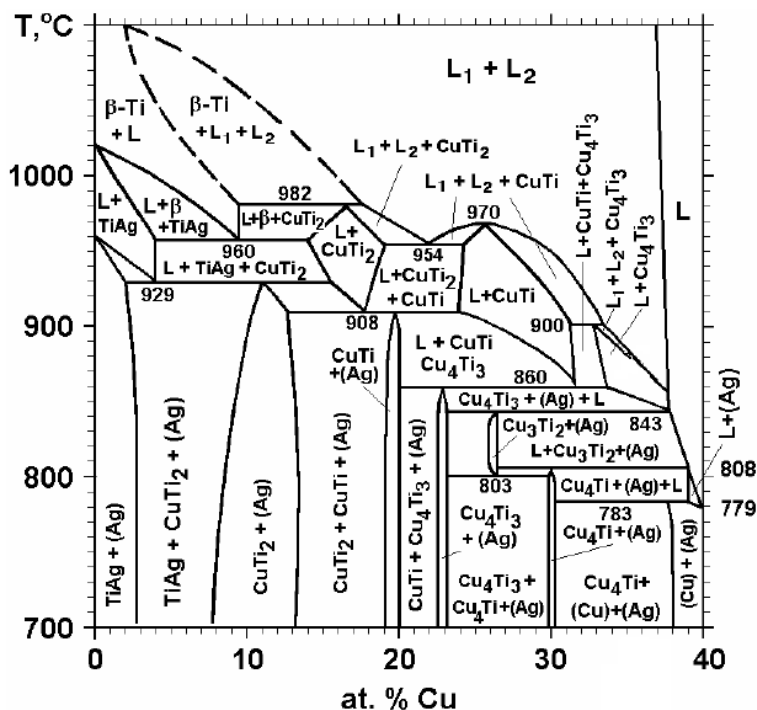
Figure 64. Vertical Cu-Ti-(60 at% Ag) section of the Ag-Cu-Ti system.
(Hirnyj & Indacochea, 2008)

A TiC reaction product is predicted for the liquid Ag-Cu-Ti alloys on diamond substrates but no reaction products were observed within the resolution of the SEM/EDS. Based on the Gibbs free energies of formation for carbides as a function of temperature (Figure 2), the formation of TiC is likely to occur at the braze alloy/diamond interface during the brazing process. The interfacial reaction product for diamond and silver-copper eutectic based filler alloys was studied by Chen et al. The results showed that there was a layer of TiC on the diamond surface (Chen, Xu, Fu, & Su, 2009). However, the TiC reaction layer was not always clearly visible because it is very thin (Buhl, Leinenbach, Spolenak, & Wegener, 2010). Previous studies also determined that the thickness of the TiC layers at the diamond interfaces varied between 50 nm and 600 nm depending on the brazing temperature and holding time (Klotz, Liu, Khalid, & Elsener, 2008). With increasing Ti content, the shear strength of the joints initially increased and then decreased (Table XVIII). The silver-copper eutectic alloy with 2 wt% Ti has

the highest average shear strength (95 MPa). The shear strength of the joints increased from 36 MPa to 95 MPa with the Ti content increasing from 0.5 wt% to 2 wt%. For silver-copper eutectic alloy with 2 wt% Ti addition, the average shear strengths increased by 163.89% as compared to that of 0.5 wt% of Ti addition. From the microstructural point of view, as illustrated in Figures 44 and 46, the intermetallic solidification product layer formed at the interface with 5 wt% Ti addition was much thicker than that of 2 wt% Ti addition. This result agrees with a previous study that concluded the shear strength of the bonds was affected by different Ti content because Ti was effective on the morphology of the interface zone. In this study, it is hypothesized that with an increasing Ti content, the number of Ti atoms migrating to the diamond surface increased, and the thickness of TiC layer increased. It was observed that the thickness of interfacial reaction layer and the amount of brittle intermetallics caused low shear strengths of the joints. In previous studies, the microstructural evolution of the interfacial reaction products and the shear strengths of diamond/steel joints brazed with Ag-Cu-Ti filler metals has been investigated. The results indicated that the shear strength of the brazed joints decreased due to the increasing thickness of the TiC layer and the formation of intermetallic phases. The thickness of interfacial reaction layer and the amount of brittle intermetallics were also related to the Ti content (Chen, Xu, Fu, & Su, 2009).

The effect of braze thickness on shear strength of brazed samples was studied in the second brazing test matrix. The highest average shear strength (54 MPa) was obtained for a joint thickness of 0.2 mm. The average shear strength for Ag-2 wt% Ti alloy was approximately constant in the braze thickness range of 0.1 to 0.2 mm (Table XIX). It was observed that the brazed samples failed in the silver braze layer. In an investigation of steel/steel joints brazed with silver as the filler metal, Bredzs et al. observed that all of the steel/steel brazed joints broke in the

middle of the silver in their work, even those with the highest tensile strength (Bredzs & Schwartzbart, 1956). For the silver braze alloy with a 2 wt% Ti addition, the Ag-2 wt% Ti/diamond interface was always stronger than the silver itself. At a lowest braze thickness of 0.025 mm, the average shear strength decreased significantly. It has been reported that a decrease of the tensile strength in extremely thin joints is due to the microscopic imperfections in the joints. The strength of steel/steel brazed joints is strongly influenced by the film thickness of the filler metal (Bredzs, 1954). The nucleation and growth of micropores results in lower tensile strengths for steel/steel brazed joints (Saxton, West, & Barrett, 1971). Finite element analyses of the stress state in silver interlayers indicated that the triaxial tensile stresses in the thinnest interlayer were approximately 10 times the yield stress of silver for steel/steel brazed joints (Klassen, Weatherly, & Ramaswami, 1992).

For the Ag-Cu-2 wt% Ti alloys evaluated as part of the braze layer thickness test matrix, the average shear strength trend is similar for the Ag-2 wt% Ti braze alloys. The highest average shear strength (95 MPa) was obtained for a joint thickness of 0.2 mm. However, the standard deviation of the brazed sample condition was the largest standard deviation (41 MPa) obtained in the brazing test matrix. It is proposed that increasing the braze joint thickness generally leads to higher residual stresses in this study. More visible cracking and larger cracks were observed on the surface region of diamond substrates for a joint thickness of 0.2 mm. There were no visible cracks in any of the samples with a joint thickness less than 0.2 mm. It is possible that thermal stresses generated from the coefficient of thermal expansion (CTE) mismatch resulted in the formation of interfacial cracks. Residual thermal stresses in the diamond substrates are caused by the different thermal expansion coefficients: $4.3\text{-}7.0 \times 10^{-6}$ K^{-1} for WC-13 wt% Co, $17\text{-}19 \times 10^{-6}$ K^{-1} for Ag-Cu eutectic, and 1.2×10^{-6} K^{-1} for diamond (Table III). The coefficient of thermal

expansion (CTE) mismatch may have caused the components of the joint to contract at different rates during cooling. It is also possible that the magnitude of residual stresses increased with increasing the thickness of brittle reaction layer. Excessive reaction can result in brittle reaction products that lower the shear strength of the diamond to WC-Co brazed joints. These thermal residual stresses between diamond and braze alloys increase with increasing product layer thickness (Klotz, Liu, Khalid, & Elsener, 2008). There is also a lattice mismatch between the diamond and the adjacent phase in the solidified filler alloy such as the intermetallic solidification product layers or TiC layers (Buhl, Leinenbach, Spolenak, & Wegener, 2010). Klotz et al. determined that the thickness of the TiC layer plays an important role in the formation of residual stresses in diamond and TiC (Klotz, Liu, Khalid, & Elsener, 2008). The formation of an interfacial TiC layer resulted in compressive stresses of 300-500 MPa in the case of CVD diamond layers deposited on Ti (Groegler, Zeiler, Hoerner, Rosiwal, & Singer, 1998).

However, for all the Ag-2 wt% Ti braze alloys in the braze layer thickness test matrix, there was no visible cracking on the surface region of diamond substrates. A ductile metal interlayer incorporated between the joining substrates can reduce the residual stresses. Silver based brazing alloys are ductile compared to Ag-Cu eutectic based brazing alloys, which can reduce the residual stresses developed during the cooling process. The ductile filler alloy deforms to accommodate the mismatch in the thermal expansion coefficient of materials (Wiese, 2001).
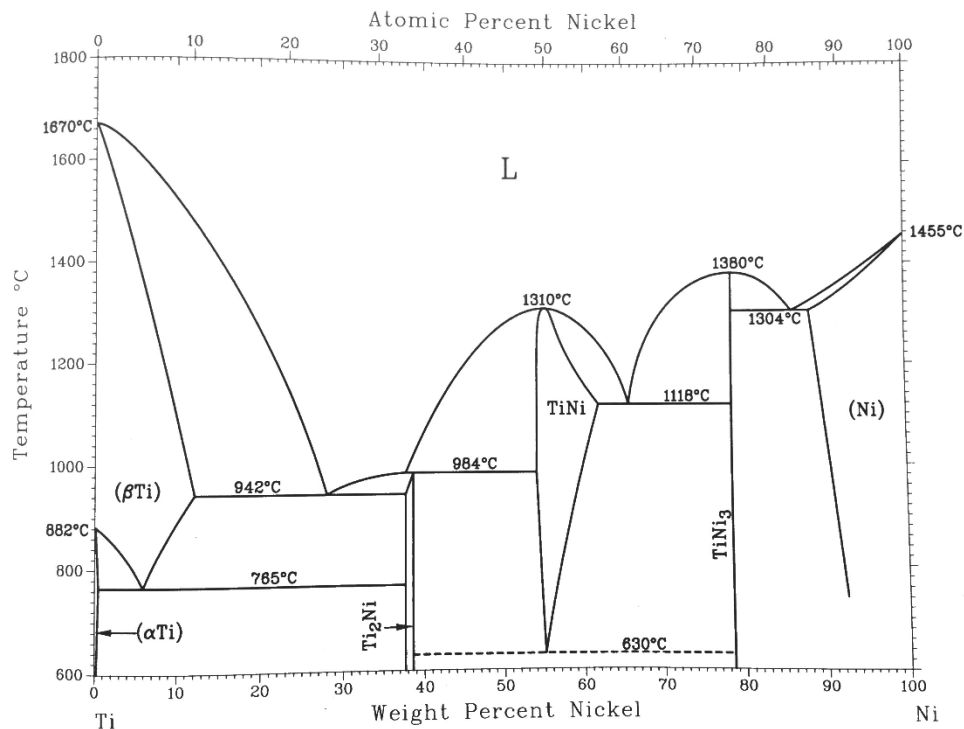
Figure 65. Ti-Ni binary phase diagram.
(Massalski, Okamoto, & ASM International, 1990)

For the optimized brazing parameters study, Ni or Cr were added into the Ag-2 wt% Ti alloy in an attempt to improve the mechanical properties of the braze samples. However, the average shear strength of the braze samples by adding Ni or Cr elements into the filler metal were lower than that of Ag-2 wt% Ti braze alloy without these additions. The average shear strengths of Ag-2 wt% Ti-2 wt% Ni (34 MPa) and Ag-2 wt% Ti-2 wt% Cr (20 MPa) decreased by 37.04% and 62.96% as compared to that of Ag-2 wt% Ti braze alloy, respectively. Based on the Ti-Ni and Ti-Cr phase diagrams (Figures 65 and 66), it is predicted that intermetallic solidification products such as TiN_3, TiNi, Ti_2Ni, or $TiCr_2$ formed at the interface during cooling. However, it was very difficult to accurately analyze the intermetallic solidification products in this study. It is possible that limited amounts of phases formed between the braze alloy and the diamond contributing to the lower of shear strength of the braze samples.
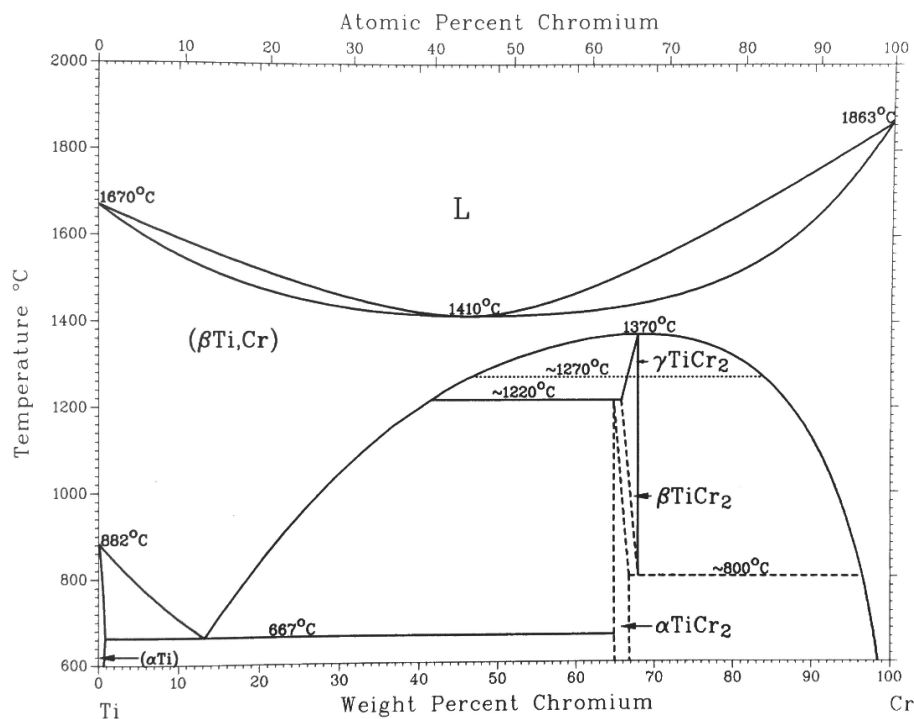
Figure 66. Ti-Cr binary phase diagram.
(Massalski, Okamoto, & ASM International, 1990)

For the silver-copper eutectic based systems in the optimized brazing test matrix, the silver-copper eutectic alloy with 2 wt% Ti has the highest average shear strength of 95 MPa when the hold time is 30 minutes and the cooling rate is 5 °C/min. No micro-cracks were observed in the cross-section with a hold time of 30 minutes and a cooling rate of 5 °C/min with Ag-Cu-2 wt% Ti alloy.

EDS line scans analysis of the interface between the braze alloy and WC-Co substrate indicated that the joint was mainly composed of a Cu-Ti rich product layer. However, this Cu-Ti rich product layer was thin and not clearly visible. Based on the Ti-Cu phase diagram (Figure 7), it is predicted that intermetallic solidification products such as $TiCu_4$, $TiCu_2$ or Ti_2Cu_3 formed at the interface during cooling of the sessile drop. Furthermore, Cu-Ti-Co rich precipitates of irregular shapes were dispersed in the braze alloy region (Figure 58). At the interface between the braze alloy region and diamond substrate, a thin Ag rich layer formed. However, it was very

difficult to accurately analyze the Cu or Ag rich product layers in this study because it was rather thin.

No titanium carbide reaction layer or other product layers were observed under the SEM when the hold time was 10 minutes. The average shear strength for silver-copper eutectic alloy with a 2 wt% Ti addition increased from 47 to 95 MPa with an increase in hold time from 10 to 30 minutes. For a hold time of 30 minutes, the average shear strengths increased by 102.13% as compared to that of 10 minutes of hold time. It seems that the longer hold time results in higher shear strength of the brazed joints. It is proposed that the reaction layers did not completely react with shorter hold times.

When the hold time was 50 minutes, a large number of micro-cracks were observed in the WC-Co substrate near the joint interface. It is proposed that a long hold time correlates with cracking in substrates. As a result, the average shear strength for the brazed joints decreased with increase in hold time from 30 minutes to 50 minutes. Buhl et al. investigated that influences of the brazing parameters on microstructure and shear strength of diamond/metal joints. The results revealed that the interlayers' thickness increased with holding time which leads to a higher percentage of brittle intermetallics in the brazing gap resulting in a decrease of the shear strength (Buhl, Leinenbach, Spolenak, & Wegener, 2010).

For the different cooling rate conditions, the brazed joints had the highest average shear strength (95 MPa) when the cooling rate was 5 °C/min (Table XXIII). The average shear strength for silver-copper eutectic alloy with a 2 wt% Ti addition decreased from 95 to 45 MPa with an increase in hold time from 5 to 10 °C/min. For a cooling rate of 5 °C/min, the average shear strengths increased by 111.11% as compared to that of 10 °C/min of cooling rate. At the interface between the braze alloy region and the substrates for a cooling rate of 5 °C/min, Cu rich

and Ag rich products formed at the interfaces. However, it was also very difficult to accurately

analyze the Cu or Ag rich product layers because the layers were too thin. It was observed that

large precipitates were uniformly dispersed in the braze alloy region. No micro-cracks were

observed in the WC-Co substrate near the joint interface. When the cooling rate was 10 °C/min,

micro-cracks were observed in the WC-Co substrate near the joint interface. Large cracks were

observed in diamond near the joint interface with a cooling rate of 25 °C/min. Therefore, a high

cooling rate correlates with cracking in substrates. As a result, the average shear strength for the

brazed joints decreased with increase in cooling rate from 5 °C/min to 10 °C/min.

5. CONCLUSIONS

(1) Polycrystalline diamond (PCD) was brazed using active metal braze alloys onto WC-13 wt% Co carbide substrates. The silver-copper eutectic alloy with addition of a 2 wt% Ti has the highest average shear strength of 95 MPa when the hold time is 30 minutes and the cooling rate is 5 °C/min.

(2) The diamond and WC-Co substrates did not bond using copper with additions of 2 wt% and 5 wt% Ti. The apparent contact angles on the WC-Co and diamond substrates using copper with additions of 2 wt% and 5 wt% Ti were ranged from 43° to 64° and both conditions were still wetting. It is proposed that the interface between the copper and diamond was weak because no reaction products or interfacial products observed and bonding was due to van der Waal's forces only.

(3) Pure copper, pure silver, and silver-copper eutectic alloys on a WC-13 wt% Co substrates all exhibited excellent wetting while exhibiting poor wetting on diamond substrates. It was observed that WC-Co is relatively easy to wet with all of the braze alloys evaluated in this study. Pure copper pure silver, and silver-copper eutectic alloys on the WC-13 wt% Co substrates exhibited excellent wetting because the addition of Co to the tungsten carbide resulted in a dissolution reaction which provided a mechanism for high wettability. However, there was no reaction mechanism available to improve the wetting of the diamond substrates.

(4) For the diamond sessile drop samples, the addition of Ti, Zr, and V decreased the apparent contact angle, which improved both the wetting and bonding behavior between the braze alloy and diamond substrate. Only intermetallic solidification products were observed at the interface for the Ag-Cu eutectic based alloys with additions of 2 wt% and

5 wt% Ti. It is predicted that the formation of TiC is thermodynamically favored at the braze alloy/diamond interface during the brazing process. However, no TiC reaction product was identified within the resolution of SEM/EDS analysis possibly because the TiC reaction layer is very thin.

(5) With increasing Ti content, the shear strength of the joints initially increased and then decreased (Table XVIII). The shear strength of the joints increased from 36 MPa to 95 MPa with the Ti content increasing from 0.5 wt% to 2 wt%. For silver-copper eutectic alloy with 2 wt% Ti addition, the average shear strengths increased by 163.89% as compared to that of 0.5 wt% of Ti addition. It is proposed that the shear strength of the bonds was affected by different Ti content because Ti was effective on the morphology of the interface zone.

(6) The average shear strength for Ag-2 wt% Ti alloy was approximately constant (47 to 54 MPa) in the braze thickness range of 0.1 to 0.2 mm. It was observed that the brazed samples failed in the silver braze layer. It is proposed that the approximately constant shear strength in this thickness range is due to the shearing of the ductile silver interlayer.

(7) The highest average shear strength (95 MPa) for the Ag-Cu-2 wt% Ti alloys was obtained for a joint thickness of 0.2 mm. However, the standard deviation (41 MPa) of the braze strengths was largest for this brazing test matrix. More visible cracking and larger cracks were observed on the surface region of diamond substrates for a joint thickness of 0.2 mm. It is possible that thermal stresses generated from coefficient of thermal expansion (CTE) mismatch resulted in the formation of interfacial cracks. It is also possible that the magnitude of residual stresses increased with increasing the thickness of brittle reaction

layer. Excessive reaction can result in brittle reaction products that lower the shear strength of the diamond to WC-Co brazed joints.

(8) Ni or Cr were added to the Ag-2 wt% Ti alloy in an effort to improve the mechanical properties of the braze samples. However, the average shear strength of the braze samples by adding Ni or Cr elements into the filler metal were actually lower than for Ag-2 wt% Ti braze alloy without an alloying addition. The average shear strengths of Ag-2 wt% Ti-2 wt% Ni (34 MPa) and Ag-2 wt% Ti-2 wt% Cr (20 MPa) decreased by 37.04% and 62.96% as compared to that of Ag-2 wt% Ti braze alloy, respectively. It is possible that limited amounts of $TiNi_3$, Ti_2Ni, $TiNi$, and $TiCr_2$ phases formed between the braze alloy and the diamond contributed to the lower of shear strength of the braze samples.

(9) No micro-cracks were observed in the cross-section with a hold time of 30 minutes and a cooling rate of 5 °C/min with Ag-Cu-2 wt% Ti alloy, which has the highest average shear strength. It was observed that a Cu-Ti intermetallic solidification product formed at the interface during cooling of the sessile drop. In addition, Cu-Ti-Co rich precipitates of irregular shapes were observed at the braze alloy region which were dispersed in the braze alloy region. However, it was very difficult to accurately analyze the Cu or Ag rich product layers in this study because it was rather thin.

(10)   The Ag-Cu eutectic-2 wt% Ti alloy has the highest average shear strength of 95 MPa when the hold time is 30 minutes. The average shear strength for silver-copper eutectic alloy with a 2 wt% Ti addition increased from 47 to 95 MPa with an increase in hold time from 10 to 30 minutes. For a hold time of 30 minutes, the average shear strengths increased by 102.13% as compared to that of 10 minutes of hold time. However, the average shear strength for the brazed joints decreased with increase in hold

time from 30 minutes to 50 minutes. It was determined that the interlayer thickness increased with increased holding time which lead to a higher percentage of brittle intermetallic phases in the braze interlayer. It is proposed that this is the reason for a decrease of the shear strength.

(11)   For the different cooling rate conditions, the average shear strength for silver-copper eutectic alloy with a 2 wt% Ti addition decreased from 95 to 45 MPa with an increase in hold time from 5 to 10 °C/min. For a cooling rate of 5 °C/min, the average shear strengths increased by 111.11% as compared to that of 10 °C/min of cooling rate. At the interface between the braze alloy region and the substrates for a cooling rate of 5 °C/min, Cu rich and Ag rich products formed at the interfaces. However, it was also very difficult to accurately analyze the Cu or Ag rich product layers because the layers were too thin. Large cracks were observed in diamond near the joint interface with a cooling rate of 25 °C/min. Therefore, a high cooling rate correlates with cracking in substrates. As a result, the average shear strength for the brazed joints decreased with increase in cooling rate from 5 °C/min to 10 °C/min.

6. FUTURE WORK

For diamond brazing, an interfacial chemical reaction is an essential aspect of the bonding mechanism. However, carbide layers formed at the interface such as TiC that were typically reported to be up 1 micron thick were not identified in this study. It is possible that these carbide layers formed but that they were too thin for the SEM resolution limits. A TEM investigation of the sessile drop and braze samples is recommended in order to accurately analyze the reaction products and intermetallic solidification products.

Based on the results of the current study, the maximum average shear strength (95 MPa) was obtained for a brazed joint heated to 810 °C with a Ag-Cu eutectic-2 wt% Ti alloy. The hold temperature for Ag-Cu eutectic-2 wt% Ti alloys was 810°C which was approximately 30°C above the melting temperature of the Ag-28 wt% Cu eutectic alloy. The shear strength of joints strongly depends on the brazing hold temperature and the hold time due to the kinetics of diffusion and the reaction of the brazing filler alloy both with the diamond and the WC-Co substrate. A study of the effect of the brazing hold temperature on the interfacial structure and the shear strength of WC-Co/diamond joints was recommended.

The average shear strength of the braze samples with additions of 2 wt% Ni or 2 wt% Cr into the filler metal actually lowered the shear strengths relative to the Ag-2 wt% Ti braze alloy. It is possible that a limited amount of $TiNi_3$, Ti_2Ni, TiNi, and $TiCr_2$ phases formed between the braze alloy and the diamond contribute to the lower of shear strength of the braze samples. It is recommended that the higher percentage of Ni and Cr are added to improve the shear strength of the braze samples using Ag with 2 wt% Ti addition. Another recommendation is that 5-15 wt% Cu was added into the filler metal in order to increase the shear strength of the braze samples using Ag with a 2 wt% Ti addition.

For the different cooling rate conditions, brazing filler alloy layer thickness increases with increasing cooling rate. It is supposed to be decreased as the cooling rate increases. In this study, the standard deviation for Ag-Cu eutectic-2 wt% Ti alloy braze sample conditions were relatively large. It is recommended that an optimized process control is applied to the brazing process.

The joint geometry can be changed to avoid pure shear by changing the stress state developed under loading and reduce the residual stresses during cooling process. In order to reduce the residual stresses, joint geometry changes are recommended. As illustrate in Figure 67, two different types of joint geometry are recommended: angle-shaped and cone-shaped. For the angle-shaped joint condition, mixed compression/shear stress state developed under loading which leads to increase the joint strength. For the cone-shaped joint condition, the increased of the joint strength caused by the mixed tension/shear and compression/shear stress state.
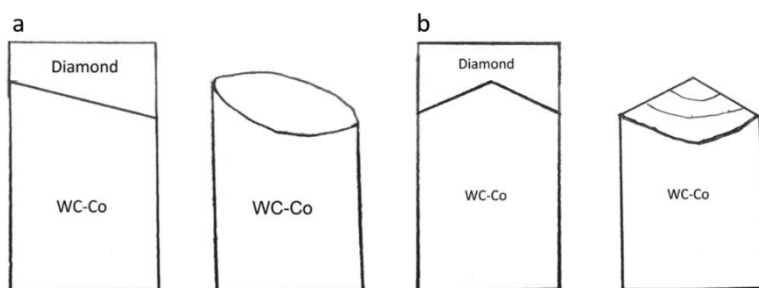
Figure 67. The modified joint geometry: a) angle-shaped, b) cone-shaped.

Residual stresses in brazed joints plays an important role in the determination of mechanical properties and lifetime of the brazed joints. The residual stresses of the brazed diamond/WC-Co joints are difficult to characterize analytically. For a future study, it is recommended that finite element methods such as ANSYS and ABAQUS be applied to calculate the theoretical residual stresses in the brazed diamond/WC-Co joint.

7. References Cited

AWS Committee on Definitions and Symbols., American Welding Society., American Welding Society. Technical Activities Committee., & American National Standards Institute. (2009). *Standard welding terms and definitions: Including terms for adhesive bonding, brazing, soldering, thermal cutting, and thermal spraying*. Miami, Fla: American Welding Society.

American Welding Society. (2007). *Brazing handbook*. Miami, FL: American Welding Society.

Akselsen, O. M. (1992). Advances in brazing of ceramics. *Journal of Materials Science*, 27, 8, 1989-2000.

ASM International Handbook Committee. (1998). *ASM handbook: Metals handbook*. Metals Park: ASM International, American Society of Materials.

Boucher, M. (1996). *Overview of the diamond industry, in Industrial Minerals*. Toronto, Canada: Blendon Information Services.

Bredzs, N. (1954). Investigation of factors determining the tensile strength of brazed joints. *Welding Research Supplement*, 33, 545-563.

Buhl, S., Leinenbach, C., Spolenak, R., & Wegener, K. (2010). Influence of the brazing parameters on microstructure, residual stresses and shear strength of diamond–metal joints. *Journal of Materials Science*, 45, 16, 4358-4368.

Buhl, S., Leinenbach, C., Spolenak, R., & Wegener, K. (2012). Microstructure, residual stresses and shear strength of diamond–steel-joints brazed with a Cu–Sn-based active filler alloy. *International Journal of Refractory Metals and Hard Materials*, 30, 1, 16-24.

Brochu, M., Pugh, M. D., & Drew, R. A. L. (2004). Brazing silicon nitride to an iron-based intermetallic using a copper interlayer. *Ceramics International*, 30, 6, 901-910.

Bredzs, H., & Schwartzbart, H. (1956). Triaxial tension testing and the brittle fracture strength of metals. *Welding Research Supplement*, 35, 610-615.

Bar-Cohen, Y., & Zacny, K. (2009). *Drilling in extreme environments: Penetration and sampling on Earth and other planets*. Weinheim: Wiley-VCH.

Cverna, F., & ASM International. (2002). *ASM ready reference*. Materials Park, Ohio: ASM International.

Callister, W. D., & Rethwisch, D. G. (2010). *Materials science and engineering: An introduction*. Hoboken, NJ: John Wiley & Sons.

Chen, Y., Xu, H., Fu, Y., & Su, H. (2009). Effect of Ti addition on shear strength of brazing diamond and Ag based filler alloy. *Key Engineering Materials*, 416,264-268.

Davis, J. R. (Ed.). (1995). *ASM Specialty Handbook: Tool Materials*. Materials Park, OH: ASM International.

Dezellus, O., & Eustathopoulos, N. (1999). The role of van der Waals interactions on wetting and adhesion in metal/carbon systems. *Scripta Materialia*, 40, 11, 1283-1288.

Dezellus, O., & Eustathopoulos, N. (2010). Fundamental issues of reactive wetting by liquid metals. *Journal of Materials Science*, 45, 16, 4256-4264.

Danielli, J. F., Rosenberg, M. D., & Cadenhead, D. A. (1972). *Progress in surface and membrane science*. New York.

Dezellus, O., Voytovych, R., Li A, P. -H., Constantin, G., Bosselet, F., and Viala, J. C. (2009). Wettability of Ti3SiC2 by Ag-Cu and Ag-Cu-Ti melts. *Journal of Materials Science*, 45, 8, 2080-2084.

Eustathopoulos, N., Nicholas, M. G., & Drevet, B. (1999). *Wettability at high temperatures*. Amsterdam: Pergamon.

Fernie, J. A., Drew, R. A. L., & Knowles, K. M. (2009). Joining of engineering ceramics. *International Materials Reviews*, 54, 5, 283-331.

Gorczyca, F. E. (1987). *Application of Metal Cutting Theory*. New York, NY: Industrial Press, Inc.

Gauthier, M. M. (Ed.). (1998). Diamond. *Engineered Materials Handbook* (Desk ed. pp. 967-968). Materials Park, Ohio: ASM International.

Galli, M., Botsis, J., & Janczak-Rusch, J. (2006). Relief of the Residual Stresses in Ceramic-Metal Joints by a Layered Braze Structure. *Advanced Engineering Materials*, 8, 3, 197-201.

Groegler, T., Zeiler, E., Hoerner, A., Rosiwal, S. M., & Singer, R. F. (1998). Microwave-plasma-CVD of diamond coatings onto titanium and titanium alloys. *Surface and Coatings Technology*, 98, 1079-1091.
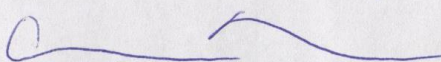
Ham, J. O., Chung, J. H., Jung, S. K., Byoun, Y. M., & Lee, C. H. (2013). Interfacial Behaviors of Vacuum Brazed Joint between Diamond Grit and Ni-13Sn-28Cr Filler Alloy. *Advanced Materials Research*, 705, 132-142.

Hirnyj, S., & Indacochea, J. E. (2008). Phase transformations in Ag70.5Cu26.5Ti3 filler alloy during brazing processes. Chemistry of Metal and Alloys, 1, 323-332.

Iida, T., & Guthrie, R. I. L. (1988). *The physical properties of liquid metals*. Oxford: Clarendon Press.

Jacobson, D. M., & Humpston, G. (2005). *Principles of brazing*. Materials Park, NY: ASM International.

Kubaschewski, O., Evans, E. L., & Alcock, C. B. (1967). *Metallurgical thermochemistry*. Oxford: Pergamon Press.

Klotz, U. E., Liu, C., Khalid, F. A., & Elsener, H.-R. (2008). Influence of brazing parameters and alloy composition on interface morphology of brazed diamond. *Materials Science & Engineering A*, 495, 265-270.

Kozlova, O., Voytovych, R., Devismes, M.-F., & Eustathopoulos, N. (2008). Wetting and brazing of stainless steels by copper-silver eutectic. *Materials Science & Engineering A*, 495, 96-101.

Klassen, R. J., Weatherly, G. C., & Ramaswami, B. (1992). Void nucleation in constrained silver interlayers. *Metallurgical Transactions A*, 23, 1, 3281-3291.

Levy, A. (1991). Thermal Residual Stresses in Ceramic-to-Metal Brazed Joints. *Journal of the American Ceramic Society*, 74, 9, 2141-2147.

Lee, C. H., Ham, J. O., Song, M. S., & Lee, C. H. (2007). The Interfacial Reaction between Diamond Grit and Ni-Based Brazing Filler Metal. *Materials Transactions*, 48, 4, 889-891.

Liu, S. X., Xiao, B., Zhang, Z. Y., & Duan, D. Z. (2016). Microstructural characterization of diamond/CBN grains steel braze joint interface using Cu-Sn-Ti active filler alloy. *International Journal of Refractory Metals and Hard Materials*, 54, 54-59.

Meier, A., Gabriel, V., Chidambaram, P. R., & Edwards, G. R. (1995). The Wettability of Copper-Manganese Alloys on Alumina and Their Potential as Direct Brazing Filler Metals. *Materials and Manufacturing Processes*, 10, 4, 625-641.

Mortimer, D. A., & Nicholas, M. (1970). The Wetting of Carbon by Copper and Copper Alloys. *Journal of Materials Science*, 5, 2, 149-155.

Massalski, T. B., Okamoto, H., & ASM International. (1990). *Binary alloy phase diagrams*. Materials Park, Ohio: ASM International.

Mirski, Z., & Piwowarczyk, T. (2011). Wettability of hardmetal surfaces prepared for brazing with various methods. *Archives of Civil and Mechanical Engineering*, 11, 2, 411-419.

Ngwenya, S. H. (2015). *Investigation and processing of 3D-polycrystalline diamond material*.

Naidich, Y. V. (1981). The Wettability of solids by liquid metals. *Progress in Surface and Membrane Science*, 14, 353-484.

Naidich, Y. V. (2007). *Strength of the Diamond-Metal Interface & Brazing of Diamonds*. Cambridge, UK: Cambridge Intl Science Pub.

Naidich, Y. V., & Kolesnichenko, G. A. (1964). Study of the wetting of diamond and graphite by liquid metals. *Soviet Powder Metallurgy and Metal Ceramics*, 2, 1, 35-38.

Naidich, Y. V., Kolesnichenko, G. A., Lavrinenko, I. A., and Motsak, Y. F. (1977). Brazing and metallization of ultrahard tool materials. Kiev, Naukova Dumka.

Prelas, M. A., Popovici, G., & Bigelow, L. K. (1998). *Handbook of industrial diamonds and diamond films*. New York: Marcel Dekker.

Richardson, F. D. (1953). The thermodynamics of metallurgical carbides and of carbon in iron. *The Journal of the Iron and Steel Institute*. 175:33-51.

Rosenqvist, T. (1974). *Principles of extractive metallurgy*. New York: McGraw-Hill.

Rado, C., Kalogeropoulou, S., & Eustathopoulos, N. (2000). Bonding and wetting in non-reactive metal/SiC systems: weak or strong interfaces? *Materials Science and Engineering A*, 276, 195-202.

Roberts, P. (2013). *Industrial brazing practice*. Boca Raton, FL: CRC Press.

Sung, C.-M. (1999). Brazed diamond grid: a revolutionary design for diamond saws. *Diamond and Related Materials*, 8, 1540-1543.

Stephenson, D. A., & Agapiou, J. S. (1997). *Metal cutting theory and practice*. New York: Marcel Dekker.

Silva, V. L., Fernandes, C. M., & Senos, A. M. R. (2016). Copper wettability on tungsten carbide surfaces. *Ceramics International*, 42, 1, 1191-1196.
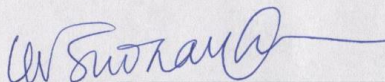
Scott, P. M., Nicholas, M., & Dewar, B. (1975). The wetting and bonding of diamonds by copper-base binary alloys. *Journal of Materials Science*, 10, 11, 1833-1840.

Saxton, H. J., West, A. J., & Barrett, C. R. (1971). Deformation and failure of brazed joints-macroscopic considerations. *Metallurgical Transactions*, 2, 4, 999-1007.

Shiue, R. K., Wu, S. K., Chen, F. Y., & Yang, T. E. (2012). Interfacial Reaction and Wettability of 72Ag-28Cu Braze on CP-Ti Substrate Using Infrared Heating. *Metallurgical and Materials Transactions A*, 43, 6, 1742-1746.

Thwaites, C. J. (1982). *Capillary joining: Brazing and soft-soldering*. Chicester: Research Studies Press.

Tillmann, W., Osmanda, A. M., Yurchenko, S., & Theisen, W. (2005). Diamond Brazing - Interfacial Reactions and Wetting. *Materialwissenschaft Und Werkstofftechnik*, 36, 8, 370-376.

Wiese, J. L. (2001). *Strength of metal-to-ceramic brazed joints* (Master's thesis). Massachusetts Institute of Technology, Cambridge, MA.

Xu, R., Indacochea, J. E., & Harren, S. V. (1992). Silicon nitride-metal active brazing: Bonding and mechanical strength. *Proceeding of 3rd International Conference on Brazing, High Temperature Brazing and Diffusion Welding*. Aachen, Germany: German Welding Society (DVS)

Yamazaki, T., & Suzumura, A. (2000). Relationship between X-ray diffraction and unidirectional solidification at interface between diamond and brazing filler metal. *Journal of Materials Science*, 35, 24, 6155-6160.
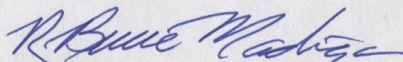
SIGNATURE PAGE

This is to certify that the thesis prepared by Zhiyong Yin entitled "Vacuum Brazing of Diamond to Tungsten Carbide" has been examined and approved for acceptance by the Department of Metallurgical and Materials Engineering, Montana Tech of The University of Montana, on this 29th day of April, 2016.
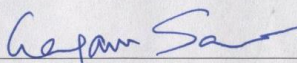
Alan Meier, PhD, Assistant Professor
Department of Metallurgical and Materials Engineering
Chair, Examination Committee

K. V. Sudhakar, PhD, Associate Professor
Department of Metallurgical and Materials Engineering
Member, Examination Committee

Bruce Madigan, PhD, Professor of Welding Engineering and Chair of General Engineering
Department of General Engineering
Member, Examination Committee

Gagan Saini, PhD, Materials Science Advisor
Halliburton Energy Services, Inc
Member, Examination Committee